2012

A Cellular Automata Model of Enantiomer Interactions with beta-Cyclodextrin

DeSoi Darren
Virginia Commonwealth University

A CELLULAR AUTOMATA MODEL OF ENANTIOMER INTERATIONS WITH β-CYCLODEXTRIN

A dissertation submitted in partial fulfillment of the requirements for the degree of Doctor of Philosophy at Virginia Commonwealth University.

by

DARREN JOSEPH DESOI
Bachelor of Science, Rowan University, 1991

Major Director: H. THOMAS KARNES, Ph.D.
PROFESSOR & GRADUATE PROGRAM DIRECTOR, DEPARTMENT OF PHARMACEUTICS

Virginia Commonwealth University
Richmond, Virginia
March, 2012

This work is dedicated to my family for their patience and continued support during times of celebration of milestones and obstacles overcome along the way. A special dedication to my wife and children who endured my absence from family vacations and getaways that were part of the journey for this part-time student. Best wishes to my son Jacob as he begins his college experience as mine comes to an end.

Acknowledgments

I would like to thank my advisor Dr. Karnes for continuously encouraging my efforts while guiding me enough to stay on track but allowing the freedom to develop as a researcher. I greatly appreciate the time you made for our discussions and your kindness when family crisis occurred during my time as your student.

I am very grateful to Dr. Lemont Kier for his guidance and enthusiasm over cellular automata. Your ideas and passion were contagious.

I am also very thankful to Dr. Chao-Kun Cheng for the hours of programming guidance and mentorship into the computer programming world.

I would also like to thank my other committee members Dr. Jurgen Venitz and Dr. Les Edinboro for their unique examination of my work to improve upon it.

Thank you to the Bioanalytical research group for their pier reviews of my numerous seminars and valued input.

Table of Contents

List of Tables

Page

List of Figures

Page

Abstract

A CELLULAR AUTMTOMATA MODEL OF ENANTIOMER INTERATIONS WITH β-CYCLODEXTRIN

By Darren Joseph DeSoi

A dissertation submitted in partial fulfillment of the requirements for the degree of Doctor of Philosophy at Virginia Commonwealth University.

Virginia Commonwealth University, 2012

Major Director: H. Thomas Karnes, Ph.D.
Professor & Graduate Program Director, Department of Pharmaceutics

The binding mechanisms of molecules to cyclodextrins continues to be studied to better explain the interactions occurring. The majority of published models focus on one-to-one molecular binding thermodynamics to explain experimental results. They rely on physical concepts of energies and forces to guide the actions of molecules expressed mathematically in terms of differential and non-linear equations. These models are limited in scope due to their complexity and are not easily expanded to study many diverse analytes. Conversely, cellular automata uses simple mathematical idealizations of systems governed by deterministic and probabilistic rules that are easily

adaptable to many types of molecular interactions. The primary goal of this research is to develop a model that is easy to use in the prediction of β-cyclodextrin chromatographic separations of enantiomers.

The model uses variegated square cells to simulate the physical environment of the molecules involved, evolving by a series of discrete time-steps referred to as iterations. Governing probabilistic rules define the physical and chemical interactions. Rules are randomly applied to all the cells of the system during each iteration and the system is updated accordingly. Micro and macro visual analysis is possible in addition to statistical output.

Results demonstrate the model's capability to use probabilistic rules for breaking of analyte-to-cyclodextrin complexes that were correlated to published experimentally determined equilibrium constants. The model was further expanded to predict the strength of interactions between enantiomer pairs to β-cyclodextrin and their potential separation. The model accurately predicted the order of strength for six enantiomer pairs. To truly predict chromatographic separation of enantiomers, the model was expanded from one-to-one interactions between enantiomers and β-cyclodextrin to a larger modeled chromatographic scale. At this scale enantiomer separation was modeled and evaluated for peak resolution and selectivity while varying column temperature, mobile phase pH and flow, and injection volumes. All results agreed well with published laboratory results. With the cost of research and development increasing, ongoing budget cuts, and the rush to get products to market first, an analytical model that can run multiple chromatographic simulations in minutes versus days could prove a valuable tool to many industries.

CHAPTER 1 Cellular Automata and the History of Enantiomer Models

1.1 Introduction

As yet, the analytical process of chromatographic enantiomer separation has not been modeled using cellular automata. This first work in the area uses mathematical systems that are easily adaptable to different enantiomer analytical processes. The binding mechanisms of analytes to cyclodextrins continues to be studied to better explain the interactions occurring. Predominantly, published models of analyte to chromatographic stationary phase interaction focus on molecular binding thermodynamics to explain experimental results. They rely on physical concepts involving energies and forces to guide the actions of molecules expressed mathematically in terms of differential and non-linear equations. Results are completely determined by the parameter sets used to describe the potential energy of the system on the specific initial conditions. This limits the scope of these models due to their complexity, making them difficult to study additional binding interactions. Conversely, cellular automata uses simple mathematical idealizations of system energies governed by deterministic and probabilistic rules that are easily adaptable to many types of molecular interactions.

"In some cases this complex behavior may be simulated numerically with just a few components. But in most cases the simulation requires too many components, and this direct approach fails. One must instead attempt to distill the mathematical essence of the process by which complex behavior is generated. The hope in such an approach is to identify fundamental mathematical mechanisms that are common to many different natural systems. Such commonality would correspond to universal features in the behavior of very different complex natural systems. To discover and analyze the mathematical basis for the generation of complexity, one must identify simple mathematical systems that capture the essence of the process. Cellular automata are a candidate class of such systems." (Wolfram 1983).

1.2 Chromatographic modeling background

The analysis of complex systems involving multiple ingredients with even more simultaneous interactions has restricted the use of models relying on complex ordinary, partial differential, and non-linear equations. These methods are limited due to their mathematical complexity. In response for the need to study more complex systems (Kier, Seybold, and Cheng 2005) Molecular dynamics and Monte Carlo simulations were developed (Leach 1996; Tildesley 1998) that examine ingredient interactions as a system driven by defined force field equations that become more complex as additional elements are included to be studied.

Differential equation models can explain properties of enantiomer chromatographic separations, but they quickly become complex and difficult to expand beyond studying the enantiomers and column of interest. As in the study of bupivacaine

enantiomer separation (Choi, Row et al. 2004). While the model did accurately predict the peak selectivity of the enantiomers under chromatographic conditions, several assumptions were built into the equations that would permit the prediction of peak shape:

- Variables are function of time and column length
- Liquid phase follows only axial dispersion flow
- Stationary phase and flow rate are constant throughout column
- Linear driving force drives intra-particle mass transfer
- Isothermal environment

One assumption directly limits the results. Having a mass transfer that is linear results in Gaussian shaped peaks, therefore peak tailing and resolution could not be modeled as found in laboratory conditions. There were many equations developed in the prediction of enantiomer selectivity, but one main equation was developed to describe the mass balance for enantiomer "i" in the mobile phase throughout the column:

$$\frac{\partial C(i,z)}{\partial t} = -u\frac{\partial C(i,z)}{\partial z} + D_L\frac{\partial^2 C(i,z)}{\partial z^2} - \frac{(1-\varepsilon)}{\varepsilon}\frac{6}{R_P}\frac{\partial q(i,z)}{\partial t}$$

C, Concentration of enantiomer "i" in mobile phase (mg/mL)

t, Time (min)

u, Interstitial velocity (m/min)

z, Axial coordinate (m)

D_L, Axial dispersion coefficient (m^2/min)

ε, Column bed porosity

R_p, Radius of particles (m)

q, Average adsorbed phase concentration of "i" (mg/mL)

The equation is composed of four main portions that describe fluid motion of enantiomers, axial dispersion of enantiomers, stationary phase properties, and finishing with the equilibrium of enantiomers on the stationary phase is described further by a competitive Langmuir isotherm:

$$q^*(i,z) = \frac{a(i)C(i,z)}{1 + \sum_{f=1}^{2} b(j)C(j,z)} \qquad \frac{\partial q(i,z)}{\partial t} = k(i)\frac{6}{R_P}(q^*(i,z) - q(i,z))$$

a and b, Enantiomers of bupivacaine

k, Mass transfer coefficient (1/min)

The Langmuir isotherm assumes that adsorption of enantiomers on a particular stationary phase site is unaffected by its neighboring sites. Therefore, enantiomer interactions with each other and steric factors do not affect modeled interactions with stationary phase. As the authors concluded, in order to develop this specific model, experimental data was needed to estimate the Langmuir isotherm coefficients. While the model does provide a prediction on the selectivity of separation for bupivacaine enantiomers, it is limited to selectivity since peak shape is Gaussian. In addition, to use this model to study additional chromatographic separations, further experimental data

would be needed along with information on column design for column bed porosity and the average size of stationary phase particles.

Molecular dynamics relies on Newton's laws of motion (Allen 1995) and assumes the second law of motion to be linear. Since this assumption does not hold true as velocities approach the speed of light, the longer a model using molecular dynamics runs, the more error is introduced. This limits the length of molecular dynamic studies typically to several nanoseconds and is not practical for studying chromatographic interactions which can last minutes. Monte Carlo simulations use random sampling applied to algorithms defining the system. After each time step, configurations that lower the energy state of the system are accepted and the system progresses; however, as the system attributes studied increases, the complexity of the algorithms limit the expandability of the model. Because of this, models of these techniques are best design for modeling one-to-one interactions.

Monte Carlo and molecular dynamic simulations can be used in combination for modeling enantiomer separations (Kim, Jung et al. 2003). The enantiomers of propranolol were modeled for separation on β-cyclodextrin stationary phase. Monte Carlo docking simulations were first run to determine the initial docking orientations with the lowest energy of propranolol enantiomers in β-cyclodextrin; however, the differences in complex energies were not conclusive due to the standard deviations:

- (R)-propranolol-β-cyclodextrin complex = - 44.43 ± 1.06 kcal/mol
- (S)-propranolol-β-cyclodextrin complex = - 43.89 ± 1.62 kcal/mol

Molecular dynamic simulations were then carried out with these complexes of the lowest energy. Molecular dynamics uses Newtonian mechanics of motion for structure

refinement of the propranolol enantiomer complex formations with β-cyclodextrin. Using NVT calculations (constant moles (N), volume (V), and temperature (T)) with a leap-frog algorithm, runs were conducted for a total run time of 100 nanoseconds (ns). From these runs an interaction energy was determined for each enantiomer complex, with a lower energy representing a more stable complex and greater retention. The (R)-propranolol-β-cyclodextrin complex was found to have an interaction energy 0.95 kcal/mol lower than the (S)-propranolol-β-cyclodextrin complex, which agreed with chromatographic retention. It was also determined that the run time was critical in obtaining accurate results, since from 0 to 20ns the (S)-propranolol-β-cyclodextrin complex had the lowest energy and hence more stable which does not agree with chromatographic results. It was also found that only in molecular dynamic simulations with runs times 10 times greater than typical simulations (Kim, Jung et al. 2003) could noticeable chiral recognition be predicted. Typical molecular dynamic simulations are carried out for less than 5ns to limit the error introduced from Newtonian mechanics, however it was concluded by the authors that longer run times are needed for accurate simulations for the prediction of chiral separation.

1.3 Cellular automata background

In the 1940's a mathematician-physicist named John von Neumann began a unique modeling design of self-reproducing biological cells later referred to as automata. With the help of Stanislaw Ulam, a fellow mathematician, they formed the foundation of the modeling technique called cellular automata. Neumann's first model involved 29 different states for cells to exist in and was cumbersome to use due to the

computations required, even though the technique was simpler than other models at the time. It was not until computers became more available in the late 70's that cellular automata interest really developed, based on the number of publications released (Wolfram 2002).

Cellular automata models are made up of several components (Wolfram 2002): a grid consisting of cells, cell shape, ingredient(s) location and amount, rules governing the behavior of ingredients, and a specified runtime or number of time steps called iterations. The cell grid determines the size and shape of the environment for interactions to occur. The cells of the grid may be empty or occupied by ingredients. Cell shape can be any shape that is capable of forming a grid (e.g. triangles, hexagons, squares) (Schwartz 1997), with square cells being the most common due to their ease of use and 4-sided tetrahedral binding configuration. Cells may be variegated, so that different rules apply to each side of the cell as in modeling chiral interactions (Kier, Seybold, and Cheng 2005).

Rules of probability govern ingredient behavior of the system and are local to the environment surrounding each ingredient known as its neighborhood. The two neighborhoods used in this model are the von Neumann and extended von Neumann neighborhoods (see Figure 1, adapted from Kier, Seybold, and Cheng 2005). The von Neumann neighborhood consists of four adjacent cells to ingredient A along the x and y axis while the extended von Neumann consists of four cells extending one cell beyond the von Neumann neighborhood. In this way the model evolves asynchronously with each iteration, potentially leading to unexpected emergent properties of the system. In

cellular automata models there are several common rules that are altered to study interactions (Kier, Seybold, and Cheng 2005):

1. Joining (J) is the factor that one ingredient will bond to another when separated by one empty cell (using extended von Neumann neighborhood). This value is changed to represent a short range attraction or repulsion.
2. Breaking probability (P_B) represents the attractive strength between two ingredients that are attached (bond strength, using von Neumann neighborhood). This probability ranges from complete repulsion between ingredients to permanent bonds forming.
3. Free Moving probability (P_M) controls whether ingredients move or not, and how fast they move verses other ingredients. A value of zero results in no movement regardless of other rules, while a value of one gives a maximum probability of moving once other rules are considered.
4. Flow factor (G) favors motions of movable ingredients in a favored direction as in mobile phase flow. Increasing values greater than zero represent increasing mobile phase flow rates.
5. Molecules rotate in three dimensional space and to represent this in two dimensions, moving ingredients are allowed to rotate 0°, -90°, +90°, and 180° each iteration.

Once the above parameters of the model are determined, the run time or number of iterations is defined as well as the number of runs to perform and average. Since

runs typically take from seconds to a few minutes, many runs are easily averaged to have a statistical measure of confidence in the results. When a run is executed, it evolves by a series of discrete time iterations as the rules are applied randomly to all the ingredients in the system asynchronously and the system is updated accordingly. Some movement rules, such as P_M, P_B, and J are applied as a single probabilistic equation since each influences the others. Results are examined visually for analyte movement at the molecular level, statistically for ingredient interactions, and system wide for averaged interaction behavior.

Cellular automata has been used to model chromatographic behavior of analytes with changes to the chromatographic system (Kier, Cheng, and Karnes 2000). When compared to what would be expected under laboratory conditions, peak shape and retention, mobile phase flow rate, and solvent polarity behaved as expected in the model. Enantiomer behavior in monolayers has also been modeled using cellular automata to study amphiphile behavior (Moa, Stine et al. 2002). A model was designed using a hexagonal grid to replicate the observed homochiral and heterochiral discrimination that occurs in the formation of monolayers. The authors decided on a cellular automata approach to represent the interactions occurring because they believed to properly model the phenomena would be “difficult to model using traditional simulation methods and perhaps impossible to model analytically” (Moa, Stine et al. 2002). Cellular automata cells have rules of movement, rotation, and binding. Each model run is started with the enantiomers randomly distributed and run for a number of iterations that results in islands of bound enantiomers. The entire system is then measured for overall interaction strength and number of cells bound together. It was

found that after 20,000 iterations the system reached equilibrium with enantiomers having an average of 2.5 attached neighbors and an interaction strength at ~75% of complete interaction of all enantiomers. Furthermore it was found that by increasing enantiomer population by 150% (from 640 cells to 1600) this decreased equilibration time to 4,000 iterations with an average number of neighbors of 2.5 and an interaction strength at 74% of possible maximum. To study homochiral interactions, movement rules where modified and 640 cells of a racemic mixture were run for 40,000 iterations. The change in run time was not explained by the authors. Enantiomer islands formed in the shape of circles or boxes that signified chiral separation, however island formation was considered incomplete due to the island structures partial formation. To study heterochiral interactions, movement rules where again modified and 1600 cells of a racemic mixture were run for 4,000 iterations. The change in cell population from homochiral studies was not explained by the authors. Formation of enantiomer islands was more complete than with homochiral interactions, with enantiomers preferring to bind to their opposite form. It was found that in racemic mixtures, heterochiral interactions had a greater number of bound neighbors and interaction strength at any given time point during the runs than homochiral interactions. The results from the study of homochiral and heterochiral interactions were determined consistent with analytical observations by several techniques (i.e. scanning probe microscopy, X-ray diffraction, fluorescence microscopy). It was suggested by the authors that using models like the one presented could be used to study adsorption of chiral molecules onto a surface and remain as interesting areas for additional research.

von Neumann

		X		
	X	**A**	**X**	
		X		

extended von Neumann

		X		
		X		
X	**X**	**A**	**X**	**X**
		X		
		X		

Figure 1: The cellular automata von Neumann and extended von Neumann neighborhoods used in the model.

1.4 Cyclodextrin chromatography background

Cyclodextrins are cyclic rings made from α-D-glucose monomers typically ranging in size from 6 to 9 glucose units (Liu and Guo 2002): α-cyclodextrin(6 units), β-cyclodextrin(7 units), γ-cyclodextrin(8 units), and δ-cyclodextrin(9 units). Cyclodextrin rings are shaped like a funnel with a hydrophobic interior of carbon and hydrophilic edges of hydroxyl groups. The wider analyte entrance end of the cyclodextrin has two secondary hydroxyl groups for every glucose unit and the narrower end has one primary hydroxyl group for every glucose unit. This results in the cyclodextrin funnel having a hydrophobic interior and a hydrophilic exterior along both ends as in Figure 2 (Chen, Chang, and Gilson 2004; adapted from Regiert 2007).

There are several proposed binding forces that affect cyclodextrin to analyte inclusion complex formation:

- Steric hindrance
- Charge transfer interaction
- van der Waals interactions
- Hydrophobic interaction
- Electrostatic interaction
- Hydrogen bonding

Steric hindrance plays a major role in determining if an inclusion complex can form. The diameter of the wide (or entrance) end of the cyclodextrin may prevent an analyte from entering or allow several analytes to enter into the inner cavity based on their size and conformation (Saenger, Takaha et al. 1998). Charge transfer interactions occur only with radicals when electrons in higher molecular orbitals of analyte move to

lower unoccupied orbitals of the cyclodextrin (Kano, Kubota et al. 1990) and are not included in this model.

Strength of cyclodextrin to analyte complexes are typically measured by their complex stability constant:

$$K = \frac{[CD \bullet A]}{[CD][A]} \qquad \text{Eq. 1}$$

where CD•A is the concentration of the analyte to cyclodextrin inclusion complex, CD is the concentration of unbound cyclodextrin, and A is the concentration of unbound analyte. The major driving forces for retention strength have been determined to be van der Waals and hydrophobic interactions, while hydrogen bonding and electrostatic interactions determine conformation of the inclusion complex (Liu and Guo 2002). Due to the imbalance of hydroxyl groups on the ends of cyclodextrin rings, twice as many at the wider end, the rings have significant dipoles. van der Waals forces most observed in cyclodextrin complexes include analyte induced dipole moment interaction with the dipole of cyclodextrins, along with the synchronization of electronic motion of the analyte and cyclodextrin. This allows for temporary dipole alignment between the molecules resulting in complex formation (Conners 1997).

The hydrophobic interior of the cyclodextrin cone attracts hydrophobic analytes to varying degrees depending on the polarity of the mobile phase. For analytes that contain polar and non-polar functional groups, the cyclodextrins may complex with just the non-polar portion of an analyte leading to potential chiral separations. Polarity of the

analyte can be correlated to the strength of the cyclodextrin complex formation (Rekharsky and Inoue 1998). Enanteomeric separation has also been observed, where due to stereochemistry, one enanteomer can position its hydrophobic portion into the cyclodextrin ring while the other enanteomer cannot due to steric hindrance or hydrogen bonding with the secondary hydroxyl groups.

With the large number of hydroxyl groups at the two ends of the cyclodextrin ring, the ring has polar properties due to electrostatic interactions. This results in cyclodextrins having significant dipole moments (Kitagawa, Chujo et al. 1988; Sakurai, Inoue et al. 1988) which can produce very specific ion-dipole complexes in non-polar solvents (Miertus, Tomasi et al. 1998), but are not of significance in aqueous systems.

Hydrogen bonding may occur at the primary OH(C6) and secondary OH(C2&3) hydroxyl groups of the glucose backbone in cyclodextrins (see Figure 3, adapted from Saenger, Takaha et al. 1998). Hydrogen binding of cyclodextrin hydroxyl groups to analytes occurs frequently at the secondary hydroxyl groups due to their proximity to the analyte as it enters the cyclodextrin cavity. This limited spatial bonding can give stereo specific chromatographic separations. Mobile phase selection is critical for hydrogen bonding to occur since solvation of the hydroxyl groups will occur if possible (Rekharsky and Inoue 1998).

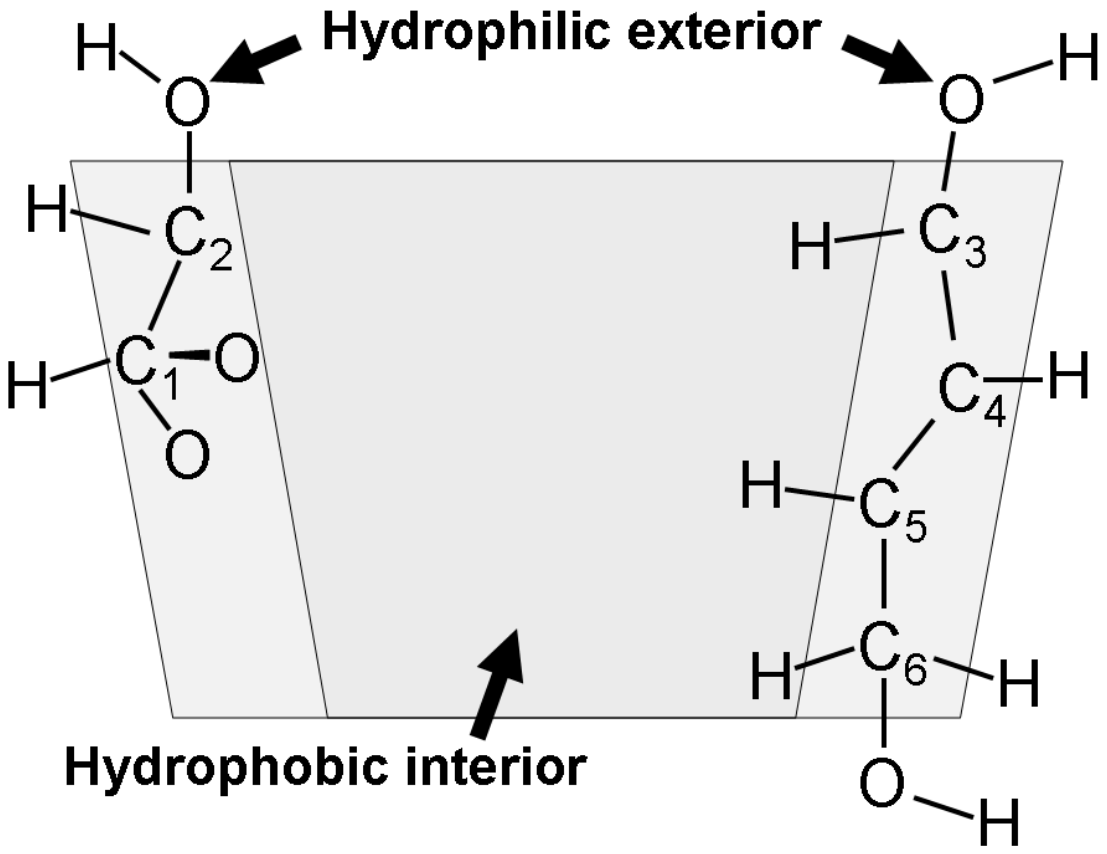

Figure 2: A cyclodextrin ring structure with a hydrophobic interior of carbon and hydrophilic edges of hydroxyl groups.

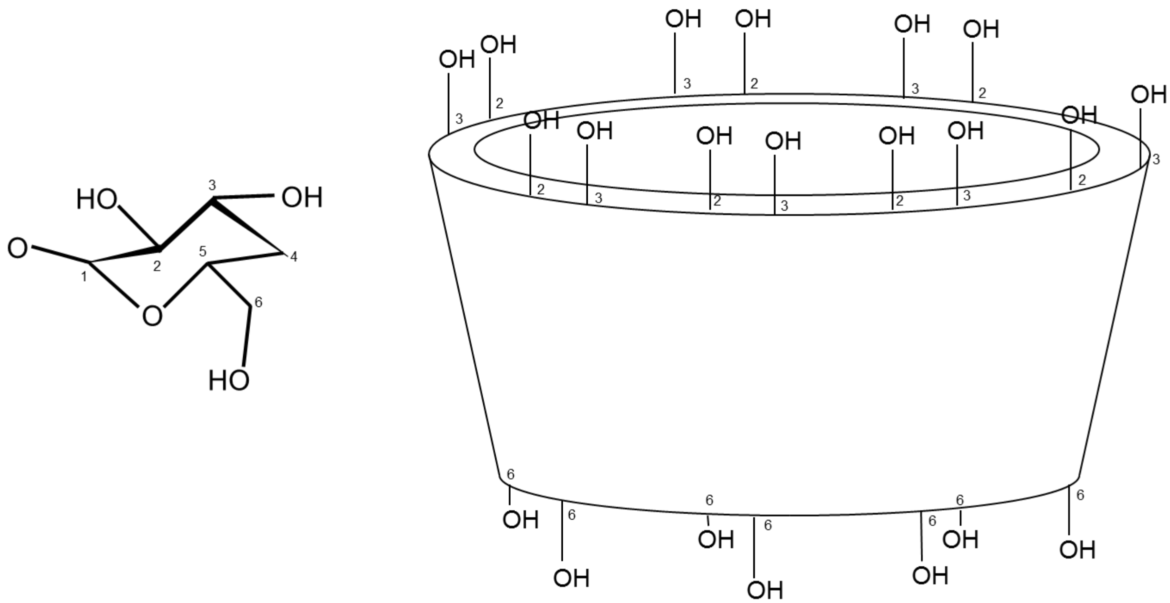

Figure 3: β-cyclodextrin ring made from an α-D-glucose monomer with primary hydroxyl groups on carbon 6 and secondary hydroxyl groups on carbons 2 and 3.

1.5 Conclusions

In today's global industries, research budgets are under continuous strain to do more with less (Abate 2003). Laboratory tests are expensive and time consuming. Reduced testing during research and development and more focused research (i.e. targeted, surgical, expedited) are constantly being examined as ways for companies to get products to market quicker with lower costs. Modeling has emerged as a way to predict chromatographic separations in the laboratory to reduce method development time, thereby reducing R&D costs. The proposed cellular automata model of β-cyclodextrin stationary phase has potential as a predictive tool for enantiomer separations, thereby reducing method development time by quickly eliminating unnecessary laboratory experiments and identifying chromatographic conditions that stand a greater chance of success, saving time and research money.

Past published models have relied on complex algorithms to study binding interactions that do not make them practical for continuous user modifications, as in study of bupivacaine enantiomers in section 1.2 were 27 variables (some requiring experimental data to estimate) must be determined before the partial differential equations can be calculated. If the chromatographic system or enantiomers are changed, then the variables need to be adjusted accordingly with additional laboratory chromatographic runs. Some published cellular automata models have been expanded to study monolayer interactions (Linyong, Stine et al. 2002), but most models are limited to one-to-one interactions that can only focus on a few analytes before becoming overly complex to use. In contrast the proposed cellular automata model uses simple probability rules that are easily expandable to study diverse chromatographic systems.

Probability rules and model environment are based on the intermolecular forces from the chemical and physical properties of the enantiomers, stationary phase, and mobile phase solvents involved. These do not require laboratory experiments to determine. Therefore changes to the enantiomers studied or the chromatographic system only requires examination of their chemical and physical properties to adjust model parameters.

The proposed cellular automata model has the flexibility to study the movement and binding actions of enantiomer to cyclodextrins while analyzing the chromatographic system as a whole, visually and statistically. This has not been accomplished to date. Predicting cyclodextrin chiral separation is even more difficult due to the stereochemical factors to consider which render traditional models very limited in scope and not easily expandable without a great depth of manipulation of the complex algorithms involved. Using the variegated cell properties of the cellular automata model which are easily modified, chiral separations will be studied. Correlation of model predictions to experimental results will be performed for validating the model. Since most published models focus on one-to-one interactions, this model will begin there but will be expanded to model chromatographic column scale to better represent an experimental environment. This will permit the incorporation of solvent/mobile phase effects like solvation, polarity of the mobile phase, varying flow rates, and temperature. Correlation to experimental data will be possible across a wide variety of analytes to study how an analyte's polarity, chiral structure, hydrophobicity, etc. affects chromatographic retention on β-cyclodextrin stationary phase. Once the model variables are correlated to enantiomer properties, it is then possible to use it to predict separation behavior.

CHAPTER 2 Cellular Automata Model Approach and Experimental Design

2.1 Introduction

High performance liquid chromatography method development can be time consuming and costly, taking weeks to develop an acceptable method or even peak separation. However, with some knowledge of the chemical properties of the analytes (enantiomers) and using the proposed model, developing a method for enantiomeric separation on β–cyclodextrin may only take hours.

The model environment is first designed to establish one-to-one interactions between a chiral molecule and β-cyclodextrin. Enantiomers have to be modeled and run individually to measure strength of the interaction. Results are then compared between the enantiomers to predict whether or not chromatographic separation is likely. Nevertheless, this one-to-one interaction does not take into account many factors that affect laboratory separations.

To be a better prediction of chromatographic separation the model needs to be expanded beyond a single analyte interaction with one stationary phase molecule. To accomplish this, the model is further expanded to included many analyte interactions. Other laboratory environmental conditions are added such as the presence of dual

solvent mobile phases and flow. This expansion of the model environment is not meant to mimic exact ratios of real life laboratory interactions within a high performance liquid chromatography column with thousands upon thousands of interactions, as this would vastly slow down the model and require significant computational power. Additionally, there may be no benefit in expanding the model to this degree, since the purpose of the model is to be designed in a way to predict chiral separations that correlate well with laboratory results in an efficient manner.

2.2 Programming environment

2.2.1 Software environment

The cellular automata model is a Java™ application executed using Eclipse Classic (versions 3.1.2 and 3.7.1, The Eclipse Foundation) as an integrated development environment. All calculations and plots are performed using Microsoft Office Excel 2003 or 2010 (Microsoft Corporation).

2.2.2 Computer hardware

All model simulations were performed on a Toshiba Satellite™ A305 laptop, with Intel Core™ Duo CPU 1.83 GHz, 3.00 GB RAM, on a Windows 7 32-bit operating system (© Windows Corporation) .

2.3 Analyte to cyclodextrin (one-to-one) model design

To properly represent a cyclodextrin ring using a two dimensional cellular automata grid of square cells, several cells are used for the cyclodextrin ring including

empty space, and a single cell for the analyte molecule (see Figure 4). Cells B0-6 make up the cyclodextrin ring, where B0, 1, and 4 represent the primary hydroxyl groups while B3 and 6 represent the upper edge of the cyclodextrin cone with the secondary hydroxyl groups. B2, 3, 5, and 6 represent the interior of the cyclodextrin. B3 and 6 may represent two portions of the cyclodextrin due to the different sets of rules assigned to the variegated analyte cell A. The variegated cell A(0-3) is an analyte with four sides, each having its own set of rules. Like enantiomers with a chiral center, the variegated cell can be modeled with four different interaction properties to represent different enantiomers. Analytes always start unbound in the interior of the cyclodextrin. This position was chosen based on the general acceptance in literature of analyte retention and positioning within cyclodextrins. Once the analyte leaves the cyclodextrin ring B cells it becomes bound to a C cell. The joining factor and breaking probability between the analyte and C cells are set so that the analyte does not become unbound. In this way, cells C1-5 are used as a detector for analyte A for its time spent interacting in the cyclodextrin cavity. Cells B and C are stationary with a free moving probability of zero. While the analyte moves freely in any direction unless acted upon by other movement rules (attractive and/or repulsive forces) by assigning a free moving probability of one. This design makes up the environment to study the one-to-one interactions of an enantiomer with a single cyclodextrin.

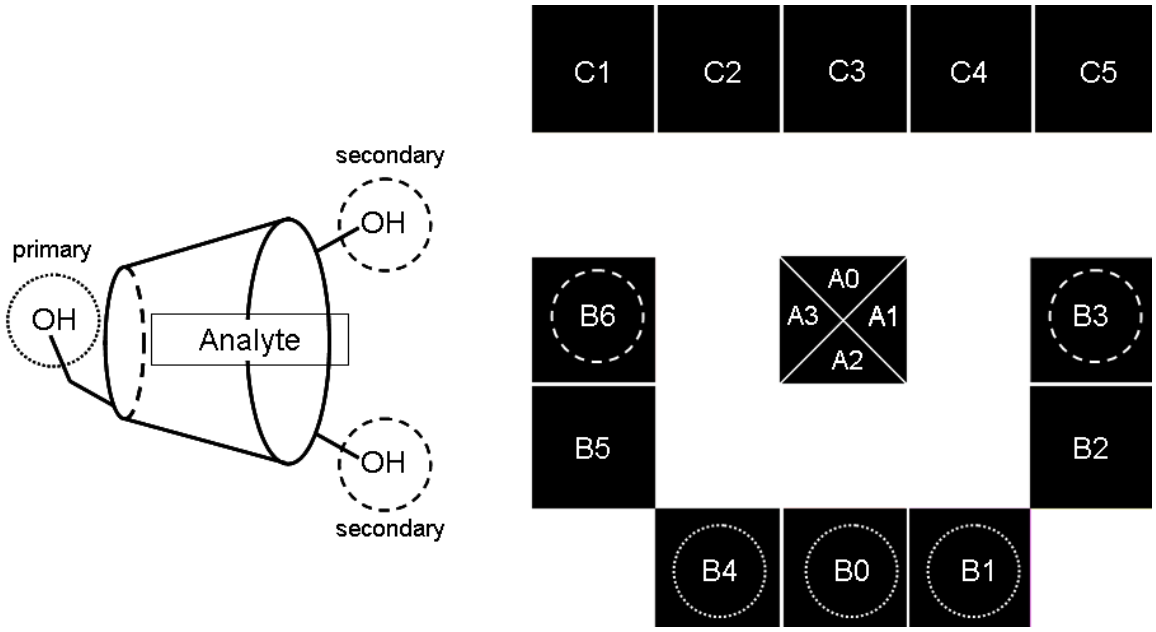

Figure 4: The two dimensional, cellular automata grid representing a cyclodextrin ring with a variegated analyte cell.

2.4 Liquid chromatographic model design

2.4.1 Expansion of cellular automata model

Up until this point the model has been designed to study only one-to-one interactions between an analyte and one β-cyclodextrin stationary phase molecule in high performance liquid chromatography. This provides useful information on the potential for enantiomer separation; however, it does not take into account many laboratory conditions that may affect the separation. To have an improved prediction on how enantiomers may separate in an high performance liquid chromatography column other factors need to be included.

Thousands of interactions occur between many analyte and stationary phase molecules depending on the amount of sample injected onto the chromatographic column and the column's design. Thousands of interactions are impractical to model, as this would vastly slow down the model and require substantial computational power. There may be no benefit in expanding the model to this degree, since the model is designed to predict chiral separations in an efficient manner and not replicate the physical environment of a chromatographic column. The number of analytes and β-cyclodextrin stationary sites needs to be increased in a manner that allows multiple site interactions as the analytes move through the column. β-cyclodextrin stationary sites are evenly spaced in an alternating manner to avoid possible solvent channels so that the analytes will have stationary phase interaction and not move through the column without interaction.

Analytes are placed randomly at the beginning of the modeled column, prior to the stationary phase, to represent the beginning of an injection of sample onto a high performance liquid chromatography column. Two different types of cellular automata cells are used representing enantiomer pairs. At the beginning of each run the analyte cells are randomly intermixed and have the ability to rotate as they move, which plays a part in their separation behavior since they are variegated cells.

Mobile phase cells are also added to the model. Two different types of cells are used so that dual solvents may be modeled. Their polarity and densities are incorporated into the model to best represent their chemical and physical properties under laboratory conditions. The mobile phase cells interact with analytes and stationary phase in various ways according to their chemical nature.

Flow (gravity factor in the model) is incorporated on analytes and mobile phase cells at equal values. The gravity parameter in the cellular automata model represents the tendency to move in a certain direction (see section 1.3). Several gravity factors were evaluated visually to determine the best value for the model. At a value of 1.0, due to other forces present, analytes cells frequently moved consistently against the downward flow of gravity. While this is acceptable for a cell or two, anything greater does not appear to model the directional movement of analytes and mobile phase under laboratory conditions. Therefore the flow was tested at higher values. As the flow was increased to a gravity factor of 2.0, there was consistent downward flow of the analytes with little movement against the mobile phase flow. A gravity factor of 2.0 was used for all runs.

2.4.2 Cellular automata grid layout

As in the one-to-one model, a β-cyclodextrin is represented using several cells (see Figure 5). The β-cyclodextrin is now made of variegated cells that are divided into two types of sites, each having their own set of interaction rules. B0 sides represent the secondary hydroxyl groups located at carbon two of the β-cyclodextrin (see Figures 2 and 3) in addition to the hydrophobic interior of the β-cyclodextrin depending on what side of the analyte cell it is interacting with. B1 sides represent the hydrophobic interior of the β-cyclodextrin, while B2 represent the primary hydroxyl groups of the β-cyclodextrin at carbon six. The outside or exterior of the β-cyclodextrin denote sites that have minimal interaction with analytes and are labeled as C.

There are two types of analyte cells in the model, A and D, to represent an enantiomer set. Analyte cells are variegated with 4 sides to represent a chiral molecule. Each side has its own set of interaction rules with stationary phase sites (B0-B2), mobile phase cells W1 or W2, and each other. Mobile phase cells are non-variegated and have the same set of interaction rules on each side (see Figure 6)

The cellular automata model environment consists of a grid of cells 40 columns wide and 800 rows long for a total of 32,000 cells to represent a chromatographic column. This grid design evolved through several steps of runs and observations. The original design was only 205 rows long, ending at the last placement of β-cyclodextrin cells. This however allowed the early eluting enantiomer cells to renter the column before the stronger retained analyte cells exited the column. The modeled column is designed as a torus with no sides, bottom, or top enabling free cell movement. With the early eluting enantiomer reentering the modeled column, it interfered with the latter

eluting enantiomer's interaction with the stationary phase. This was unacceptable so the grid was extended to 300, 400, 450, and finally 800 rows to eliminate this problem. The first 10 rows of the grid does not contain any cyclodextrin cells so that analyte cells may start there at the beginning of each run to represent a sample injection. One hundred of each analyte are randomly placed within this space so that analytes are intermixed with each other and mobile phase cells. Various amounts of analyte were tried before deciding on 100. Analyte amount was reduced to 50 and increased to 200; however, 100 provided the best interaction relationship with the number of stationary phase sites, resulting in proper peak shape.

β-cyclodextrin cells begin at row eleven in the orientation as in Figure 5. The first 10 rows are left for analyte cells A and D along with mobile phase to simulate injection of analytes onto the modeled column. This orientation was chosen to avoid analytes being pushed into the β-cyclodextrin funnel shape by flow if the open end was faced upward, with the analyte having to push against mobile phase flow to exit. Conversely, if the cyclodextrin was faced downward, analytes would have to move against the flow to enter the cyclodextrin. Oriented on its side the β-cyclodextrin sites have analytes enter due to their attraction or lack thereof. The side direction that the β-cyclodextrin faces does not matter since all moving cells may exit one side of the grid and reappear on the opposite side, eliminating analyte and mobile phase cell movement boundaries. β-cyclodextrin sites were placed in a manner so that they are spaced five cells apart on any side. Figure 7 shows the placement of the first ten β-cyclodextrin stationary phase sites. This type of placement continues until a total of one hundred β-cyclodextrin sites

exist, so that stationary phase is present from rows 10 to 204. The remaining 595 rows are left empty for mobile phase at the start of each run. These rows provide an area for the analytes to move into after their interaction with the stationary phase sites. It is in these rows that the analytes will be examined, as in high performance liquid chromatography when analytes leave the column and continue onward to the detector.

Placement of mobile phase cells is random; however, several factors need to be considered to determine their concentration: empty space available in the grid after placement of stationary phase and analytes, empty space left to allow for ingredient cell movement, concentration of solvent in mobile phase, and density of solvent at varying temperatures. Of the 32,000 available cells, only 31,100 are available once analytes (A and D) and cyclodextrin sites are subtracted out. It has been previously demonstrated in aqueous systems that 69% occupancy of the cell grid allows for water cells to behave chemically similar to actual conditions (Kier and Cheng 1994). In the chromatographic system modeled (Feitsma, Zeeuw et al. 1985), the mobile phase consists of 62.5% water, 31.5% acetonitrile, and 6.0% methanol. Since acetonitrile and methanol both have the potential for hydrogen bonding, albeit weaker than water (Chaudhari and Lee 2004) their model probabilities would be the same. For simplicity, the model will consist of a two solvent mobile phase, 62.5% water and 37.5% acetonitrile. Additionally, taking into account the density of the solvents involved (Weast 1988; Khimenko and Gritsenko 1980) results in equation 2:

$$W = 31100 \times 0.69 \times C \times \rho \qquad \text{Eq. 2}$$

31100, number of empty cells in grid

0.69, percent of occupied space

C, concentration of solvent in mobile phase

ρ, density of solvent

Using equation 2, the cell concentration of water and acetonitrile was determined for each chromatographic temperature modeled (see Table 1). The calculated number of cells for each solvent were placed randomly throughout the grid. See Figure 8 for an example of a model generated environment (note: only the upper portion is displayed due to space constraints). Appendix B shows portions of the cellular automata file "desoi2.inf" that places the cells in the grid.

Table 1: Cell population of water and acetonitrile at varying temperatures.

	Density		Number of Cells	
	Water	ACN	Water	ACN
Temperature	W1	W2	W1	W2
24	0.9973	0.7793	13376	6271
31	0.9954	0.7716	13350	6209
37	0.9934	0.7650	13323	6156
44	0.9907	0.7573	13287	6094
50	0.9881	0.7507	13252	6041
57	0.9848	0.7430	13208	5979

In addition to location in the grid, cell type and orientation are defined. Cell types are defined in the string file "desoi2.str" (Appendix C) and are as follows:

- A = 0
- D = 1
- B0 = 2

- B1 = 3
- B2 = 4
- W1 = 5
- W2 = 6

Orientation values are from 0 to 4 and are only relevant for cells that do not move and rotate, since orientation determine which direction the variegated sides face at the beginning at the run.

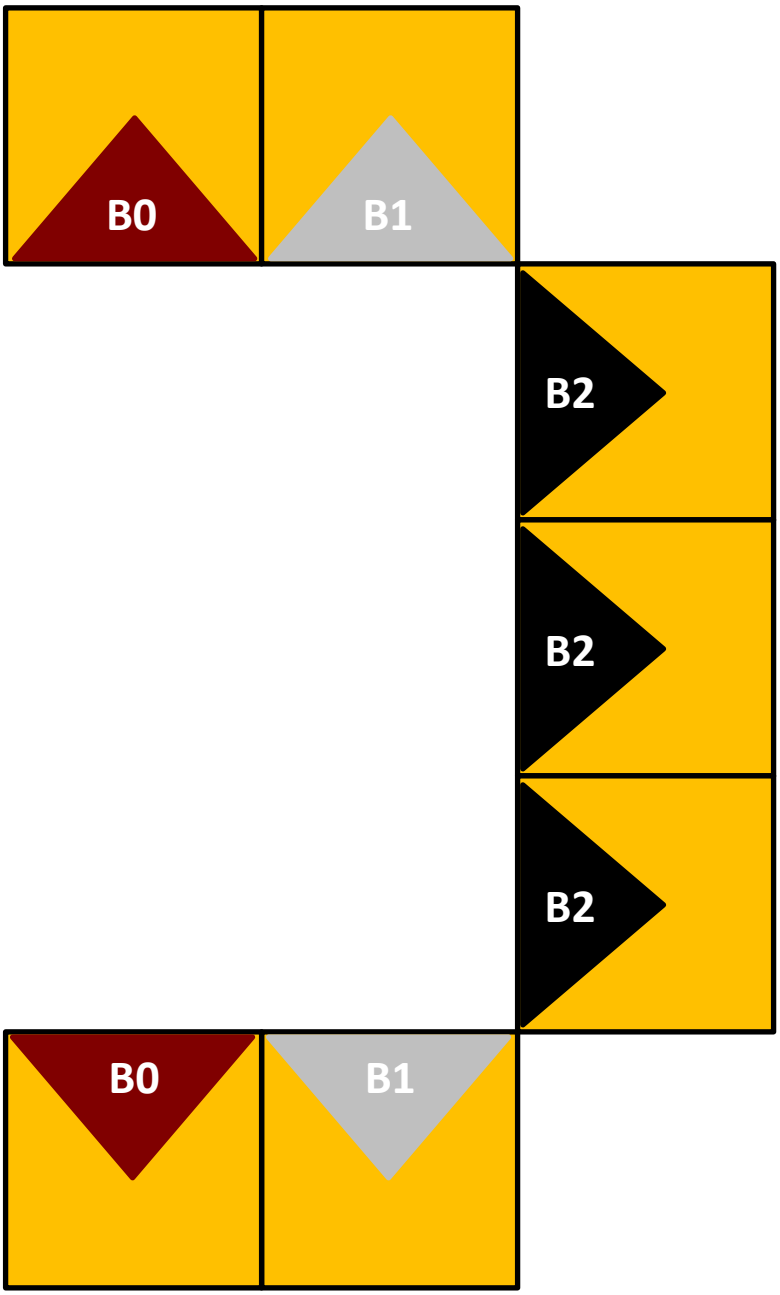

Figure 5: The two dimensional, cellular automata grid representing a cyclodextrin ring with a variegated analyte cell for chromatographic scale.

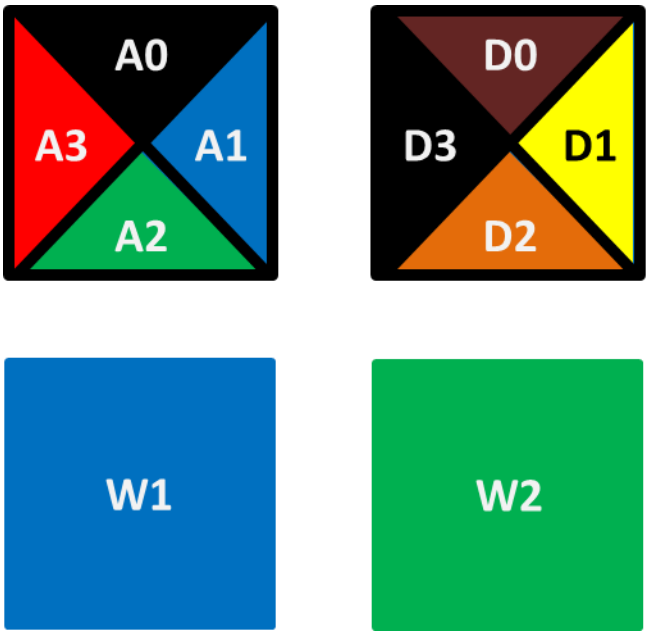

Figure 6: Analyte cells A and D with variegated sides to represent chiral molecules and non-variegated mobile phase cells W1 and W2.

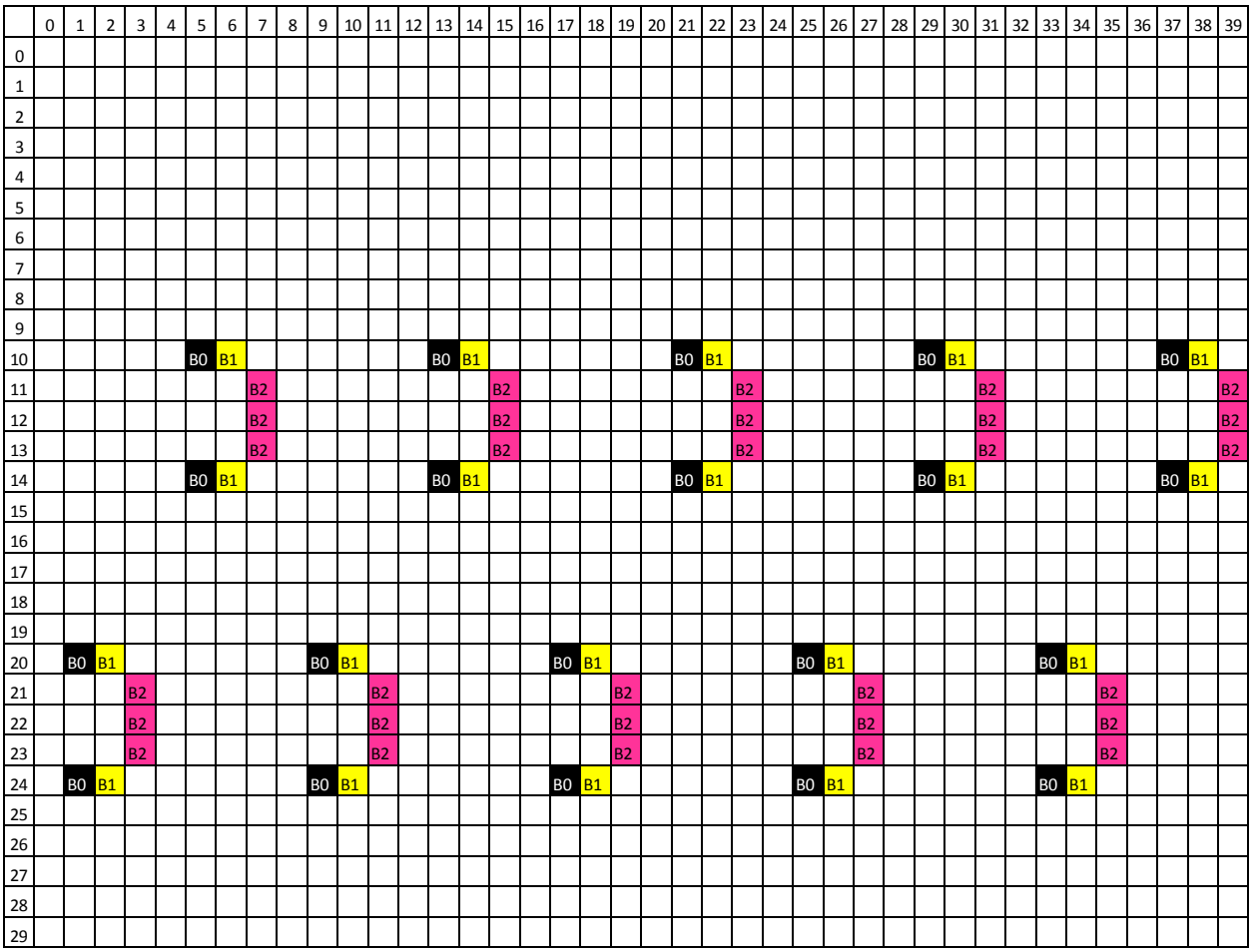

Figure 7: Cyclodextrin grid layout for the first 30 rows of the cellular automata environment

Figure 8: Model generated chromatographic scale environment with analyte, cyclodextrin, and mobile phase cells.

2.5 Conclusions

The computer hardware and Eclipse Classic software used have an impact on the speed of analysis at the chromatographic scale. Typical run times were seven minutes. When run on a 64 bit system with faster processors (main and video) with more memory, the run time was approximately three minutes. It was found that running without graphical display cut this time even further. It is recommend that the model be run on a 64 bit system. It should be noted that once one run has begun, parameters of the model may be changed and a new run started. In this manner many runs can be performed simultaneously.

The one-to-one interaction model is simplistic by nature. While it does provide a prediction of the strength of enantiomer binding with β-cyclodextrin, several factors are not accounted for. Solvent interactions are not accounted for along with the influence of mobile phase flow. Competitive interaction of the enantiomer pairs with the β-cyclodextrin cannot be studied since each enantiomer is analyzed individually. Despite these limitations, the model is sufficient for its intended purpose as are the majority of published models that treat interactions as if in a vacuum.

Escalating the model to a chromatographic scale would not simply be increasing the number of enantiomer to β-cyclodextrin interactions. With the introduction of the additional ingredients, many rules of interaction must be considered:

- Enantiomer to β-cyclodextrin
- Enantiomer to mobile phase
- Enantiomer to enantiomer
- Mobile phase to β-cyclodextrin

- Mobile phase to mobile phase

Each type of interaction has its own probabilistic rules that allow each model run to evolve in a dynamic manner based on general chemical principals of the molecules involved. The greater number of types of interactions in addition to the larger number of ingredients to interact results in dramatic increase in the number of interactions versus the one-to-one model. To analyze the results from the model, more complex analysis is required to go from the raw data of cell locations to generating chromatograms using Excel.

CHAPTER 3 Validation of Cellular Automata Model

3.1 Introduction

The model is first tested for basic functionality to verify that the modeled cyclodextrin retains analytes (one-to-one interaction) and that retention rules affect retention with acceptable reproducibility. Model rules are then optimized to the interaction forces of the complex formation as well as correlated to published experimentally determined equilibrium complex stability constants.

The model is then expanded to confirm that the variegated analyte cell performs as anticipated for a chiral molecule. Model rules are correlated to enantiomer-(β-cyclodextrin) overall binding energies to develop the model's rule equations. The rules are then used to predict the retention strength and chromatographic separation of six drug enantiomer sets with similar aromatic characteristics in their nonionic state (see Figure 9). Enantiomers were modeled without consideration of solvent environment, as if in a vacuum. Only enantiomers and stationary phase molecules are modeled, which is a common approach in models of one-to-one interactions. Model results are then compared to published, experimentally determined results.

One-to-one enantiomer interactions with β-cyclodextrin have been the focus of the model so far, which has similarly been accomplished using other modeling techniques. However, to predict how enantiomers will separate in the lab, one-to-one

interactions are not sufficient. That is why the model is expanded to chromatographic scale, incorporating solvents, mobile phase flow, and multiple stationary phase sites for β-cyclodextrin. Enantiomers of mandelic acid and brompheniramine are modeled and compared to published chromatographic results for their selectivity. Cyclohexylphenylglycolic acid, which is similar to mandelic acid with the hydrogen on the chiral carbon replaced with cyclohexane, is modeled at varying mobile phase temperatures, flow rates, sample loads, and pH. The results are compared vs. published chromatographic results for selectivity, resolution, peak tailing and capacity factors.

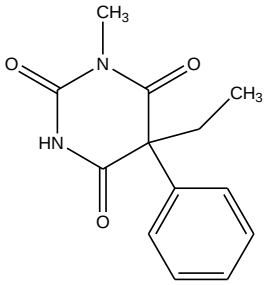

N-Methylphenobarbitone
(MPB)

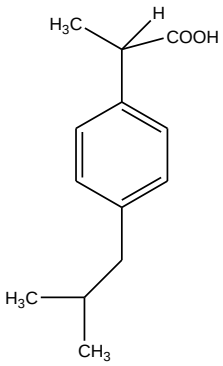

Ibuprofen
(IBP)

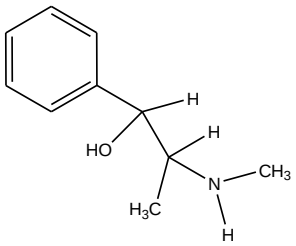

Ephedrine (RS/SR) (EF)
Pseudoephedrine (RR/SS) (PF)

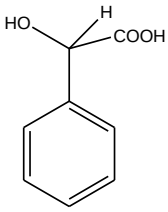

Mandelic acid
(MA)

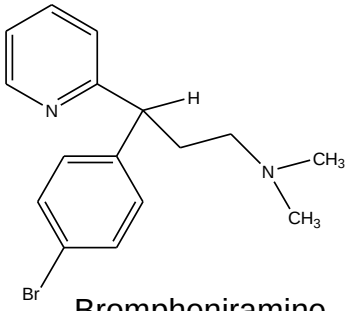

Brompheniramine
(BP)

Figure 9: The six enantiomer pairs used in the cellular automata model to predict their chromatographic retention.

3.2 Cellular automata model rule testing

3.2.1 Model movement rule testing for basic functionality in on-to-one interactions

Analyte interaction with cyclodextrin involves insertion of a portion or all of the analyte into the cyclodextrin interior. Therefore, the time an analyte is in this position is used to measure the strength of an analyte-cyclodextrin complex. Once the analyte leaves the cyclodextrin and binds to cells C, the analyte-cyclodextrin complex is considered to no longer exist. The number of iterations required for the analyte to bind to C is a direct measure of complex strength. Each result reported is the average of 100 runs. From 100 runs, the number of iterations required for 95% of the analytes to bind to C is considered the time required for the complex to end. This number of iterations is reported as “iterations to escape”. Six results, for a total of 600 runs, are determined for each reported value along with a relative standard deviation and confidence interval.

Before modeling experimental cyclodextrin complexes, model performance is evaluated. To do this the following questions are considered: does the model retain analytes and does retention of analyte change with changes to the breaking probability and joining factor between the cells of analyte and cyclodextrin?

Previous studies of water molecule interaction demonstrate that joining and breaking variables have the relationship of log J = -1.5 P_B + 0.6 (Kier, Seybold et al. 2000). This relationship is a reasonable approach to cyclodextrin interactions since the hydrophobic behavior of cyclodextrins has been shown using molecular dynamics simulations (Geiger, Rahman et al. 1979; Jorgensen, Ravimohan et al. 1985), and other

model based techniques (Blokzijl and Engberts 1993; Hummer, Pratt et al. 1996; Ohmine and Tanaka 1993).

To confirm that the model forms analyte-cyclodextrin complexes and that the retention changes with rule changes, breaking probability and joining factor are varied in the model from very strong to very weak analyte-cyclodextrin bonding strength. Bonding was modeled from the strongest interaction that was not permanent at a breaking probability of 0.05, to the weakest interaction with very little bonding and a breaking probability of 0.95. A total of 28 different value sets for the variables are evaluated to represent analytes forming strong to weak interactions with the cyclodextrin. A run time of 10,000 iterations is used to allow for the strongest bonding interactions to end. The number of iterations required for 95% of each analyte condition to leave the cyclodextrin is reported in Figure 10.

The cyclodextrin model forms a stronger complex and retains analytes longer as the breaking probability and joining factor were adjusted to do so. At a breaking probability of 0.95, representing the weakest of interactions, the analyte was retained for only 13 iterations with a 95% confidence interval of 1 iteration. Modeling a very strong interaction with a breaking probability of 0.05, the analyte was retained for 7,060 iterations with a confidence interval of 901 iterations. Therefore, the model performed as anticipated. Additionally, the 95% confidence interval of each result increases as retention was increased. This is consistent with the chromatographic phenomena of band broadening. Typically the longer an analyte is retained on the stationary phase, the broader the chromatographic peak (Skoog 1985). Therefore, the modeled

stationary phase performs similarly to isocratic chromatography systems in terms of retention band broadening.

The strength of cyclodextrin complexes is commonly compared by referring to the complex stability constant of the complex. The log of analyte-cyclodextrin complex stability constants have shown to have a linear relationships when examining hydrophobic (Matsui and Mochida 1979) and van der Waals interactions (Sanemasa, Deguchi et al. 1994). Therefore, the log of iterations for analytes to escape from the cyclodextrin is compared to that of the joining factor for linearity. The plot of joining factor vs. log(iterations to escape) gives an equation of log(iterations to escape) = 0.8242(J) + 0.9457 with a coefficient of determination of 0.9959 (Figure 11). This demonstrates a linear relationship with no bias, since the y intercept of 0.9457 means that a joining factor of 0 gives "iterations to escape" of 9. When the weakest interaction was modeled to represent little to no bonding, the analyte required 13 iterations to escape. Any iterations less than this represents no significant bonding, therefore 9 iterations is reasonable for non-bonding interaction.

The next step is to see if different sites within the cyclodextrin retain differently and if similar sites retain similarly as is expected in cyclodextrin bond formation. The beginning premise is that B0 should retain longer than B3 and B6 since B0 is deeper inside the cyclodextrin, requiring a longer time for the analyte to exit the cyclodextrin. B3 and B6 are located at equal but opposite locations in the cyclodextrin so they should retain similarly (see Figure 4). The same 28 sets of joining and breaking values used for binding strength are evaluated for B0, 3, and 6 with a run time of 100 iterations

(n=6). The number of iterations required for the analyte to leave the cyclodextrin complex 95% of the time is reported (see Figure 12).

The model forms a stronger complex and retains analytes longer at B0 vs. B3 and B6 within 95% confidence intervals. Additionally B3 and B6 retain the analytes equivalently within 95% confidence intervals. Accordingly, the model performs as anticipated. These results confirm that retention of the analyte in the modeled cyclodextrin ring can be modified at specific sites with repeatable results and that the model replicates chromatographic stationary phase behavior.

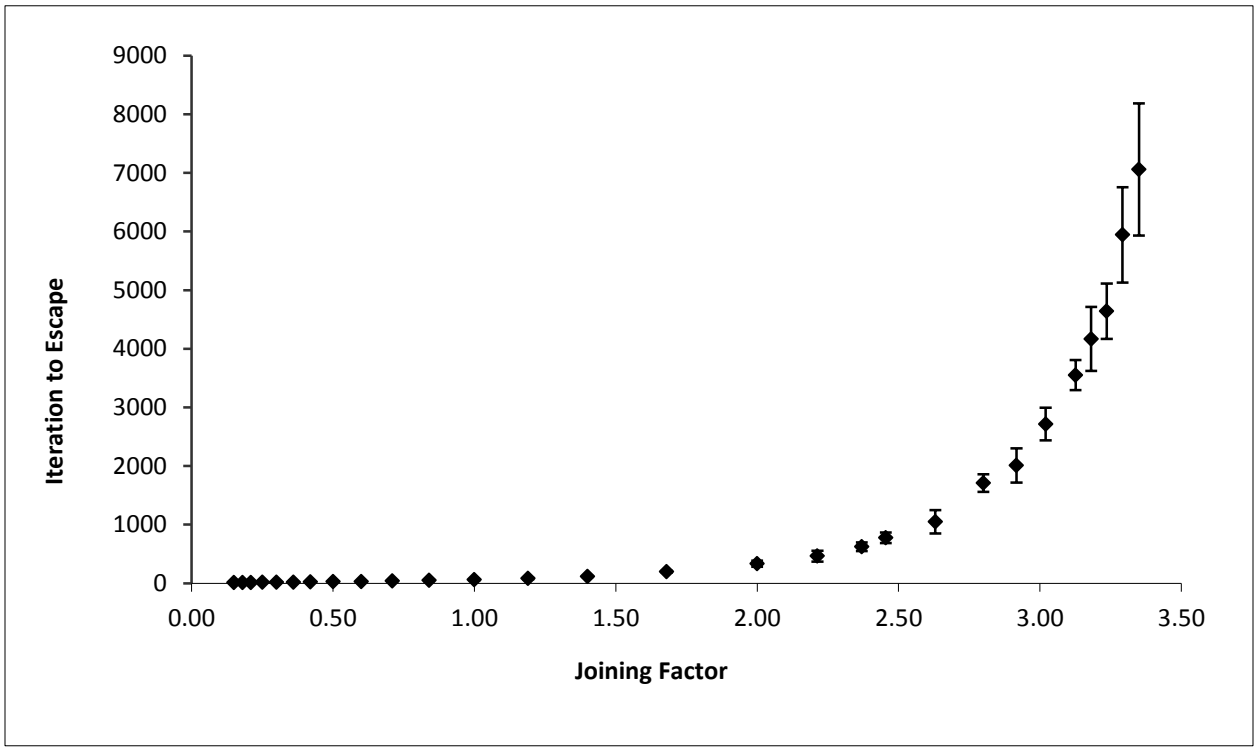

Figure 10: Escape iterations vs. joining factor with the 95% confidence interval expressed along the y-axis.

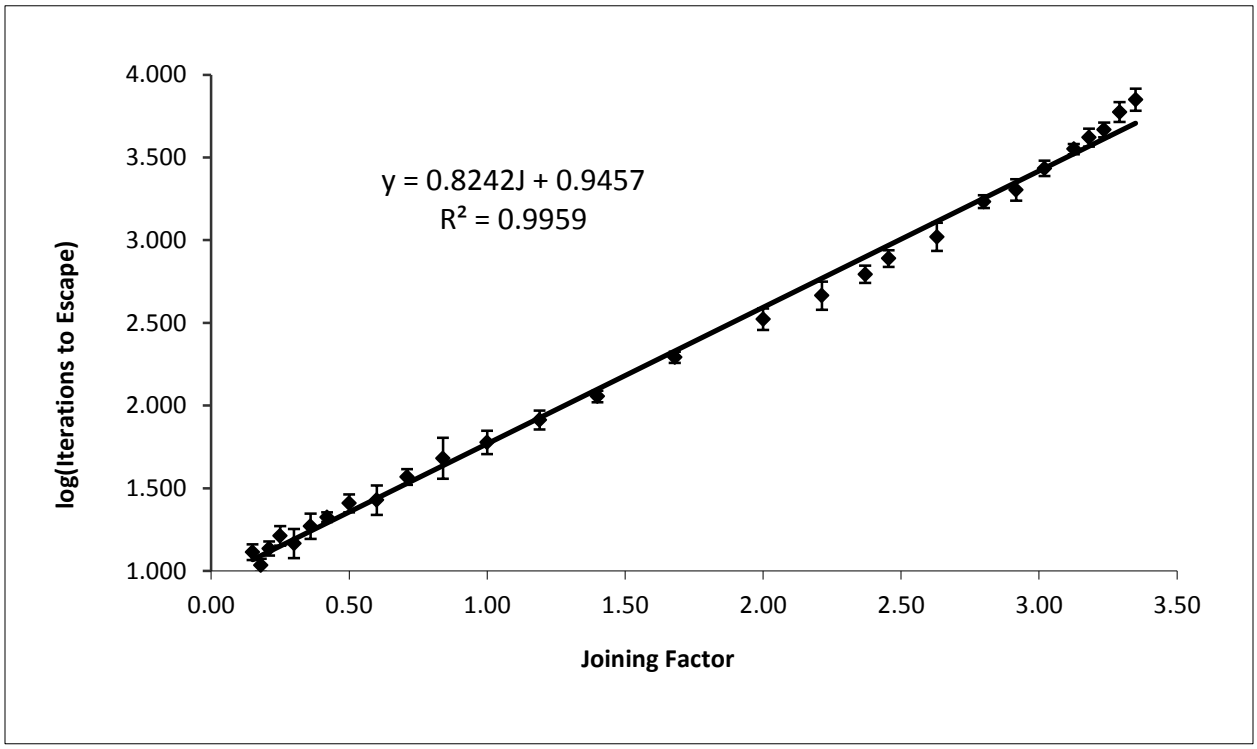

Figure 11: Log(Escape Iterations) vs. joining factor with the 95% confidence interval expressed along the y-axis.

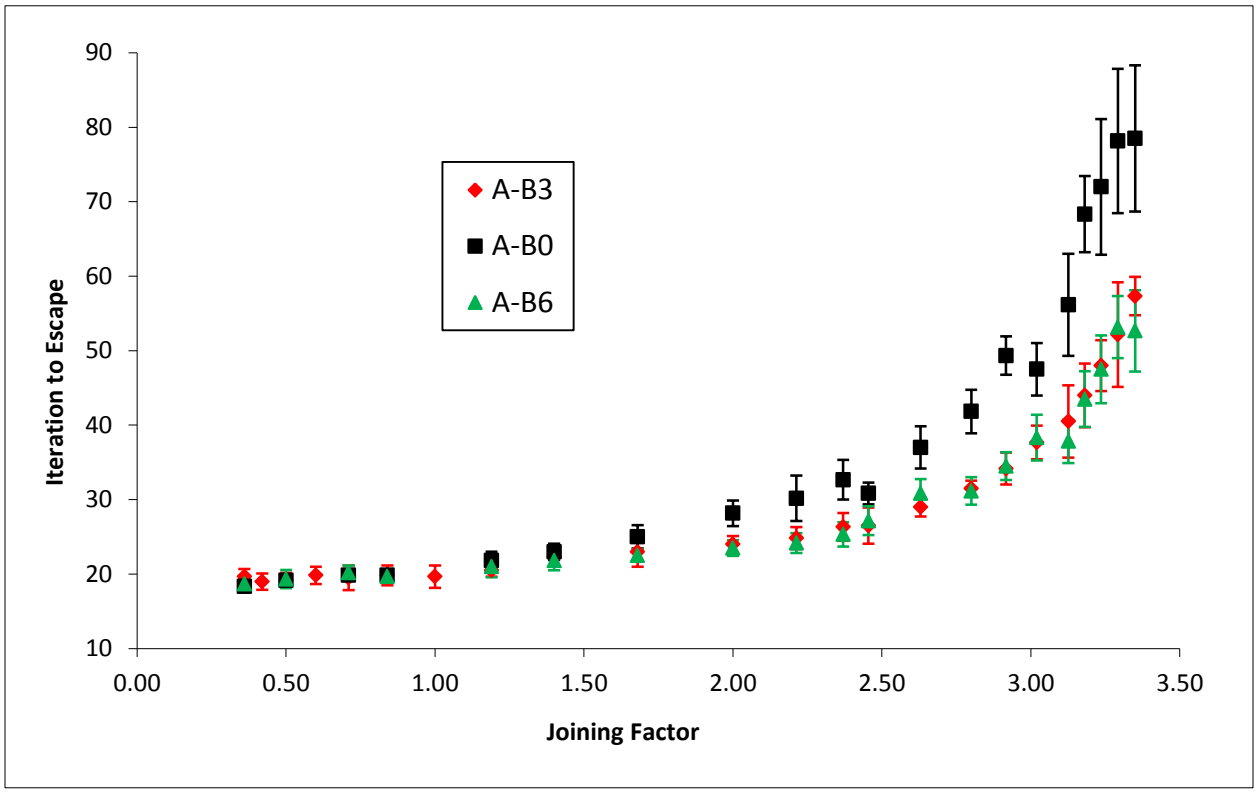

Figure 12: Twenty eight sets of joining and breaking values used for binding strength are evaluated for B0, 3, and 6 with the number of iterations required for the analyte to leave the cyclodextrin complex 95% of the time reported.

3.2.2 Model movement rule testing for enantiomeric behavior

Before modeling enantiomer experimental published data, model performance is evaluated for the variegated enantiomer cell A. To do this the following questions are evaluated: with just an inner β-cyclodextrin cavity interaction occurring how does the model retain the enantiomer cell, does the retention of the enantiomer cell increase when retention is modeled at the secondary hydroxyl sites (cells B3 and B6) in addition to retention at the inner β-cyclodextrin cavity.

The length of time an enantiomer remains in the β-cyclodextrin ring is used to measure the strength of an enantiomer-(β-cyclodextrin) complex. Each result reported is the average of 1000 runs. From 1000 runs, the number of iterations required for 95% of the enantiomers to leave the β-cyclodextrin complex and bind to C is considered the time required for the complex to end. Six results, for a total of 6000 runs, are determined for each reported value along with a relative standard deviation and 95% confidence interval.

To test that the model retains an enantiomer with just an inner β-cyclodextrin cavity interaction occurring, the breaking probability and joining factor of the variegated enantiomer cell to several β-cyclodextrin cells are varied at 5 values to simulate strong to neutral (equal attraction and repulsion) retention interactions (see Table 2). The binding variables were adjusted in this way for interactions between A1 and A3, representing the phenyl portion of the enantiomer with B2, 3, 5, and 6 representing the inner hydrophobic β-cyclodextrin cavity (see Figure 4). The log of analyte-(β-cyclodextrin) complex stability constants were shown to have linear relationships when examining hydrophobic (Ohmine and Tanaka 1993) and van der Waals interactions

(Sanemasa, Deguchi et al. 1994), therefore, the log of the iterations for enantiomers to escape from the β-cyclodextrin is compared to that of the joining factor (see Figure 13). This comparison gives a non-linear relationship of log (iterations to escape) = $0.0765J^2$ - 0.0089J + 1.5266 with a coefficient of determination of 0.9963. Under the strongest interaction conditions the enantiomer takes 233 iterations (±14, 95% CI) to exit the β-cyclodextrin and 35 iterations (±2, 95% CI) under neutral interaction conditions. This confirms that the model retains enantiomers longer as the breaking probability and joining factor were adjusted to do so but in a non-linear manner. Non-linear interaction may be the result that not all of the enantiomer cell sides are interacting equally. The next step is to see if retention of the enantiomer cell increases when interaction is added at the secondary hydroxyl sites.

Table 2: Complexation model values for joining factor and breaking probability.

P_B	J	P_B	J
Strong Bond	Strong Attraction	0.050	3.350
		0.114	2.690
		0.195	2.030
		0.309	1.369
Neutral	Neutral	0.500	0.708

In addition to the inner β-cyclodextrin binding described previously, binding to the secondary hydroxyl sites (cells B3 and B6) is added by adjusting the binding variables for interactions between A0 to B3 and 6. Breaking probability and joining factor were set as previously as in Table 2. Under these binding conditions, log (iterations to escape) = $0.0767J^2$ - 0.0033J + 1.5334 with a coefficient of determination of 0.9974

(see Figure 14). Under the strongest interaction conditions the enantiomer takes 248 iterations (±15, 95% CI) to exit the β-cyclodextrin. While the enantiomer with two binding interactions is retained longer in the β-cyclodextrin than with just one interaction (248 and 233 iterations respectively), the 95% confidence intervals show little difference statistically. Nevertheless this is only one interaction between an enantiomer analyte and one β-cyclodextrin stationary phase molecule. Very small differences can lead to enantiomer separation, since under normal chromatographic conditions many thousands of these interactions are possible. Figure 15 demonstrates that the enantiomer with two binding interactions is retained longer in the cyclodextrin than with just one interaction under all retention conditions. Accordingly, the model performs as anticipated with analytes retained longer as the number and strength of interactions are increased. If analytes had consistently exited the cyclodextrin after just a few interactions, then changing breaking probability would not have affected retention. This was critical in establishing the model, for if probability of breaking did not affect analyte retention inside the cyclodextrin then further development of the model would be unsuccessful. These results confirm that retention of an enantiomer in the modeled β-cyclodextrin can be modified at specific binding sites with repeatable results and that the model can replicate enantiomer chromatographic behavior.

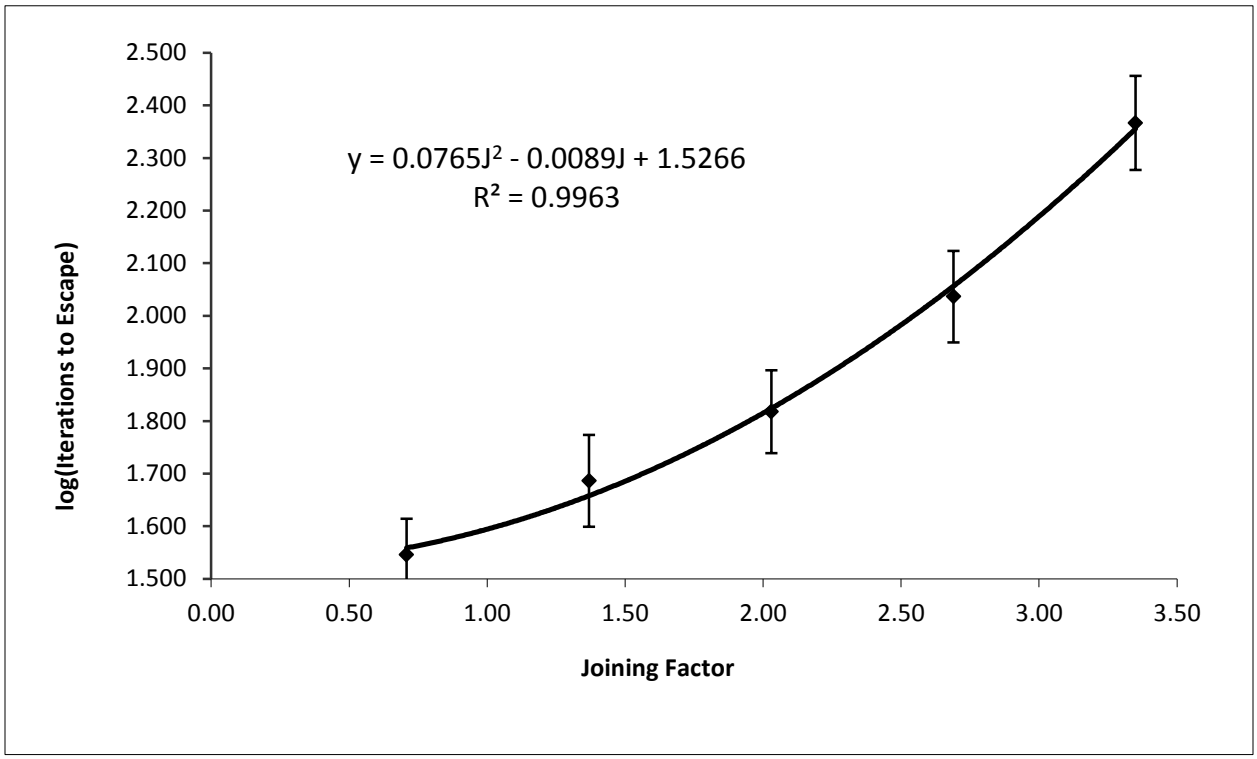

Figure 13: Log(Iterations to Escape) vs. joining factor with the 95% confidence interval expressed along the y-axis for variegated cell A1, 2 interactions with B2, 3, 5, 6.

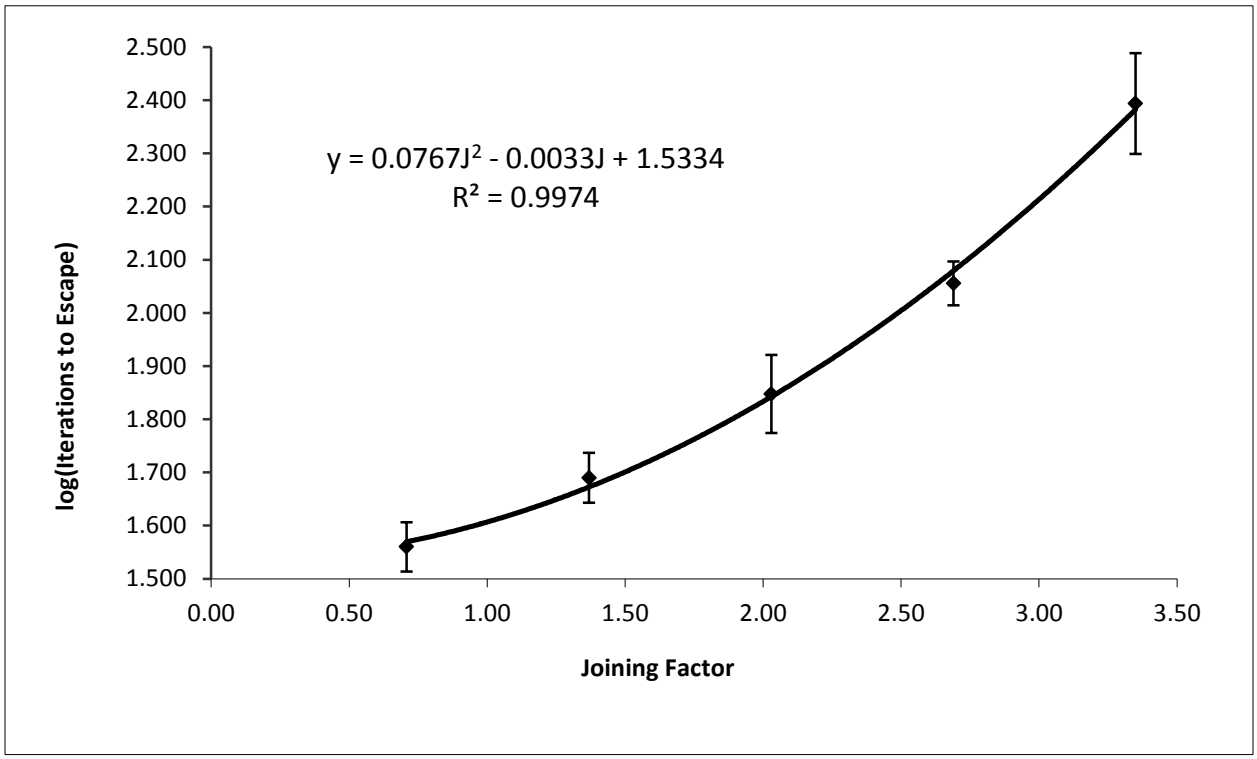

Figure 14: Log(Iterations to Escape) vs. joining factor with the 95% confidence interval expressed along the y-axis for variegated cell A1, 2 interactions with B2, 3, 5, 6 and A0 with B3, 6.

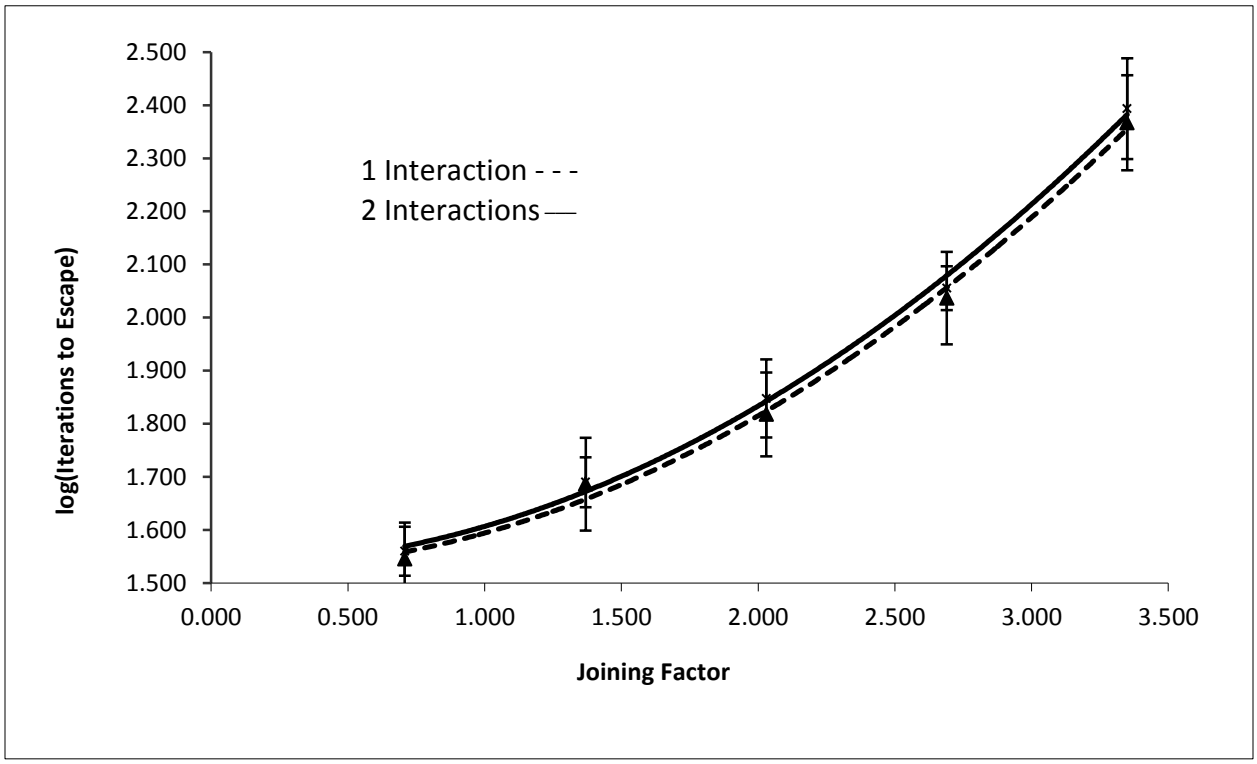

Figure 15: Log(Iterations to Escape) vs. joining factor with the 95% confidence interval expressed along the y-axis for variegated cell A1, 2 interactions with B2, 3, 5, 6 vs. A1, 2 interactions with B2, 3, 5, 6 and A0 with B3, 6.

3.3 Development of model rules

3.3.1 Development of model rule equations for stability constants

By developing the model's probability and factor equations from a diverse and large quantity of published chromatographic experimental data, an optimal modeling of one-to-one molecular binding strengths between analytes and cyclodextrins should be achievable. In correlating the model to experimental data from published literature, several limitations must be acknowledged. The model is examining a one-to-one analyte to cyclodextrin interaction, where experimental data covers both one-to-one through chromatographic scale interactions. Solvation is not yet accounted for in the model, while the experimental data used is in solvent environments. Furthermore, the literature references determined complex stability constants by numerous techniques: calorimetry, gas chromatography, UV spectroscopy, potentiometry, and others. All of these contribute to differences between the model and experimental design that may impact modeling results.

By examining 968 complex stability constants (K) of cyclodextrin inclusion complexes (Rekharsky and Inoue 1998), it is possible to estimate the log K for very weak through very strong bonds. Since values for breaking probability and joining factor are known for these bonds from the previous modeling experiments, they are correlated to log K in Table 3.

Table 3: Complexation model values across log K range.

	Weak Bond	Strong Bond
J, Joining Factor	0.15	3.35
P_B, Breaking Probability	0.95	0.05
log K, Complex Stability Constant	0.25	5.50

It was previously described in section 3.2.2 that the log of analyte-(β-cyclodextrin) complex stability constants have linear relationships when examining hydrophobic and van der Waals interactions, the two strongest interaction energies modeled. Therefore, there should be a linear relationship between the joining factor that models these energies and log K, which gives the following equations:

$$J = 0.610 \times \log K \qquad \text{Eq. 3}$$

$$P_B = (\log J - 0.6) / -1.5 \qquad \text{Eq. 4}$$

Using these relationships, log K vs. log of iterations for analyte to escape will be compared.

3.3.2 Development of model equations for enantiomeric interactions

3.3.2.1 Development of model rule equations

The development of breaking probability and joining factor values take into account the major bonding interactions in the enantiomers studied: van der Waals,

hydrophobicity, hydrogen binding at the primary and secondary hydroxyl groups, and steric interactions. It should be noted that values for variables represent the overall behavior of the possible interactions and not the specific energy of these interactions. Joining factor is calculated from breaking probability, therefore, the breaking probability formula is derived for A0 (hydrogen binding with secondary hydroxyl groups of β-cyclodextrin), and A1,3 (binding and steric forces within β-cyclodextrin).

A starting breaking probability value of 0.5 means that there is equal attraction and repulsion force between the analyte and β-cyclodextrin. A probability of 0.0 represents a bond that has zero probability of breaking. Since a value of zero is not representative of the chromatographic environment of the model, the lower limit for breaking probability is set at 0.05 to signify a very strong attractive interaction but one that can separate. This value range is the basis for the breaking probability equation. Hydrogen bonding is the only modeled attractive force for the enantiomers with the secondary hydroxyl groups of the β-cyclodextrin. Of the enantiomers modeled, N-methylphenobarbitone has the highest potential for hydrogen bonding interaction with 2 Nitrogen and 3 Oxygen atoms. With O-H···N having a bond strength of ~6.9 kcal/mole and O-H···O ~5.0 kcal/mole (Ege 2003), N-methylphenobarbitone has a possible total hydrogen bonding potential of 28.8 kcal/mole. This represents the highest hydrogen bonding potential of the enantiomer group studied. Although the likelihood of all the nitrogen and oxygen atoms bonding at once is unlikely due to their structural separation, varying interactions are possible as molecules move. The hydrogen bonding potential for the enantiomers studied is therefore relative to 28.8 kcal/mole. Taking this into

account, a maximum breaking probability of 0.05, and a starting value of 0.50, results in the equation for the breaking probability of A0 with cells B3 and B6 (see Figure 4) to be:

$$P_{B(A0)} = 0.50 - \frac{H_{\text{sec.}}}{28.8 kcal/mole} \times 0.45 \qquad \text{Eq. 5}$$

0.50, Equal attraction and repulsion value

$H_{sec.}$, Potential hydrogen bonding for enantiomer at secondary hydroxyl groups of the β–cyclodextrin (additive from N and O atoms)

28.8 kcal/mole, Maximum hydrogen bonding potential of enantiomers studied

0.45, Maximum decrease in breaking probability

Unlike the interactions at the secondary hydroxyl groups, a breaking probability for the interior cavity of β-cyclodextrin must take into account, van der Waals forces, hydrophobicity for the portion of analyte inside β-cyclodextrin, hydrogen bonding in β-cyclodextrin, and steric hindrance inside β-cyclodextrin. The induced dipole of the analyte contributes to the overall van der Waals interaction and is proportional to its size (Grimme 2008). Decahydronaphthalene is one of the larger molecules that enters the β-cyclodextrin cavity (Rekharsky and Inoue 1998). Therefore its van der Waals volume, ~60% of β-cyclodextrin's internal volume, is used as the maximum likely to interact with β-cyclodextrin. To calculate its volume and portions of enantiomers that enter the β-

cyclodextrin cavity, the method of Atomic and Bond Contributions of van der Waals volume (VABC) is used (Zhoa, Zissimos et al. 2003). This technique uses the number of atom types present, number of bonds formed, and the number of aliphatic and aromatic rings in the molecule to calculate its van der Waals volume. The authors provided and Excel spreadsheet to perform the calculations. The technique was validated by comparing the results of VABC for 677 organic compounds to computer determined van der Waals volumes. VABC results were found to be equivalent to convention, but more computationally intensive calculated results that require van der Waals radii, inter-atomic distances, and angles of bonds.

$$V_{vdW} = \Sigma \text{ all atom contributions} - 5.92N_B - 14.7R_A - 3.8R_{NA} \quad \text{Eq. 6}$$

N_B, number of bonds = total number of atoms – 1 + R_A +R_{NA}

R_A, number of aromatic rings

R_{NR}, number of non-aromatic rings

Using VABC, decahydronaphthalene has a van der Waals volume (V) of 156.8 $Å^3$. This represents the highest probable van der Waals bonding potential currently modeled which is typically less than 1kcal/mole (Saenger, Takaha et al. 1998). This volume is used later to proportion the van der Waals contribution in the enantiomers studied relative to their van der Waals volume entering the β-cyclodextrin cavity.

In aqueous environments one of the strongest bonding forces occurring between enantiomers and the β-cyclodextrin cavity is hydrophobicity. The hydrophobic bonding energy of a molecule is determined by assuming that the overall hydrophobic bond energy is the sum of each group or atom of the molecule. Decahydronaphthalene is again used as the molecule to have a maximum hydrophobic bonding potential calculated to be 10.0 kcal/mole. This value is used to proportion hydrophobic bonding potential in the enantiomers studied. The portions of enantiomers that can undergo hydrophobic attraction (W) are calculated in the same manner (Kakitani and Yomosa et al. 1980).

Hydrogen bonding in the interior of β-cyclodextrin is also possible, and contributes to the overall enantiomer bonding to β-cyclodextrin. Nitrogen in analytes that enter the β-cyclodextrin cavity may undergo a hydrogen bonding attraction (Liu and Guo 2002; Aree, Hoier et al. 1998), albeit a weak interaction at ~0.7 kcal/mole. Brompheniramine is the only enantiomer containing nitrogen, in its pyridine ring, that is likely to enter hydrophobic β-cyclodextrin cavity due to pyridine's hydrophobic properties. Therefore hydrogen bonding on the interior of β-cyclodextrin is limited in the model to 0.70 kcal/mole.

In addition to the above attractive forces for enantiomers towards cyclodextrin, steric hindrance from the enantiomer may inhibit it entering β-cyclodextrin. β-cyclodextrin has an interior volume of 262 $Å^3$ (Saenger, Takaha et al. 1998). The assumption in the model is that any substitution onto the portion of the enantiomer entering β-cyclodextrin (typically the phenyl group) would hinder the enantiomer

complex proportionally to its van der Waals volume (Durham 1996). It should be noted that due to cyclodextrin's ability to undergo conformational changes and that cyclodextrins have two open ends, it is possible for some larger molecules to enter β-cyclodextrin partially (Chen, Gilson et al. 2004).

Once more, a breaking probability of 0.5 means that there is equal bonding attraction and repulsion force between the analyte and β-cyclodextrin, which is the starting value for breaking probability. van der Waals, hydrophobic, and hydrogen bonding combine to have a total potential bonding energy of 11.7 kcal/mole (see Table 4).

Table 4: Bonding Energy Contributions for $P_{B(A1,3)}$

	max kcal/mole	% contribution	Contribution to 0.45 of $P_{B(A1,3)}$
van der Waals	1.0	8.5	0.038
Hydrophobic	10.0	85.5	0.385
Hydrogen bonding	0.7	6.0	0.027

All three energy contributions are evaluated for their potential contribution to the lowering of breaking probability resulting in a stronger bonding interaction. Taking into account all of the attracting and repulsing forces, the resulting equation for the breaking probability of A1 and 3 with cells B2, 3, 5, and 6 is shown in equation 7:

$$P_{B(A1,3)} = 0.5 - \left(\frac{V}{156.8\text{Å}^3} \times 0.038 + \frac{W}{10.0 kcal\ /\ mole} \times 0.385 + \frac{H}{0.7 kcal\ /\ mole} \times 0.027 \right) + \left(\frac{S}{262\text{Å}^3} \times 0.45 \right)$$

V, van der Waals volume of portion of enantiomer in β-cyclodextrin cavity

156.8 $Å^3$, Decahydronaphthalene van der Waals volume

0.038, van der Waals contribution to 0.45 of $P_{B(A1,3)}$

W, Hydrophobic bonding energy of enantiomer in β-cyclodextrin cavity

10.0 kcal/mole, Modeled maximum hydrophobic bonding potential

0.385, Hydrophobic contribution to 0.45 of $P_{B(A1,3)}$

H, Hydrogen bonding energy of enantiomer in β-cyclodextrin cavity

0.7 kcal/mole, Modeled maximum hydrogen bonding potential

0.027, Hydrogen bonding contribution to 0.45 of $P_{B(A1,3)}$

S, van der Waals volume of the substitution onto the portion of the enantiomer entering the cyclodextrin

262 $Å^3$, β-cyclodextrin interior volume

0.45, Maximum steric inhibition of $P_{B(A1,3)}$

Equations 5 and 7 are used to determine $P_{B(A0)}$ and $P_{B(A1,3)}$ for each enantiomer set. By developing the model's probability and joining factor equations from fundamental bonding interactions, a model of one-to-one molecular binding strengths between the enantiomers and β-cyclodextrin is achieved. In correlating the model to experimental data from published literature, several limitations must be acknowledged. The model is examining a one-to-one enantiomer to β-cyclodextrin interaction, where selectivity experimental data represents chromatographic scale interactions. Solvation is not

accounted for in the model, while the chromatographic experimental data used is in a solvent environment. These may contribute to differences between the model and experimental data, impacting modeling results.

3.3.2.2 Development of P_B values from equations

Equations 5 and 7 are used to generate the breaking probability for $P_{B(A0)}$ and $P_{B(A1,3)}$ respectively and their corresponding joining factor for the six drug enantiomer sets in their nonionic state (see Figure 9). For all enantiomers except for the enantiomer brompheniramine (S), the main interaction is with the phenyl group. Brompheniramine (S) however prefers the insertion of the pyridine ring into the β-cyclodextrin (Durham 1996). Hydrophobic attraction (W) is modeled the same for N-methylphenobarbitone, ephedrine, pseudoephedrine, and mandelic acid since the phenyl group enters the cyclodextrin. Brompheniramine has one less hydrogen regardless of which ring enters β-cyclodextrin and therefore has a slightly lower W value. Ibuprofen has a higher W value due to isobutyl on the phenyl ring. Hydrogen bonding (H) in the interior of β-cyclodextrin only occurs for brompheniramine (S) enantiomer at 0.7 kcal/mole due to the pyridine ring. Steric hindrance occurs in several enantiomers. Using the VABC method (Zhoa, Zissimos et al. 2003) ibuprofen has the largest steric interference (75.1$Å^3$) from the isobutyl group on the phenyl ring that enters the cyclodextrin cavity for interactions to occur. N-methylphenobarbitone (S) has steric interference (23.5$Å^3$) from the two oxygen atoms near the phenyl ring that lack much mobility due to their double bonds. N-methylphenobarbitone (R) has additional steric

interference from the methyl group which now interferes with the phenyl ring entering the cyclodextrin cavity for a total steric interference of 48.0Å^3. Brompheniramine (R) has steric interference from the bromine (26.5Å^3), where the brompheniramine (S) has none since the pyridine group enters the cyclodextrin cavity (Durham 1996).

$P_{B(A0)}$ focuses on the bonding occurring along the outer ring of the β-cyclodextrin with the secondary hydroxyl groups. As previously mentioned, O-H···N and O-H···O have a hydrogen bond potential of 6.9 kcal/mole 5.0 kcal/mole respectively. Using this, hydrogen binding at the β-cyclodextrin's secondary hydroxyl groups (H_{sec}) is determined for each enantiomer by summing the potential hydrogen sites taking into consideration the steric orientation of the enantiomers. Once the phenyl ring enters β-cyclodextrin, N-methylphenobarbitone enantiomers have the best chance of hydrogen bonding at the para positioned oxygen and meta positioned two nitrogens. The ortho positioned oxygens are positioned close to the phenyl ring in the interior of the cyclodextrin and unlikely to interact. In ibuprofen the torsion angles of the attached chiral center and isobutyl group allow ibuprofen (S) to potentially have the two oxygens of the carboxylic acid group interact to form hydrogen bonds, where ibuprofen (R) only has one possible oxygen interaction (Durham 1996). This is similar to mandelic acid where mandelic acid (S) has three potential oxygen interactions and mandelic acid (R) only has one. Ephedrine (SR and RS) and pseudoephedrine (SS) prefer conformations with β-cyclodextrin that allow for hydroxyl and amino hydrogen bonding interactions. While pseudoephedrine (RR) has a conformation that does not favor any hydrogen bonding interactions based on potential energy plots (Durham 1996). Brompheniramine (S)

prefers a conformation with β-cyclodextrin where the pyridine ring is in the cyclodextrin cavity, allowing for one amino interaction on the cyclodextrin outer ring. Brompheniramine (R) however prefers the bromophenyl portion entering the cyclodextrin cavity allowing for one amino interaction and a pyridine interaction with the cyclodextrin outer ring (Durham 1996). The pyridine may undergo hydrogen bonding with the cyclodextrin secondary hydroxyl groups on the outer ring with a strength of about 3 kcal/mol (Dimitrova, Galabov et al. 2004). Values for $P_{B(A0)}$ and $P_{B(A1,3)}$ are calculated for the enantiomers using the above determinations (see Table 5).

Table 5: Equation variable values for enantiomers.

	V	W	H	S	H_{sec}	$P_{B(A1,3)}$	$P_{B(A0)}$
MPB (S)	79.85	4.6	0.0	23.5	18.8	0.3439	0.2063
MPB (R)	79.85	4.6	0.0	48.0	18.8	0.3860	0.2063
IBP (S)	79.85	7.4	0.0	75.1	10.0	0.3247	0.3438
IBP (R)	79.85	7.4	0.0	75.1	5.0	0.3247	0.4219
EF (SR)	79.85	4.6	0.0	0.00	11.9	0.3035	0.3141
EF (RS)	79.85	4.6	0.0	0.00	11.9	0.3035	0.3141
PF (SS)	79.85	4.6	0.0	0.00	11.9	0.3035	0.3141
PF (RR)	79.85	4.6	0.0	0.00	0.0	0.3035	0.5000
MA (S)	79.85	4.6	0.0	0.00	15.0	0.3035	0.2656
MA (R)	79.85	4.6	0.0	0.00	5.0	0.3035	0.4219
BP (S)	73.55	4.4	0.7	0.00	6.9	0.2858	0.3922
BP (R)	79.85	4.4	0.0	26.52	9.9	0.3568	0.3453

3.3.3 Development of model equations for the chromatographic system

3.3.3.1 Development of model equations for mandelic acid and brompheniramine

In the one-to-one model, several interactions were addressed for mandelic acid and brompheniramine. Hydrogen binding between the enantiomers at the secondary

hydroxyl groups of the β–cyclodextrin, along with van der Waals, hydrophobicity, hydrogen binding, and steric interactions at the interior of the β–cyclodextrin. Using this previous work, equation 5 is used to determine breaking probability of A0 (S-enantiomer) and D0 (R-enantiomer) with cell B0 of the cyclodextrin. Equation 7 is used to determine breaking probability of A1-3 and D1-3 with B0 and B1.

With a system that now includes additional forces that result in further movement, such as attractive and repulsive forces on the analytes from mobile phase interactions and flow, interaction of the analytes with each other, and with the primary hydroxyl groups of the cyclodextrin should be incorporated. It has been previously shown that for mandelic acid the main interaction is in the interior of the β–cyclodextrin with the phenyl group (Durham 1996). Since the phenyl group is hydrophobic, there should be a repulsion force with the primary polar hydroxyl groups of the β-cyclodextrin, hence an increase in the breaking probability between the two. In equation 7, the hydrophobic energy of a molecule was determined by the sum of each group or atom of the molecule. Using this same approach, and that decahydronaphthalene is again used as the molecule to have a maximum hydrophobic energy at 10.0 kcal/mole (Kakitani and Yomosa et al. 1980), the following equation is developed:

$$P_{B(B2)} = 0.5 + \left(\frac{W}{10.0 kcal / mole} \times 0.45 \right) \qquad \text{Eq. 8}$$

W, Hydrophobic energy of enantiomer in cyclodextrin cavity

10.0 kcal/mole, Modeled maximum hydrophobic energy potential

0.45, Maximum inhibition of $P_{B(B2)}$

A starting breaking probability value of 0.5 means that there is equal attraction and repulsion force between the analyte and the primary hydroxyl groups of β-cyclodextrin, therefore repulsion due to the hydrophobicity of the phenyl group will increase the value of $P_{B(B2)}$ with sides A1-3 and D1-3 of the mandelic acid enantiomers. All other mandelic acid interactions with β-cyclodextrin were either considered improbable or insignificant and assigned a breaking probability of 0.5.

It has been shown that the brompheniramine (S) enantiomer prefers the insertion of the pyridine ring into the β–cyclodextrin while the (R) enantiomer prefers the insertion of the para-substituted phenyl group (Durham 1996). For (R)-brompheniramine then, equation 8 is used to determine the hydrophobic repulsive force between D1-3 and B2. (S)-brompheniramine though has the potential for hydrogen bonding from the pyridine group with the primary hydroxyl groups of the cyclodextrin (Dimitrova, Galabov et al. 2004). Equation 8 should not be used to predict the interaction between A1-3 and B2, rather an equation for attractive forces involving hydrogen bonding like equation 5. (S)-brompheniramine has the potential for the nitrogen from the pyridine to bond with the primary hydroxyl groups of the β-cyclodextrin. With O-H···N having a bond strength of ~6.9 kcal/mole (Ege 2003), and pyridine undergoing hydrogen bonding with a strength of ~3 kcal/mol (Dimitrova, Galabov et al. 2004) equation 9 results:

$$P_{B(B2)} = 0.50 - \left(\frac{H_{prim.}}{6.9 kcal\ /\ mole} \times 0.45 \right) \qquad \text{Eq. 9}$$

0.50, Equal attraction and repulsion value

$H_{prim.}$, Potential hydrogen bonding for enantiomer from N

6.9 kcal/mole, Maximum hydrogen bonding potential

0.45, Maximum decrease in breaking probability

Again, a starting breaking probability value of 0.5 means that there is equal attraction and repulsion force between the analyte and the primary hydroxyl groups of β-cyclodextrin, therefore attraction due to the hydrogen bonding of the pyridine group will reduce the value of $P_{B(B2)}$ with sides A1-3 of the (S)-brompheniramine.

3.3.3.2 Development P_B values for mandelic acid and brompheniramine

Breaking probabilities and their corresponding joining factors (using equation log J = -1.5 P_B + 0.6 (Kier, Seybold et al. 2000)), are calculated for the enantiomers of mandelic acid and brompheniramine using the equations from sections 3.3.2.1 and 3.3.3.1 for interactions with β-cyclodextrin (see Table 6).

Table 6: Breaking probability and joining factors for mandelic acid and brompheniramine with β–cyclodextrin cells.

Interaction			
Mandelic Acid		P_B	J
A0	B0	0.2656	1.591
A0	B1	0.5000	0.7079
A0	B2	0.5000	0.7079
A1	B0	0.3035	1.396
A1	B1	0.3035	1.396
A1	B2	0.7070	0.3463
A2	B0	0.3035	1.396
A2	B1	0.3035	1.396
A2	B2	0.7070	0.3463
A3	B0	0.3035	1.396
A3	B1	0.3035	1.396
A3	B2	0.7070	0.3463
Mandelic Acid		P_B	J
D0	B0	0.4219	0.9271
D0	B1	0.5000	0.7079
D0	B2	0.5000	0.7079
D1	B0	0.3035	1.396
D1	B1	0.3035	1.396
D1	B2	0.7070	0.3463
D2	B0	0.3035	1.396
D2	B1	0.3035	1.396
D2	B2	0.7070	0.3463
D3	B0	0.3035	1.396
D3	B1	0.3035	1.396
D3	B2	0.7070	0.3463

Interaction			
Brompheniramine		P_B	J
A0	B0	0.3922	1.027
A0	B1	0.5000	0.7079
A0	B2	0.5000	0.7079
A1	B0	0.2858	1.484
A1	B1	0.2858	1.484
A1	B2	0.3043	1.392
A2	B0	0.2858	1.484
A2	B1	0.2858	1.484
A2	B2	0.3043	1.392
A3	B0	0.2858	1.484
A3	B1	0.2858	1.484
A3	B2	0.3043	1.392
Brompheniramine		P_B	J
D0	B0	0.3453	1.208
D0	B1	0.5000	0.7079
D0	B2	0.5000	0.7079
D1	B0	0.3568	1.161
D1	B1	0.3568	1.161
D1	B2	0.6980	0.3573
D2	B0	0.3568	1.161
D2	B1	0.3568	1.161
D2	B2	0.6980	0.3573
D3	B0	0.3568	1.161
D3	B1	0.3568	1.161
D3	B2	0.6980	0.3573

Other interactions also require breaking probabilities and joining factors:

- Enantiomer to mobile phase
- Enantiomer to enantiomer
- Mobile phase to β-cyclodextrin

- Mobile phase to mobile phase

Enantiomer interaction with mobile phase (water and acetonitrile) should involve no overall significant attraction or repulsion. Although competing interactions of repulsion (water with benzene) and attraction (hydrogen bonding) are acknowledged, they should work against each other. Therefore, all enantiomer interactions with mobile phase were assigned the breaking probability of 0.5 (no attraction or repulsion).

Enantiomer to enantiomer interaction also has competing interactions. Hydrophobic attraction may occur between benzene portions of the enantiomers and hydrogen bonding attraction between the alpha hydroxy acids may occur. Nevertheless repulsing interactions will occur when the opposite portions of the enantiomers interact, therefore enantiomer interactions were assigned the breaking probability of 0.5.

Mobile phase interactions with β-cyclodextrin are a little more complex since water (W1) and acetonitrile (W2) will behave differently in the hydrophobic interior and hydroxyl groups of the cyclodextrin. At the B0 cells of the cyclodextrin, which represent both the secondary hydroxyl sites and the upper hydrophobic interior of the cyclodextrin, water is attracted due to hydrogen binding but repelled due to the hydrophobicity. Since these forces are opposite, a breaking probability of 0.5 is assigned. B1 represents the stronger hydrophobic interior of the cyclodextrin, an environment where water would be repelled. Therefore a breaking probability of 1.0 is assigned between water and B1. B2 cells denote the primary hydroxyl groups that water will be attracted to due to hydrogen binding. The breaking probability between water and the B2 cells follows the same probability of water-water interactions, varying with temperature described later. The

exterior of the β-cyclodextrin (C0) is considered to have no attractive or repulsive forces with either mobile phase solvent and has a breaking probability of 0.5 with each.

Like water, acetonitrile has the same competing interactions as water at B0 and is assigned a breaking 0.5. In the hydrophobic interior of the cyclodextrin acetonitrile is not repelled like water and has a breaking probability of 0.5. At the primary hydroxyl groups, acetonitrile may have some attraction and repulsion and is therefore given a value of 0.5 (see Table 7).

Table 7: Breaking probability and joining factors for mandelic acid and brompheniramine with mobile phase cells.

Interaction		P_B	J
A0-3	W1	0.5000	0.7079
D0-3	W2	0.5000	0.7079
A0-3	A0-3	0.5000	0.7079
A0-3	D0-3	0.5000	0.7079
D0-3	D0-3	0.5000	0.7079
W1	B0	0.5000	0.7079
W1	B1	1.000	0.1259
W1	B2	vary with temperature	vary with temperature
W2	B0	0.5000	0.7079
W2	B1	0.5000	0.7079
W2	B2	0.5000	0.7079

Solvents of the mobile phase interact but vary with temperature. Since temperature variation in the chromatographic system will be studied, then these interaction changes need to be accounted for. Water breaking probabilities vary with

temperature (Kier, Seybold, and Cheng 2005). Acetonitrile breaking probabilities vary with temperature but are different than water since its liquid range is -45.7°C to 81.6°C (Weast 1988) (see Table 8). Breaking probabilities of 0.00 to 1.00 are used to cover the liquid range of acetonitrile temperature.

Table 8: Breaking probability and joining factors for water (W1) and acetonitrile (W2) with each other.

	Temperature, °C					
	24	31	37	44	50	57
W1-W1						
P_B	0.240	0.310	0.370	0.440	0.500	0.570
J	1.74	1.36	1.11	0.871	0.708	0.556
W1-W2 W2-W2						
P_B	0.544	0.599	0.647	0.702	0.749	0.805
J	0.608	0.503	0.426	0.352	0.300	0.247

3.3.3.3 Development of model equations for cyclohexylphenylglycolic acid

In the development of model equations for mandelic acid and brompheniramine, several types of interactions were considered. To study these interactions further another enantiomer set was chosen, cyclohexylphenylglycolic acid. It is similar to mandelic acid except that a hydrogen has been replaced with cyclohexane (see Figure 16). Where mandelic has minimal chiral separations since the only chiral discriminating characteristic is the different interactions of the alpha hydroxy acid, cyclohexylphenylglycolic acid has the potential for different interactions between the

benzene and cyclohexane groups in the interior of the β–cyclodextrin. Equations 5, 7, and 8 should be used to calculate the appropriate breaking probabilities, but they need to be adapted to the new molecule being analyzed.

With O-H···O having a bond strength of ~5.0 kcal/mole (Ege 2003), cyclohexylphenylglycolic acid has a possible total hydrogen bonding potential of 15.0 kcal/mole. This represents the highest hydrogen bonding potential due from the alpha hydroxy acid with the secondary hydroxyl groups of β-cyclodextrin. Taking this into account, a maximum P_B of 0.05, and a starting value of 0.50, results in the equation for the breaking probability of A0 and D0 with cell B0:

$$P_{B(B0)} = 0.50 - \frac{H_{\text{sec.}}}{15.0 kcal\ /\ mole} \times 0.45 \qquad \text{Eq. 10}$$

0.50, Equal attraction and repulsion value

$H_{sec.}$, Potential hydrogen bonding for enantiomer (additive of O atoms)

15.0 kcal/mole, Maximum hydrogen bonding potential

0.45, Maximum decrease in breaking probability

A breaking probability for the interior cavity of β-cyclodextrin takes into account, van der Waals forces, hydrophobicity for the portion of analyte in β-cyclodextrin, and steric hindrance inside β-cyclodextrin. Hydrogen bonding in the interior of the β-

cyclodextrin is no longer incorporated since neither benzene or cyclohexane are likely to interact in this manner.

Cyclohexylphenylglycolic acid contains both a benzene and cyclohexane that may enter the β–cyclodextrin hydrophobic interior. It has been shown with brompheniramine that different groups attached to the chiral carbon can have preferential interaction with the interior of the β–cyclodextrin (Durham 1996). However, benzene and cyclohexane do not differ enough in their van der Walls volume (79.85$Å^3$ and 98.66$Å^3$) (Zhoa, Zissimos et al. 2003) or hydrophobic binding potential (4.6Å and 5.8Å) (Kakitani and Yomosa et al. 1980) to explain significant chromatographic separation. It has been shown with mandelic acid that the phenyl group preferably enters the β–cyclodextrin cavity, but there is also enough volume for cyclohexane to enter either interchangeably or simultaneously. Other studies have demonstrated this type of interaction, as in fenoprofen (Choi, Jung et al. 2000) where one enantiomer prefers the insertion on one benzene ring into the β–cyclodextrin, while the other prefers both benzene rings (161$Å^3$ van der Waals volume) to form interactions within the β–cyclodextrin. Combined, benzene and cyclohexane have a van der Waals volume 178$Å^3$ compared to the internal volume of β–cyclodextrin 262$Å^3$ (Saenger, Takaha et al. 1998). Due to cyclodextrin's ability to undergo conformational changes and that they have two open ends, it is possible for even larger molecules to enter β-cyclodextrin partially (Chen, Gilson et al. 2004). Since cyclohexane and β–cyclodextrin may change their spatial conformation, one enantiomer of cyclohexylphenylglycolic acid may have this type of interaction while the other enantiomer has only the original benzene

interaction. Chromatographic retention and selectivity have been demonstrated to improve as the hydrogen on the chiral center of mandelic acid is replaced with larger substituted groups (Feitsma, Zeeuw et al. 1985), evidence that the second group plays an important role in increasing the selectivity of the retention interaction. Therefore the proposal that cyclohexane plays a role in the interaction of retention will be incorporated into the model. *d*-cyclohexylphenylglycolic acid (D cell) is retained the least in the system studied (Feitsma, Zeeuw et al. 1985) and will be modeled with the phenyl group entering the β–cyclodextrin interior, while *l*-cyclohexylphenylglycolic acid (A cell) will be modeled with the phenyl and/or cyclohexane interacting with the β–cyclodextrin interior.

As explained in section 3.3.2.1, one of the strongest bonding forces occurring between enantiomers and the β-cyclodextrin cavity is hydrophobicity. Benzene and cyclohexane combined have a maximum hydrophobic bonding potential (W) at 10.4 kcal/mole. Since neither the phenyl or cyclohexane group have additional groups attached, steric hindrance will not be included.

Once more, a breaking probability of 0.5 means that there is equal bonding attraction and repulsion force between the analyte and β-cyclodextrin, which is the starting value for P_B. van der Waals and hydrophobic bonding combine to have a total potential bonding energy of 11.4 kcal/mole (see Table 9).

Table 9: Bonding Energy Contributions for $P_{B(B0,1)}$ with A and D1-3.

	max kcal/mole	% contribution	Contribution to 0.45 of $P_{B(B0,1)}$
van der Waals	1.0	8.8	0.040
Hydrophobic	10.4	91.2	0.410

Taking into account the attracting interactions involved, the resulting equation for the breaking probability of A1-3 and D1-3 with B0 and B1 is shown in equation 11:

$$P_{B(B0,1)} = 0.5 - \left(\frac{V}{178.5\text{Å}^3} \times 0.040 + \frac{W}{10.4 kcal / mole} \times 0.410 \right) \quad \text{Eq. 11}$$

V, van der Waals volume of portion of enantiomer in cyclodextrin cavity

178.5 $Å^3$, Benzene and cyclohexane van der Waals volume

0.040, van der Waals contribution to 0.45 of $P_{B(B0,1)}$

W, Hydrophobic bonding energy of enantiomer in cyclodextrin cavity

10.4 kcal/mole, Modeled maximum hydrophobic bonding potential

0.410, Hydrophobic contribution to 0.45 of $P_{B(B0,1)}$

As in equation 8, the phenyl or cyclohexane groups will not have an attraction to the primary hydroxyl groups due to their hydrophobic nature. Therefore, there should

be a repulsion between the two. Equation 12 is identical to equation 8 except the maximum hydrophobic energy is now increased:

$$P_{B(B2)} = 0.5 + \left(\frac{W}{10.4 kcal / mole} \times 0.45 \right)$$ Eq. 12

W, Hydrophobic energy of enantiomer in cyclodextrin cavity

10.4 kcal/mole, Modeled maximum hydrophobic energy potential

0.45, Maximum inhibition of $P_{B(B2)}$

Repulsion due to the hydrophobicity of the phenyl cyclohexane groups will increase the value of $P_{B(B2)}$ with sides A1-3 and D1-3 of the cyclohexylphenylglycolic acid enantiomers.

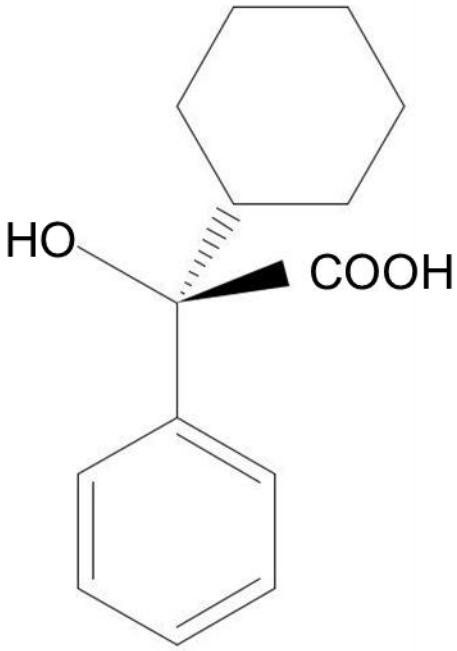

Figure 16: Cyclohexylphenylglycolic acid (CHPGA).

3.3.3.4 Development P_B values for cyclohexylphenylglycolic acid

Using the variables discussed in the previous section, their values are determined for each enantiomer (see Table 10). The breaking probabilities with corresponding joining factors are calculated for the cyclohexylphenylglycolic acid enantiomers using equations 10, 11, and 12 for their interactions with β-cyclodextrin (see Table 11).

Table 10: Equation variable values for cyclohexylphenylglycolic acid enantiomers.

	V	**W**	**H_{sec}**
l-Cyclohexylphenylglycolic acid (A)	178.51	10.4	15
d-Cyclohexylphenylglycolic acid (D)	79.85	4.6	15

Table 11: Breaking probability and joining factors for *l*-Cyclohexylphenylglycolic acid and *d*-Cyclohexylphenylglycolic acid with β–cyclodextrin cells.

Interaction			
l-Cyclohexylphenylglycolic acid		P_B	J
A0	B0	0.0500	3.350
A0	B1	1.000	0.1260
A0	B2	1.000	0.1260
A1	B0	0.0500	3.350
A1	B1	0.0500	3.350
A1	B2	0.9500	0.1500
A2	B0	0.0500	3.350
A2	B1	0.0500	3.350
A2	B2	0.9500	0.1500
A3	B0	0.0500	3.350
A3	B1	0.0500	3.350
A3	B2	0.9500	0.1500
d-Cyclohexylphenylglycolic acid		P_B	J
D0	B0	0.0500	3.350
D0	B1	1.000	0.1260
D0	B2	1.000	0.1260
D1	B0	0.3008	1.409
D1	B1	0.3008	1.409
D1	B2	0.6990	0.3560
D2	B0	0.3008	1.409
D2	B1	0.3008	1.409
D2	B2	0.6990	0.3560
D3	B0	0.3008	1.409
D3	B1	0.3008	1.409
D3	B2	0.6990	0.3560

Interactions between A0 and D0 representing the alpha hydroxy acid and the hydrophobic interior of the β-cyclodextrin are unlikely and were assigned a breaking probability of 1. All other interactions involving mobile phase solvents and enantiomers are values in Tables 7 and 8.

3.4 Conclusions

Once the physical environment of the model was defined, the breaking probabilities and their accompanying joining factors of the interactions had to be determined. To determine the breaking probabilities, the appropriate equations to do so had to be developed for recognized chemical interaction forces. This was an evolutionary process as the model was expanded from one-to-one general analyte interactions with β-cyclodextrin, to enantiomer retention studies, and eventually expansion to a chromatographic scale.

With the first interactions studied being the testing of the model for basic functionality, the equation were rather straight forward. A solid foundation in these equations was critical as the model was expanded to comparing results to analyte complex stability constants.

Testing enantiomeric behavior expanded the model to use variegated cells which proved critical in studying more complex enantiomers. New interaction energies were introduced into the equations. It should be emphasized that the goal was to incorporate the additional interaction energies involved into the model at an appropriate level, not to determine their exact values that occur at the molecular level. As the model was expanded to the chromatographic scale, many more interactions needed to be incorporated into the model. This resulted in new equations involving new interaction energies to consider. The foundation of all equations are based on generally excepted chemical and physical properties of the molecules involved.

CHAPTER 4 Correlation of Model Results to Published Results

4.1 Introduction

The cellular automata model was developed in a stepwise manner, examining results of one type interaction and then expanding the model to a more complex one:

- One-to-one analyte interactions with β-cyclodextrin
- One-to-one enantiomer interactions with β-cyclodextrin
- Chromatographic scale enantiomer interactions with β-cyclodextrin
- Chromatographic scale interactions with changing chromatography conditions

At each point in the evolution of the model, it was evaluated against published modeled or laboratory results.

One-to-one analyte interactions were compared to complex stability constants of analytes and β-cyclodextrin. This demonstrated the models ability to form interactions of similar strength to published results. One-to-one interactions between enantiomers and β-cyclodextrin were modeled to compare results with the potential binding energies of the complexes formed. Chromatographic conditions such as mobile phase solvent interaction and flow were not yet considered. Although a good predictor for the potential for chromatographic separation, it is still limited since additional factors contribute the ability to separate and analyze peaks.

Further expansion of the model to the chromatographic scale gives a better prediction of chromatographic separation since selectivity, peak tailing and resolution, and capacity factors are examined. Interpretation of the model results become more complex as model raw data files are imported into Excel and graphed to create chromatograms.

To compare the chromatographic model expansion results to previous one-to-one studies, mandelic acid and brompheniramine are again modeled and the results evaluated. Conditions that affect chromatographic separation are then evaluated for cyclohexylphenylglycolic acid enantiomers: system temperature, mobile phase flow rate, pH of mobile phase, and injection volume. The non-linear adsorption isotherms of the system are also examined.

4.2 Correlation of model results to complex stability constants

For the model to predict binding strengths between analytes and cyclodextrins, the relationship between the amount of time an analyte stays within the cyclodextrin versus log K must be understood. To do this, twenty eight value sets (n=6) are used for the variables across the log K range of 0.25 – 5.5. A comparison of log (iterations to escape) vs. log K gives a linear relationship (coefficient of determination, 0.9924) expressed as log(iterations to escape) = 0.5026 x log K +0.9394 (Figure 17). This demonstrates a linear relationship with no bias, since the y intercept of 0.9394 means that a log K of 0 gives “iterations to escape” of 9. As previously demonstrated, any iterations less than 13 represents no significant bonding.

Since analyte retention is now correlated to log K, and since the joining factor and breaking probability can be calculated from experimental log K values, the model is tested to see if it accurately predicts the retention order of different analytes when compared to experimental data. Using 65 analytes whose log Ks were experimentally determined (Blokzijl and Engberts 1993) that span weak to strong retention with small to larger differences in log K, joining factor and breaking probability were determined for each using equations 3 and 4. All analytes are run with a run time of 2000 iterations (n = 6). The model accurately predicted the relative retention strength/elution order of all 65 analytes (see Table 12). The model's %RSD for analytes ranged from 3.2 to 22.5%, which compares reasonably well with the experimental %RSD range of 0.4 to 45.8%. Additionally, it is clear that the model accurately predicts elution order for large and very small differences in log K, as in butanoic acid (log K = 1.511) and benzoate (log K = 1.559).

Table 12: Experimental log K vs. model retention.

Analytes	Host	Experimental		Iterations >0.95		Model
		log K	%RSD	mean (n=6)	%RSD	% Increase Retention
4-cyanophenol	α	**2.24**	0.4%	103.3	3.2%	
4-chlorophenol	α	**2.43**	0.4%	125.2	14.7%	**21.1%**
cyclohexanone	α	**1.34**	4.5%	40.0	17.2%	
cyclohexanol	α	**1.89**	1.1%	83.5	10.0%	**108.8%**
2,5-hexanediol	α	**1.41**	7.1%	50.3	4.7%	
1,5-hexanediol	α	**1.54**	3.9%	51.3	7.1%	**2.0%**
1,6-hexanediol	α	**2.01**	1.0%	92.0	11.6%	**82.8%**
1,2-hexanediol	α	**2.27**	4.0%	113.5	8.3%	**125.5%**
3-hexanol	α	**2.19**	2.7%	115.7	20.6%	
2-hexanol	α	**2.45**	0.8%	141.2	13.9%	**22.0%**
1-hexanol	α	**2.58**	1.9%	147.8	7.3%	**27.8%**
(2-methoxyphenethyl)ammonium	α	**1.14**	2.6%	33.5	11.8%	
(3-methoxyphenethyl)ammonium	α	**1.23**	0.8%	39.5	17.9%	**17.9%**
(4-methoxyphenethyl)ammonium	α	**1.48**	0.7%	54.3	16.5%	**62.2%**
(1-methylhexyl)ammonium	α	**2.642**	0.2%	173.2	14.1%	
(1-methylheptyl)ammonium	α	**3.053**	0.2%	263.7	13.1%	**52.3%**
2,7-naphthalenedisulfonate	α	**0.98**	6.1%	31.8	16.2%	
2-naphthalenedisulfonate	α	**2.56**	0.4%	147.0	17.4%	**361.8%**
3-nitrophenol	α	**2.09**	1.0%	95.0	10.6%	
4-nitrophenol	α	**2.34**	1.7%	121.5	14.1%	**27.9%**
2-nitrophenol	α	**3.70**	29.7%	515.5	8.3%	**442.6%**
3-nitrophenolate	α	**2.31**	0.4%	116.5	12.9%	
4-nitrophenolate	α	**3.26**	2.1%	306.5	11.4%	**163.1%**
3-nitrophenyl acetate	α	**1.72**	0.0%	63.7	15.5%	
4-nitrophenyl acetate	α	**1.92**	0.0%	72.5	20.4%	**13.9%**
1,5-pentanediol	α	**1.49**	0.7%	51.5	20.8%	
1,2-pentanediol	α	**1.89**	1.6%	77.5	17.2%	**50.5%**
3-pentanol	α	**1.85**	1.1%	81.5	9.7%	
2-pentanol	α	**2.00**	1.5%	94.8	15.9%	**16.4%**
1-pentanol	α	**2.44**	0.8%	130.2	22.5%	**59.7%**
1,2-propanediol	α	**0.48**	45.8%	16.3	20.8%	
1,3-propanediol	α	**0.63**	6.3%	21.5	15.8%	**31.6%**
2-adamantylammonium	β	**3.87**	1.3%	625.7	20.1%	
1-adamantylammonium	β	**3.95**	1.3%	626.3	18.0%	**0.1%**
1-adamantylmethylammonium	β	**4.48**	1.8%	1305.8	11.2%	**108.7%**
butanoic acid	β	**1.511**	0.9%	51.8	11.3%	
benzoate	β	**1.559**	0.3%	59.2	11.0%	**14.1%**
benzoic acid	β	**2.737**	0.1%	193.7	15.3%	**273.6%**
trans-1,2-cyclohexanediol	β	**2.00**	2.0%	92.3	12.2%	
cis-1,2-cyclohexanediol	β	**2.43**	1.6%	137.5	16.3%	**48.9%**
hexanoate	β	**1.830**	0.6%	74.5	22.0%	
hexanoic acid	β	**2.467**	0.3%	162.8	21.1%	**118.6%**
3-(2-hydroxyphenyl)propionate	β	**1.908**	0.6%	89.2	15.2%	

3-(4-hydroxyphenyl)propionate	β	**2.473**	0.2%	133.0	9.5%	**49.2%**
3-*O*-methyldopamine	β	**0.63**	23.8%	18.5	16.1%	
4-*O*-methyldopamine	β	**1.71**	0.6%	70.0	12.0%	**278.4%**
(3-methylphenyl)acetate	β	**1.08**	4.6%	28.5	10.1%	
(4-methylphenyl)acetate	β	**1.61**	1.2%	52.7	8.3%	**84.8%**
naphthalene	β	**2.83**	0.0%	205.7	18.0%	
1-naphthaleneacetate	β	**4.35**	1.1%	1028.2	6.1%	**399.9%**
1-naphthyl acetate	β	**2.19**	0.0%	94.5	16.1%	
2-naphthyl acetate	β	**2.51**	1.2%	138.3	12.9%	**46.4%**
3-nitrophenolate	β	**2.07**	3.4%	96.2	12.4%	
4-nitrophenolate	β	**2.76**	0.7%	202.7	18.2%	**110.7%**
pentanoate	β	**0.92**	23.9%	30.7	21.3%	
pentanoic acid	β	**1.96**	0.5%	79.2	17.9%	**158.2%**
2-propanol	β	**0.41**	19.5%	14.2	15.5%	
1-propanol	β	**0.65**	21.5%	19.7	13.0%	**38.8%**
4-chloro-4-[(4-hydroxyphenyl)azo]benzoate	γ	**4.16**	0.5%	894.2	13.1%	
2-chloro-4-[(4-hydroxyphenyl)azo]benzoate	γ	**4.30**	4.0%	953.2	10.4%	**6.6%**
2-naphthalenesulfonate	γ	**1.58**	1.9%	53.3	16.4%	
2,7-naphthalenedisulfonate	γ	**2.58**	0.8%	156.2	13.4%	**192.8%**
2-[(4-hydroxyphenyl)azo]benzoate	γ	**3.28**	1.8%	324.3	12.8%	
3-[(4-hydroxyphenyl)azo]benzoate	γ	**4.04**	0.2%	752.7	16.9%	**132.1%**
4-[(4-hydroxyphenyl)azo]benzoate	γ	**4.15**	1.2%	860.0	3.8%	**165.2%**

Although the model accurately predicts analyte elution order, correctly determining log K from model retention would demonstrate model accuracy when compared to experimental data. Using the iterations to escape from the data collected and the rearranging of the equation relationship from Figure 17 to solve for log K, log(iterations to escape) = 0.5026 x log K + 0.9394, the model determined log K is compared to experimental values (see Figure 18). The model and experimental log K have strong correlation with a coefficient of determination of 0.9960. The model's determined log K is slightly biased high with a slope of 0.9159 and an intercept of +0.15; however, the standard error of the slope is ±0.06 for model predicted log K and may contribute to this bias. The experimental log K range of 0.25 to 5.5 originally correlated to joining factor and breaking probability may need adjusting to better represent the

strength of the complexes formed. Additionally, the model is simplified verses experimental systems as previously explained which may contribute to the slight bias.

To determine the predictive power of the model, several parameters were evaluated (Tropsha, Gombar et al. 2003) using generally accepted statistical tests for models of chemical properties:

Cross-validated correlation coefficient, $q^2 = 1 - \frac{\sum_{i=1}^{test}(y_i - \hat{y}_i)^2}{\sum_{i=1}^{test}(y_i - \bar{y})^2} > 0.5$ Eq. 12

y_i , Measured log K

$\hat{y}_i$, Predicted log K

$\bar{y}$, Average log K

Coefficient of determination, $R^2 > 0.6$

Coefficients of determination, $\frac{(R^2 - R_0^2)}{R^2} < 0.1$ Eq. 13

R^2 , Coefficient of determination

R_0^2 , Coefficient of determination with intercept forced through origin

Slope, $0.85 \leq k \leq 1.15$

If all parameters are met then the model demonstrated acceptable predictability. The cross-validated correlation coefficient was 0.9854, which being greater than 0.5 is indicative of a predictive model. A coefficient of determination of 0.9960 has a suitable quality of the fit between the predicted values of the model and experimental values.

The coefficients of determination was 0.0131, confirming that the model's slope does not differ greatly from one with an intercept through the origin. A slope of 0.9727 when forced through the origin also showed minimal bias. Additionally the mean prediction error was determined to be 0.0350 and a root mean squares error of 0.1065 demonstrates accuracy throughout the predicted population. It is concluded that the model is predictive within the boundaries of examining one-to-one molecular binding strengths between analytes and cyclodextrins.

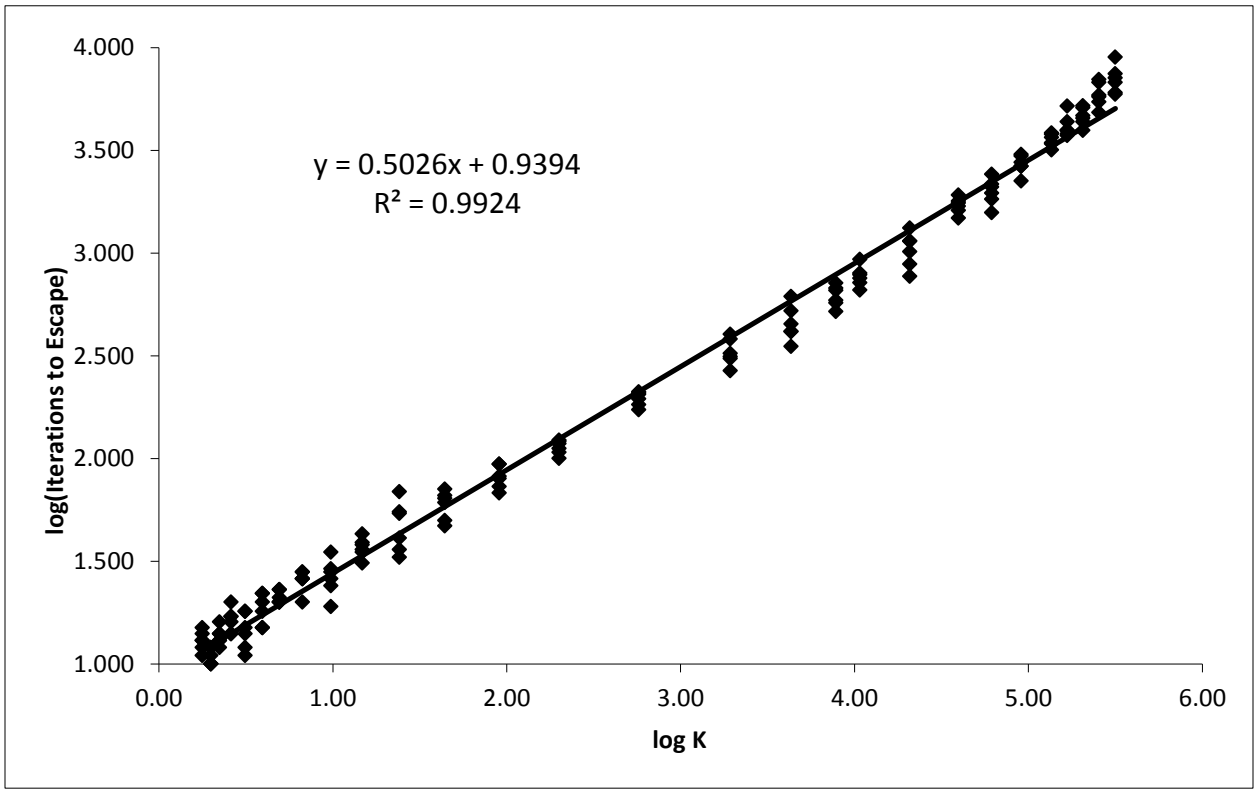

Figure 17: Log(Escape Iterations) vs. log K across the log K range of 0.25 – 5.5, resulting in a linear relationship.

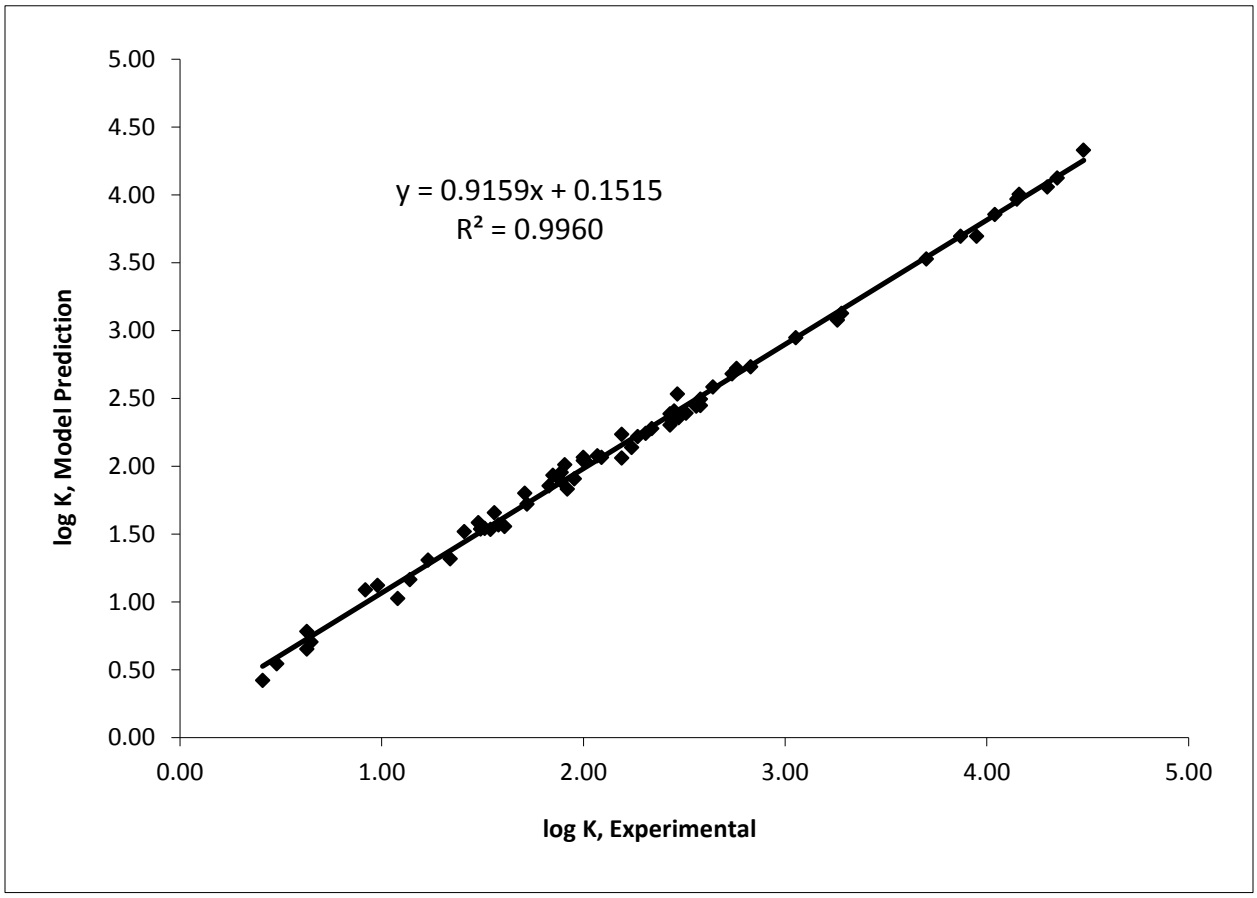

Figure 18: The model determined and experimental log K demonstrate a good correlation with a coefficient of determination of 0.9960.

4.3 Correlation of model results for enantiomeric chromatographic separations

Results of the model were compared to published potential binding energies of the enantiomer-(β-cyclodextrin) complexes and high performance liquid chromatography selectivity data (see Table 13 (Durham, D. 1996; Han and Armstrong 1989) and Figure 19) demonstrating that the model accurately predicts enantiomer retention in β-cyclodextrins and the lack thereof. Using the determined values for $P_{B(B0)}$ and $P_{B(B1,3)}$, each enantiomer was run with enough iterations to allow the complex to terminate with 95% of the enantiomers leaving the cyclodextrin. This is a measure of the strength of the enantiomer-(β-cyclodextrin) bonding interactions.

Table 13: Model retention, potential energy differences, and high performance liquid chromatography results compared

	Iterations to Escape (ITE)	P.B.E.	ΔITE	ΔP.B.E.	HPLC Selectivity, ∝
MPB (S)	48.2 (±1.18)	130.87	2.83	2.33	1.11
MPB (R)	45.3 (±1.20)	128.54			
IBP (S)	**49.5 (±1.10)**	**131.62**	**1.33**	**0.92**	**ns**
IBP (R)	**48.2 (±1.18)**	**130.70**			
MA (S)	**51.8 (±0.94)**	**140.36**	**0.67**	**0.05**	**1.05**
MA (R)	**51.2 (±0.33)**	**140.31**			
EF (RS)	**51.5 (±1.10)**	**137.65**			
EF (SR)	**51.7 (±1.20)**	**137.66**	**0.17**	**0.01**	**ns**
PF (RR)	50.3 (±0.83)	139.00			
PF (SS)	51.5 (±1.58)	139.57	1.17	0.57	1.12
BP (S)	52.0 (±1.52)	140.49	5.17	6.80	1.13
BP (R)	46.8 (±1.38)	133.69			

The model predicts that brompheniramine would separate to the greatest extent with a difference in iterations to escape (ΔITE) of 5.17. This agrees with the differences in potential binding energy (ΔPBE) of enantiomer-(β-cyclodextrin) complexes of 6.80

kcal/mole, where a value close to or greater than one predicts sufficient complexation for high performance liquid chromatography separation (Durham 1996). Moreover, high performance liquid chromatography selectivity ($\propto$, selectivity factor) for brompheniramine demonstrates the greatest selectivity at 1.13 (Durham 1996; Han and Armstrong 1989). N-methylphenobarbitone is predicted to have the next greatest separation with an ΔITE of 2.83. This agrees with the published ΔPBE of 2.33 kcal/mole and a selectivity of 1.11. Pseudoephedrine is predicted to have separation by the model with an ΔITE of 1.17. Published ΔPBE for pseudoephedrine of 0.57 kcal/mole does not indicate much separation; however, a chromatographic selectivity of 1.12 does. NMR analysis has demonstrated that both pseudoephedrine and ephedrine have nearly identical positioning of the phenyl ring in the cyclodextrin cavity, and that any separation occurring is due to hydrogen bonding along the cyclodextrin outer edge (Mularz and Petersheim et al. 1988). Therefore the pseudoephedrine separation occurring will be highly dependent on the surrounding mobile phase environment.

Ibuprofen, mandelic acid, and ephedrine do not have significant chromatographic separation, with only mandelic acid having a selectivity factor of 1.05, while ibuprofen and ephedrine are not separated. This agrees with model predictions for ephedrine (ΔITE of 0.17) and mandelic acid (ΔITE of 0.67), except ibuprofen has an ΔITE of 1.33 predicting chromatographic separation. Ibuprofen has an ΔP.B.E. of 0.92 predicting the possibility of separation. It appears that one-to-one modeling is insufficient in predicting ibuprofen selectivity.

Model results are graphically displayed (see Figure 19) showing iteration to escape with their 95% confidence intervals as error bars. It clearly displays the

separation of brompheniramine and N-methylphenobarbitone enantiomers, with less separation for ibuprofen. It also demonstrates lack of separation of mandelic acid, ephedrine, and pseudoephedrine. This demonstrates that the model can predict enantiomer retention in β-cyclodextrins and the lack thereof that agrees with published chromatographic separations (with the exception of pseudoephedrine), along with the degree of the retention relative to changes in potential binding energies of the complexes formed.

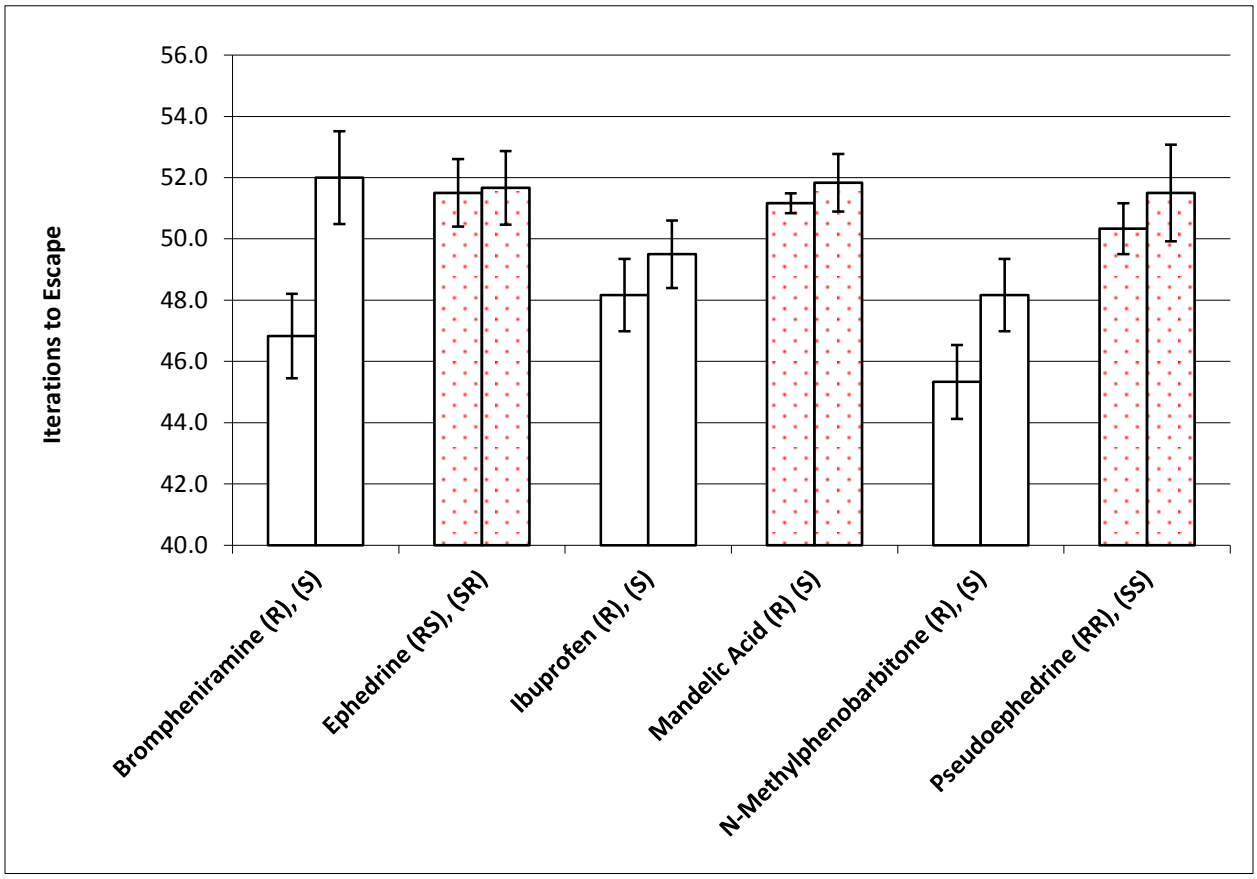

Figure 19: Iterations to Escape vs. enantiomers modeled with the 95% confidence interval expressed along the y-axis to graphically display separation and the lack of separation of enantiomers.

4.4 Correlation of model results for chromatographic scale separations

4.4.1 Mandelic acid and brompheniramine model results

4.4.1.1 Interpretation of model data into chromatograms

Before the model data output can be compared to the selectivity of laboratory generated chromatograms, it must be transformed from columns of numbers in a Windows Notepad file into an Excel "X Y (Scatter)" graph (© Windows Corporation). In order to do this several steps are involved.

The cellular automata model output is a data file that reports cell population, location of D (R-enantiomer) and A (S-enantiomer) of mandelic acid, and brompheniramine in the following format:

- Run iteration
- Row
- A average population at the above iteration
- A standard deviation
- D average population at the above iteration
- D standard deviation

The run iteration is the iteration in the run that is being observed. Since runs go into thousands of iterations, it was decided to record every 10^{th} iteration. The row represents how far through the column a cell has moved, with row 204 being the end of the modeled column (see section 2.4.2). The cell average population is the average population of cells A or D at that row at a specific point in time (e.g. iteration). For the analysis of mandelic acid and brompheniramine, each run reported was the average of

60 runs. This number of runs was reached by first only taking one run that repeated 10 times, and reporting the average. This did not provide good peak shape in the Excel generated chromatograms. Peak population had not yet achieved enough reproducibility around the peak maximum to plot. Peaks were split into several maximums. As in the one-to-one interaction studies, it was decided to rerun the model 5 more times and take the average of the 6 runs. This resulted in a total of 60 runs. Excel chromatograms now had appropriate peak shape, with a single peak maximum that when retained longer resulted in wider peaks with greater tailing as in typical chromatography. Therefore, a single run that repeated 60 times was performed. Comparison of the two approaches demonstrated that one run that repeats 60 times is the simplest approach resulting in the same peak shape as in the above average of 6 runs.

Enantiomers cell location of A and D were examined when 90% (or 90 of the 100 cells) were past the last β–cyclodextrin cells at row 204. With 90% of the enantiomer cells eluted from the stationary phase, the cell population was sufficient to generate Excel chromatograms. At lower percentages of elution, peaks were distorted with a tailing shoulder that represented enantiomer cells still in the stationary phase. This model measurement is taking a snapshot of cell location of every enantiomer cell at a particular iteration. Note that the number of iterations for A and D will be different depending on their retention by the β–cyclodextrin cells resulting a in degree of separation. Once an iteration is determined for the average number of cells A where 90 have moved beyond row 204, all row data for that iteration is imported into Excel. This

is repeated for D cells. Since this results in a large number of rows (i.e. 800 rows), the sum of every ten rows is determined and a new table is calculated (see Table 14).

Table 14: Model data output for brompheniramine of iteration and cell location, A being Brompheniramine (S), and D Brompheniramine (R).

row	iteration	A	iteration	D
140	12580	0.1	11250	0.0
150	12580	0.2	11250	0.1
160	12580	0.7	11250	0.4
170	12580	1.0	11250	0.7
180	12580	2.1	11250	1.5
190	12580	3.2	11250	3.9
200	12580	4.8	11250	7.0
210	12580	6.4	11250	11.6
220	12580	9.0	11250	14.2
230	12580	11.0	11250	16.9
240	12580	13.1	11250	16.7
250	12580	12.8	11250	11.0
260	12580	11.0	11250	8.2
270	12580	9.5	11250	4.2
280	12580	6.8	11250	1.9
290	12580	3.8	11250	1.0
300	12580	2.5	11250	0.5
310	12580	1.2	11250	0.2
320	12580	0.4	11250	0.0
330	12580	0.3	11250	0.0
340	12580	0.1	11250	0.0
total cells =		100		100

Rows 140 to 349 were used since this range contained all 100 cells of both enantiomers. Though, the difference between time of elution from the stationary phase,

the difference in iterations, has not been accounted for as can be seen in the Excel chromatogram (Figure 20).

To correct for this, the time or iterations between the enantiomers needs to be accounted for since the earlier eluting enantiomer continues to move with flow as the other enantiomer is being retained in the column. To do this the flow rate in rows/iteration was determined. This was accomplished by setting the breaking probabilities of the analytes equivalent to the mobile phase and determining how many iterations it takes for unretained cells to move in just mobile phase beyond row 205. By doing this the flow rate is determined and the row position of the early eluting D cells can be calculated (see Table 15):

$$R_D = R + (I_A - I_D) \times Flow \qquad \text{Eq. 12}$$

R_D, Row for D population

R, Row uncorrected

I_A, Iteration for cells A

I_D, Iteration for cells D

Flow, rows/iteration

Table 15: Model data output for brompheniramine with cell location D adjusted for mobile phase flow.

Row	Row	A	Row adjusted for flow	D
140	140	0.1	179	0.0
150	150	0.2	189	0.1
160	160	0.7	199	0.4
170	170	1.0	209	0.7
180	180	2.1	219	1.5
190	190	3.2	229	3.9
200	200	4.8	239	7.0
210	210	6.4	249	11.6
220	220	9.0	259	14.2
230	230	11.0	269	16.9
240	240	13.1	279	16.7
250	250	12.8	289	11.0
260	260	11.0	299	8.2
270	270	9.5	309	4.2
280	280	6.8	319	1.9
290	290	3.8	329	1.0
300	300	2.5	339	0.5
310	310	1.2	349	0.2
320	320	0.4	359	0.0
330	330	0.3	369	0.0
340	340	0.1	379	0.0
	total cells =	100		100

With the corrected row position for D cells, new Excel chromatograms are generated See Figure 21 for brompheniramine and Figure 22 for mandelic acid enantiomers. The Excel chromatograms were generated using a “X Y (Scatter)” chart with straight lines and a moving average of 2. It should be noted that peaks are in order of row location, therefore they are in the opposite order of typical chromatograms. Additionally the peaks themselves are reversed in shape with tailing being on the left side of the peak. For this study only selectivity is being evaluated and compared to published results from

section 4.3, therefore peak shape and elution order will not be altered since this will not affect selectivity calculations.

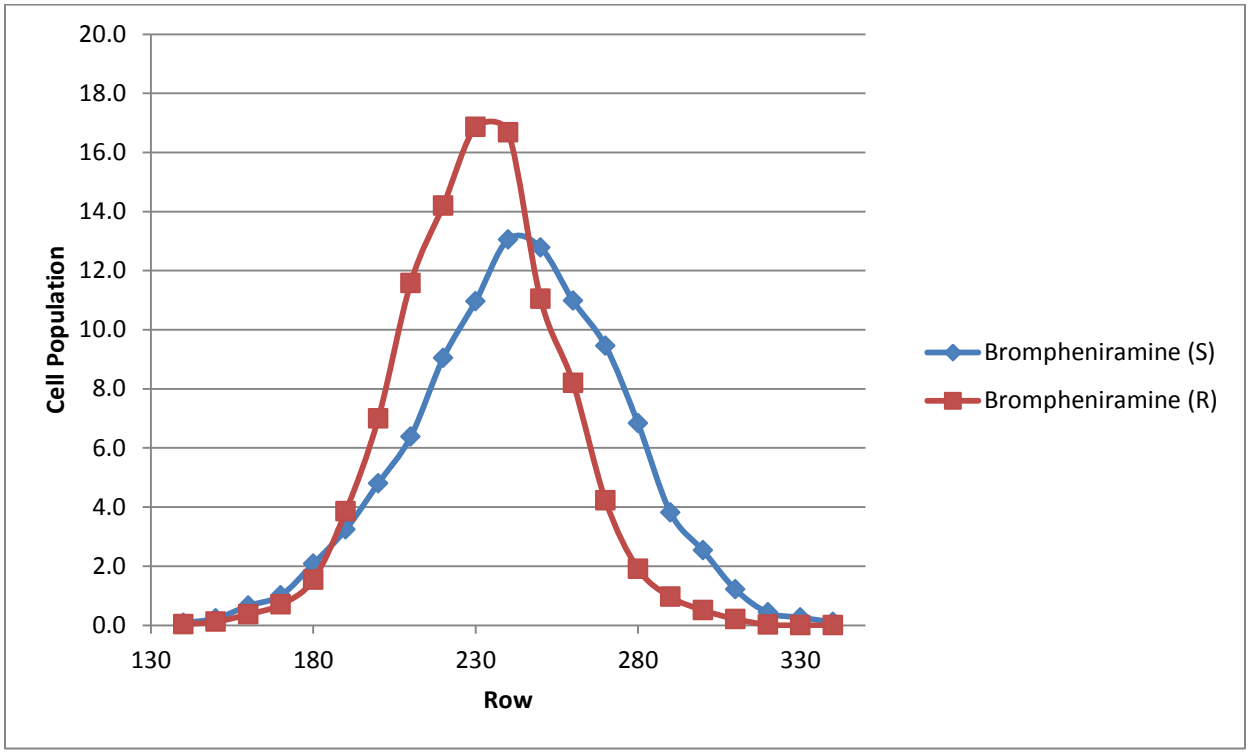

Figure 20: Excel chromatogram of brompheniramine enantiomers without iterations accounted for.

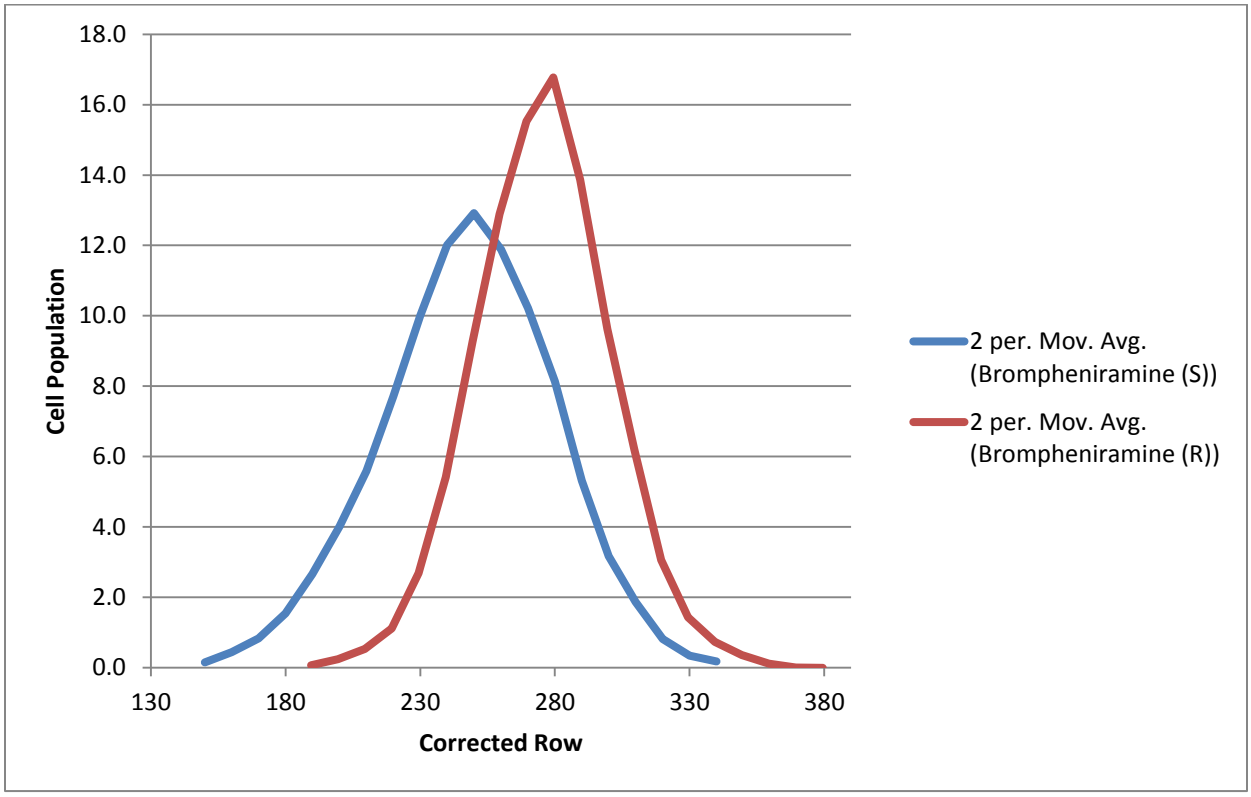

Figure 21: Excel chromatogram of brompheniramine enantiomers.

.

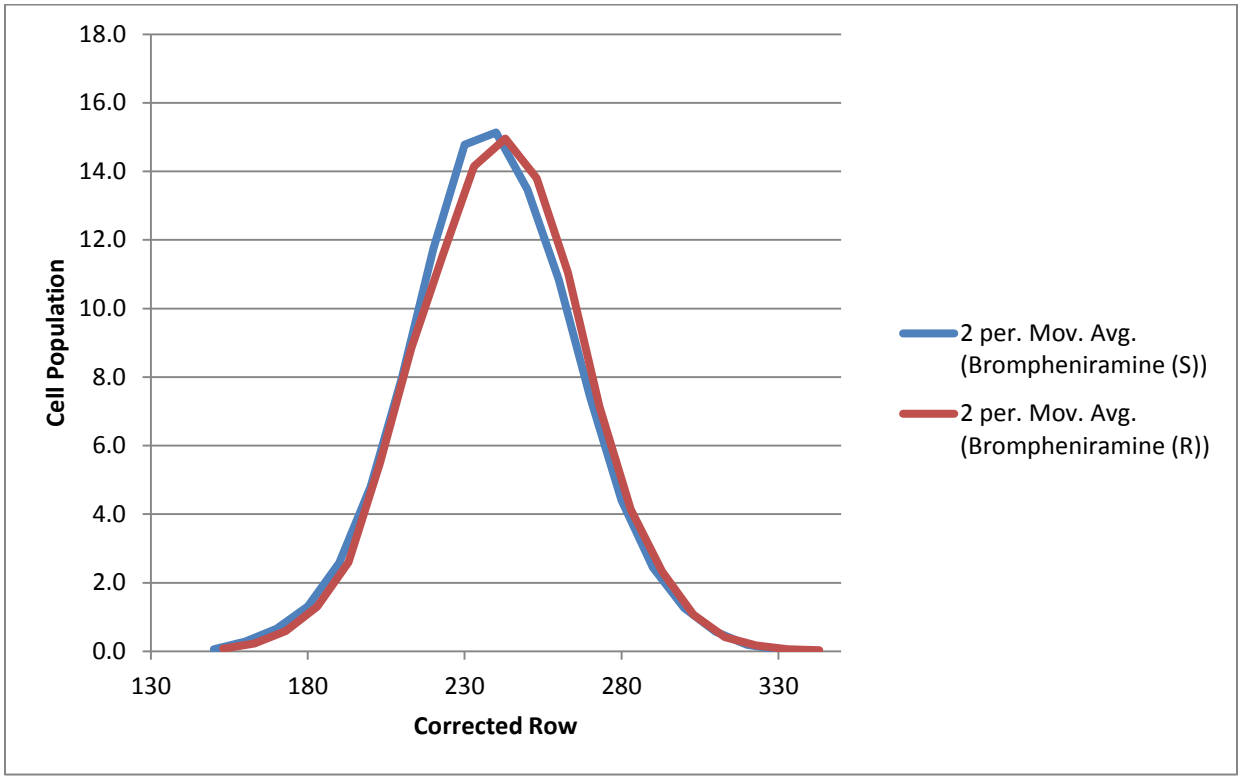

Figure 22: Excel chromatogram of mandelic acid enantiomers.

4.4.1.2 Mandelic acid and brompheniramine results evaluation

In high performance chromatography, the selectivity between peaks on a chromatogram is calculated by:

$$\alpha = k_B^{'} / k_A^{'} \qquad \text{Eq. 13}$$

$k'_B = (t_R - t_0) / t_0$, Retention factor of analyte B

$k'_A = (t_R - t_0) / t_0$, Retention factor of analyte A

t_R, Retention time of analyte

t_0, Void retention time

Since the Excel generated chromatograms are not traditional and do not have a void retention time, selectivity was evaluated by two different techniques. First by finding the row location of the population maximum for the enantiomer from data as in Table 15. The ratio of the row location for each enantiomer set was determined. Another approach was to take the ratio of the number of iterations to elute for the enantiomers. Results were the compared to published results in Table 16.

Table 16: Selectivities of modeled enantiomers vs. published selectivities.

	Selectivity Published	Selectivity by Row	Selectivity by Iteration
Mandelic acid	1.05	1.01	1.01
Brompheniramine	1.13	1.12	1.12

Mandelic acid had a laboratory selectivity of 1.05, resulting in hardly any separation (Durham 1996). Evaluating the model results, selectivity by maximum row population gave a value of 1.01 and by iteration a value of 1.01. While these values are lower than laboratory results, the model accurately predicts that insufficient separation will occur. Brompheniramine has a greater laboratory separation with a selectivity of 1.13, while the model predicts a row and iteration selectivity of 1.12 and 1.12, respectively. Here, the model correctly predicts brompheniramine enantiomer selectivity with greater chromatographic separation. Therefore, the model accurately predicts the lack of chromatographic selectivity in mandelic acid while predicting greater selectivity with brompheniramine enantiomers.

Predicting chromatographic selectivity is useful; however, it does not consider all of the measurements on how well the peaks are separated. Brompheniramine enantiomers have greater selectivity but are still not baseline resolved (see Figure 21). Peak tailing and resolution provide even more information on prediction of peak separation. To accomplish this, more information from the model results is needed.

4.4.2 Cyclohexylphenylglycolic acid model results

4.4.2.1 Interpretation of model data into chromatograms

In predicting the chromatographic separation of cyclohexylphenylglycolic acid enantiomers, more than selectivity is needed. Peak shape needs to be examined. To accomplish this more information from the model is extracted. Along with flow rate, void retention time will be determined. From this, capacity factors will be compared to published values. Tailing factors and resolution will be determined manually from the

Excel chromatograms (see Figures 23 and 24 respectively). With this information, enantiomer separation is examined more closely.

It was previously demonstrated that a run with 60 repetitions produced Excel chromatograms with appropriate peak shape (section 4.4.1.1). To run with a number of repetitions that produces reliable results, but is also efficient, several runs were made and the chromatograms were evaluated. Runs with 10, 50, and 100 repetitions were performed. Ten repetitions resulted in a peak shape that was distorted and not ideal. Although for examining selectivity and a rough estimation for resolution, 10 repetitions may be sufficient. Fifty repetitions had appropriate peak shape with a single maximum and peak tailing. One hundred repetitions did not improve the precision of selectivity and only a slight improvement on peak shape. Therefore 50 repetitions was chosen, and all runs preformed going forward were run this way.

Void retention (I_0 in iterations) was determined by setting breaking probabilities of the analytes equivalent to the mobile phase and determining how many iterations it takes for unretained cells to move through the stationary phase cells beyond row 205. Flow rate (rows/iteration) was then determined by taking the 205 rows the unretained analytes traveled and dividing by the void retention. Retention factors may now be determined:

$$k' = ((I_R - I_0) / I_0) / T \qquad \text{Eq. 14}$$

I_R, Retention iterations of analyte

I_0, Void retention iterations

T, Tailing factor of analyte

The number of retention iterations represents when 99% (or 99 of the 100 cells) are past the last β–cyclodextrin cells at row 204. This is an increase in the percentage of 90% from the previous analysis of mandelic acid and brompheniramine. Measuring at 99% elution from the β–cyclodextrin stationary phase gave greater repeatability of the peak shape; however, the retention iteration is the iteration for elution at the tail end of the peak. To account for peak shape, the retention factor is divided by the tailing factor. Selectivity is now calculated directly from equation 15.

$$\alpha = k_A^{'} / k_D^{'} \qquad \text{Eq. 15}$$

k'_D = Retention factor of analyte D

k'_A = Retention factor of analyte A

As before with mandelic acid and brompheniramine, once an iteration is determined for the average number of cells A, where 99 have moved beyond row 204, all row data for that iteration is imported into Excel. This is repeated for D cells. Every ten rows are summed (see Table 17); however, the difference between time of elution from the stationary phase, the difference in iterations of A (*l*-cyclohexylphenylglycolic acid) and D (*d*-cyclohexylphenylglycolic acid), has not yet been accounted for.

Table 17: Model data output at 24°C of iteration and cell location, A being *l*-cyclohexylphenylglycolic acid, and D *d*-cyclohexylphenylglycolic acid.

Row	Iteration	A	Iteration	D		Row	Iteration	A	Iteration	D
10	9390	0.0	6490	0.0		410	9390	5.9	6490	2.1
20	9390	0.0	6490	0.0		420	9390	6.4	6490	1.4
30	9390	0.0	6490	0.0		430	9390	5.2	6490	0.6
40	9390	0.0	6490	0.0		440	9390	5.8	6490	0.3
50	9390	0.0	6490	0.0		450	9390	5.9	6490	0.1
60	9390	0.0	6490	0.0		460	9390	5.6	6490	0.2
70	9390	0.0	6490	0.0		470	9390	6.0	6490	0.0
80	9390	0.0	6490	0.0		480	9390	5.3	6490	0.0
90	9390	0.0	6490	0.0		490	9390	4.4	6490	0.0
100	9390	0.0	6490	0.0		500	9390	4.1	6490	0.0
110	9390	0.0	6490	0.0		510	9390	3.5	6490	0.0
120	9390	0.0	6490	0.0		520	9390	1.8	6490	0.0
130	9390	0.0	6490	0.0		530	9390	1.5	6490	0.0
140	9390	0.0	6490	0.0		540	9390	1.1	6490	0.0
150	9390	0.1	6490	0.1		550	9390	0.4	6490	0.0
160	9390	0.1	6490	0.1		560	9390	0.3	6490	0.0
170	9390	0.1	6490	0.1		570	9390	0.2	6490	0.0
180	9390	0.2	6490	0.2		580	9390	0.1	6490	0.0
190	9390	0.1	6490	0.2		590	9390	0.0	6490	0.0
200	9390	0.1	6490	0.2		600	9390	0.0	6490	0.0
210	9390	0.2	6490	0.2		610	9390	0.0	6490	0.0
220	9390	0.1	6490	0.2		620	9390	0.0	6490	0.0
230	9390	0.1	6490	0.6		630	9390	0.0	6490	0.0
240	9390	0.2	6490	1.4		640	9390	0.0	6490	0.0
250	9390	0.3	6490	2.8		650	9390	0.0	6490	0.0
260	9390	0.3	6490	3.2		660	9390	0.0	6490	0.0
270	9390	0.7	6490	3.8		670	9390	0.0	6490	0.0
280	9390	0.6	6490	4.8		680	9390	0.0	6490	0.0
290	9390	0.6	6490	5.4		690	9390	0.0	6490	0.0
300	9390	0.7	6490	5.6		700	9390	0.0	6490	0.0
310	9390	1.1	6490	7.1		710	9390	0.0	6490	0.0
320	9390	1.3	6490	8.2		720	9390	0.0	6490	0.0
330	9390	1.6	6490	8.1		730	9390	0.0	6490	0.0
340	9390	2.2	6490	8.2		740	9390	0.0	6490	0.0
350	9390	2.1	6490	7.7		750	9390	0.0	6490	0.0
360	9390	3.3	6490	7.7		760	9390	0.0	6490	0.0
370	9390	3.9	6490	6.6		770	9390	0.0	6490	0.0
380	9390	4.5	6490	6.1		780	9390	0.0	6490	0.0
390	9390	5.9	6490	3.9		790	9390	0.0	6490	0.0
400	9390	6.0	6490	2.9		800	9390	0.0	6490	0.0

Enantiomer population row position is now determined by knowing the enantiomer iteration, row position, and void iteration :

$$Row_A = Row \times (I_R - I_0)/10000 \qquad \text{Eq. 16}$$

Row_A, Row relative position adjusted for iteration

Row, Row position unadjusted

I_R, Retention iterations of analyte

I_0, Void retention iterations

10000, factor to normalize Row_A to a manageable number

With the row position now representing a relative position to the time the enantiomers were retained by the stationary phase to each other and the void retention (see Table 18), Excel chromatograms are generated for cyclohexylphenylglycolic acid using a “X Y (Scatter)” chart with straight lines and a moving average of 6 (see Figure 25). Using a straight line plot gave point to point lines, making it difficult to determine the peak tangent lines for calculation of resolution (see Figure 24). A moving average of 6 was used in the Excel plots to better define the peaks curvature that eliminated this problem. Note that the peaks are reversed in shape with tailing being on the left side of the peak. To correct this, the row populations of each enantiomer are reversed and re-plotted resulting in a more conventional chromatogram (see Figure 26).

Table 18: Model data output at 24°C of adjusted cell location for retention, A being *l*-cyclohexylphenylglycolic acid, and D *d*-cyclohexylphenylglycolic acid.

Row	Row adjusted for Retention	A	Row adjusted for Retention	D		Row	Row adjusted for Retention	A	Row adjusted for Retention	D
10	8	0.0	5	0.0		410	318	5.9	199	2.1
20	16	0.0	10	0.0		420	326	6.4	204	1.4
30	23	0.0	15	0.0		430	334	5.2	209	0.6
40	31	0.0	19	0.0		440	341	5.8	214	0.3
50	39	0.0	24	0.0		450	349	5.9	219	0.1
60	47	0.0	29	0.0		460	357	5.6	224	0.2
70	54	0.0	34	0.0		470	365	6.0	228	0.0
80	62	0.0	39	0.0		480	372	5.3	233	0.0
90	70	0.0	44	0.0		490	380	4.4	238	0.0
100	78	0.0	49	0.0		500	388	4.1	243	0.0
110	85	0.0	53	0.0		510	396	3.5	248	0.0
120	93	0.0	58	0.0		520	404	1.8	253	0.0
130	101	0.0	63	0.0		530	411	1.5	258	0.0
140	109	0.0	68	0.0		540	419	1.1	262	0.0
150	116	0.1	73	0.1		550	427	0.4	267	0.0
160	124	0.1	78	0.1		560	435	0.3	272	0.0
170	132	0.1	83	0.1		570	442	0.2	277	0.0
180	140	0.2	87	0.2		580	450	0.1	282	0.0
190	147	0.1	92	0.2		590	458	0.0	287	0.0
200	155	0.1	97	0.2		600	466	0.0	292	0.0
210	163	0.2	102	0.2		610	473	0.0	296	0.0
220	171	0.1	107	0.2		620	481	0.0	301	0.0
230	178	0.1	112	0.6		630	489	0.0	306	0.0
240	186	0.2	117	1.4		640	497	0.0	311	0.0
250	194	0.3	122	2.8		650	504	0.0	316	0.0
260	202	0.3	126	3.2		660	512	0.0	321	0.0
270	210	0.7	131	3.8		670	520	0.0	326	0.0
280	217	0.6	136	4.8		680	528	0.0	330	0.0
290	225	0.6	141	5.4		690	535	0.0	335	0.0
300	233	0.7	146	5.6		700	543	0.0	340	0.0
310	241	1.1	151	7.1		710	551	0.0	345	0.0
320	248	1.3	156	8.2		720	559	0.0	350	0.0
330	256	1.6	160	8.1		730	566	0.0	355	0.0
340	264	2.2	165	8.2		740	574	0.0	360	0.0
350	272	2.1	170	7.7		750	582	0.0	365	0.0
360	279	3.3	175	7.7		760	590	0.0	369	0.0
370	287	3.9	180	6.6		770	598	0.0	374	0.0
380	295	4.5	185	6.1		780	605	0.0	379	0.0
390	303	5.9	190	3.9		790	613	0.0	384	0.0
400	310	6.0	194	2.9		800	621	0.0	389	0.0

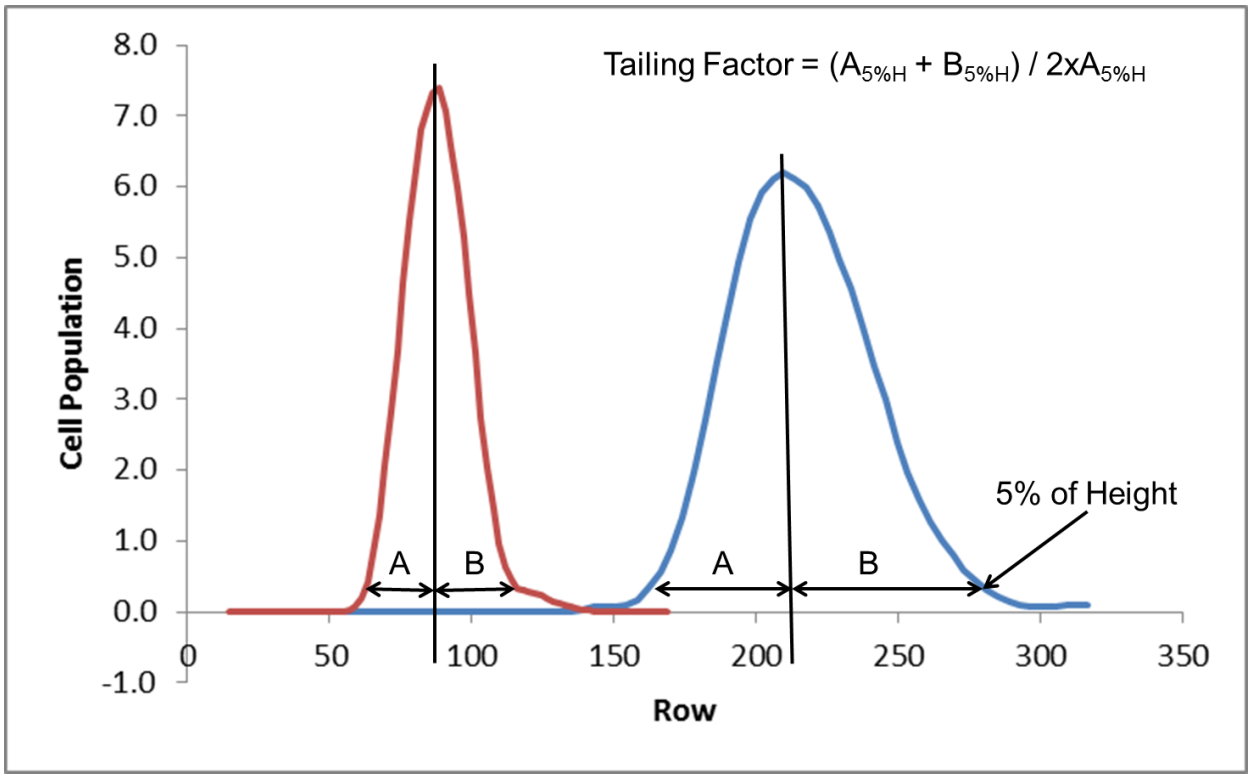

Figure 23: Technique of manual calculation of tailing factor on Excel chromatogram.

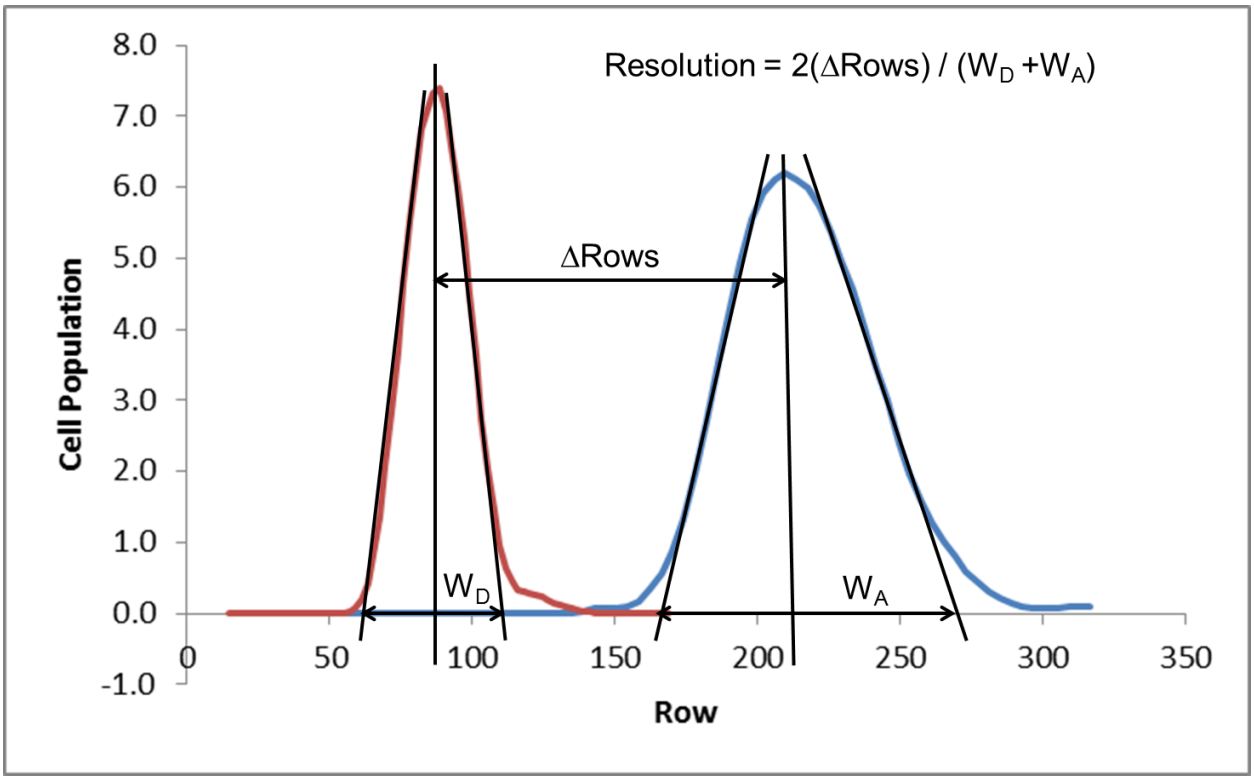

Figure 24: Technique of manual calculation of resolution on Excel chromatogram.

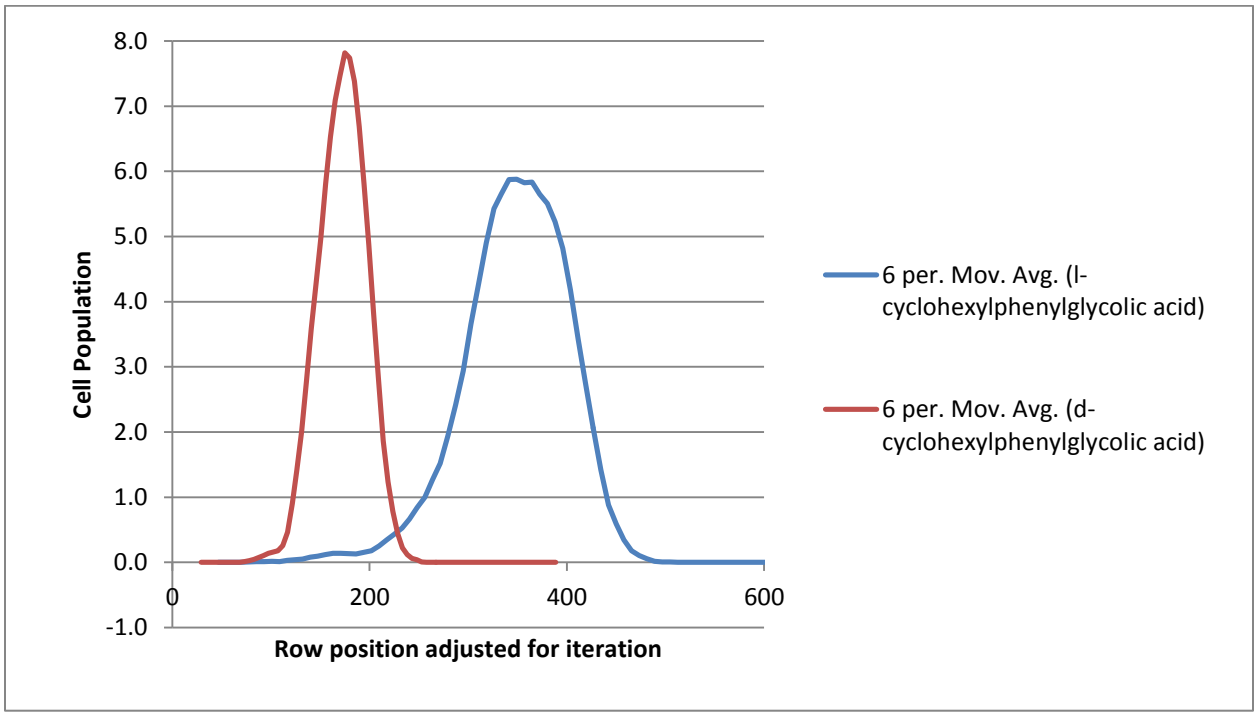

Figure 25: Excel chromatogram of cyclohexylphenylglycolic acid enantiomers at 24°C with inverted cell populations.

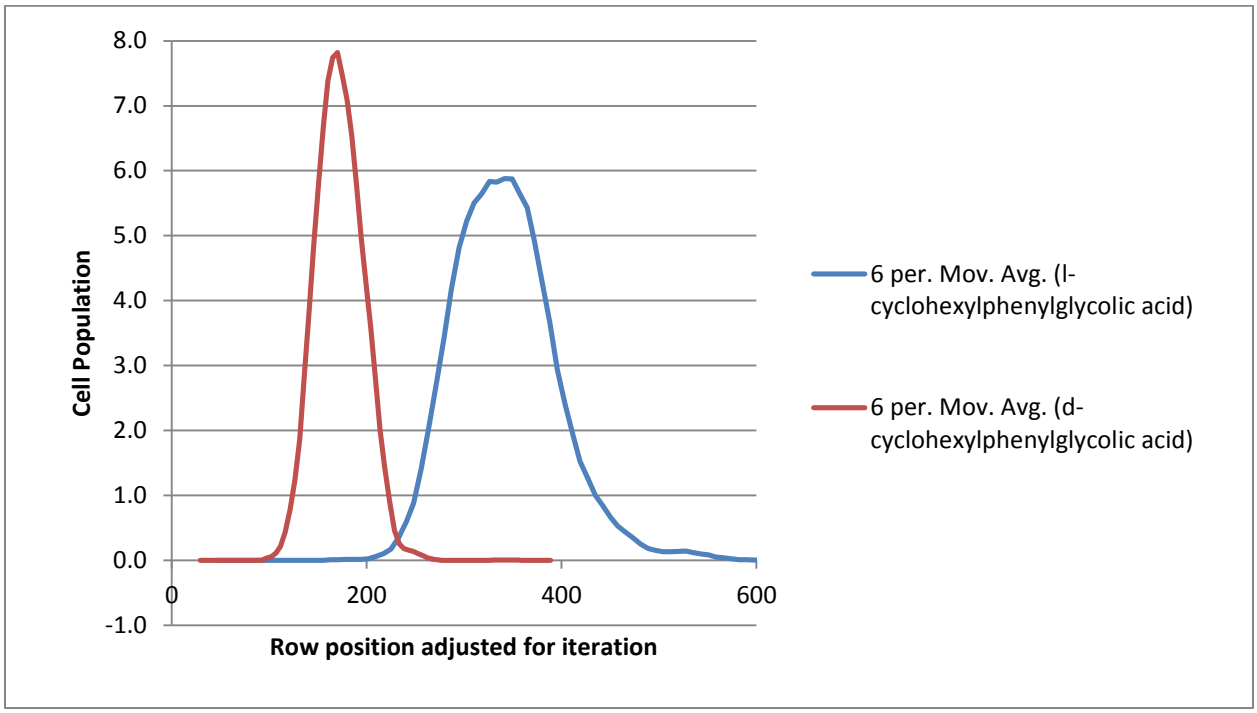

Figure 26: Excel chromatogram of cyclohexylphenylglycolic acid enantiomers at 24°C.

4.4.2.2 System temperature variation

When complexes form between the enantiomers of cyclohexylphenylglycolic acid with β-cyclodextrin, the strength of those complexes can be affected by temperature (Hinze 1981). Because interactions of analytes with the interior of β-cyclodextrin are slow relative to other chromatographic interactions (Feitsma, Zeeuw et al. 1985), slower mass transfer between the enantiomers and the interior of the β-cyclodextrin can affect the resolution of the enantiomers. Higher temperatures can increase the speed of this mass transfer, decreasing retention time while increasing peak resolution as in the modeled chromatographic conditions of 24°C and 57°C (see Figures 26 and 27). This was demonstrated in the laboratory (Feitsma, Zeeuw et al. 1985). The chromatographic system in Feitsma's was run at 24, 31, 37, 44, 50, and 57 degrees Celsius. Using the solvent cell populations from Table 1 and model probabilities and factors from Table 8, the model was run at these temperatures.

Model results and published laboratory results (Feitsma, Zeeuw et al. 1985) are compared in Table 19 and Figure 28.

Table 19: Chromatographic resolution of cyclohexylphenylglycolic acid enantiomers vs. temperature.

Temperature, °C	24	31	37	44	50	57
Lab Resolution	1.41	1.47	1.47	1.57	1.53	1.63
Model Resolution	1.24	1.32	1.35	1.46	1.53	1.64
Lab Resolution calculated	1.14	1.25				1.51

It was first observed that the model predicted enantiomer resolutions did increase with an increase in modeled temperature, as in the laboratory results. However, the slopes of the model resolutions differed from laboratory results at 0.012 vs. 0.006 respectively. As can be seen in Figure 28, the plots of laboratory and model resolutions do not overlap. In fact the greatest difference is at the lowest temperature of 24°C. This difference decreases as the temperature is increased, with the laboratory and model results converging at 50°C. Upon examination of the laboratory results, it was discovered that peak resolution was calculated assuming a Gaussian shaped peak (Feitsma, Zeeuw et al. 1985) using the equation:

$$R = (t_{R,l} - t_{R,d}) / 2(\sigma_l + \sigma_d) \qquad \text{Eq. 17}$$

R, Resolution

$t_{R,l}$, Retention time of l-cyclohexylphenylglycolic acid

$t_{R,d}$, Retention time of d-cyclohexylphenylglycolic acid

σ_l, Peak width of l-cyclohexylphenylglycolic acid at ½ peak height

σ_d, Peak width of d-cyclohexylphenylglycolic acid at ½ peak height

Of the three chromatograms provided in the publication at different temperatures (24, 31, and 57°C), they were found to have tailing factors that ranged from 3.9 to 2.3. The assumption of a Gaussian shaped peaked therefore appeared non-ideal. The chromatograms from the publication were enlarged on a copy machine and the resolutions were calculated manually using the technique from Figure 24. It was found

that the laboratory resolutions where now lower than the previously reported laboratory resolutions, with a slope of 0.011. The change in model resolution was now more parallel to laboratory results. Model results also fall in between the two different techniques of interpreting reported laboratory resolutions.

There was still the question as to why model results and reported laboratory results converge as temperatures increase, agreeing at 50 and 57°C. Laboratory chromatograms show that d-cyclohexylphenylglycolic acid tailing factor decreases from 3.88 at 31°C to 2.25 at 57°C. While l-cyclohexylphenylglycolic acid decreased slightly from 2.67 to 2.50. Therefore the peaks are becoming more Gaussian at higher temperatures and equation 17 is more appropriate to use as temperatures increase. As the peaks become more Gaussian, resolution values from equation 17 will approach values calculated from baselines peak widths as in the model.

Since higher temperatures decrease retention time of the enantiomers by increasing the speed of mass transfer, selectivity between the peaks may decrease as temperature increases. This was demonstrated in the laboratory (Feitsma, Zeeuw et al. 1985). Model results and published laboratory results are compared in Table 20 and Figure 29. Selectivity values of the model are nearly equivalent to the laboratory values as seen in Table 20. When plotted vs. temperature, the decreasing slope of selectivities with increasing temperature of both laboratory and model results nearly overlap with identical slopes of -0.005.

Table 20: Chromatographic selectivity of cyclohexylphenylglycolic acid enantiomers vs. temperature.

Temperature, °C	24	31	37	44	50	57
Lab Selectivity	1.57	1.53	1.50	1.47	1.44	1.40
Model Selectivity	1.56	1.53	1.50	1.48	1.42	1.38

Model resolution values fall between two different techniques of interpreting laboratory peak resolution and the differences between model and laboratory results are explainable due to peak shape. Therefore, it is correct in concluding that the model accurately predicts the resolution of cyclohexylphenylglycolic acid enantiomers under varying temperature conditions. Additionally, the model accurately predicts the selectivity of the laboratory chromatographic results. By this technique, the separation of cyclohexylphenylglycolic acid enantiomers can be modeled for chromatographic temperature optimization.

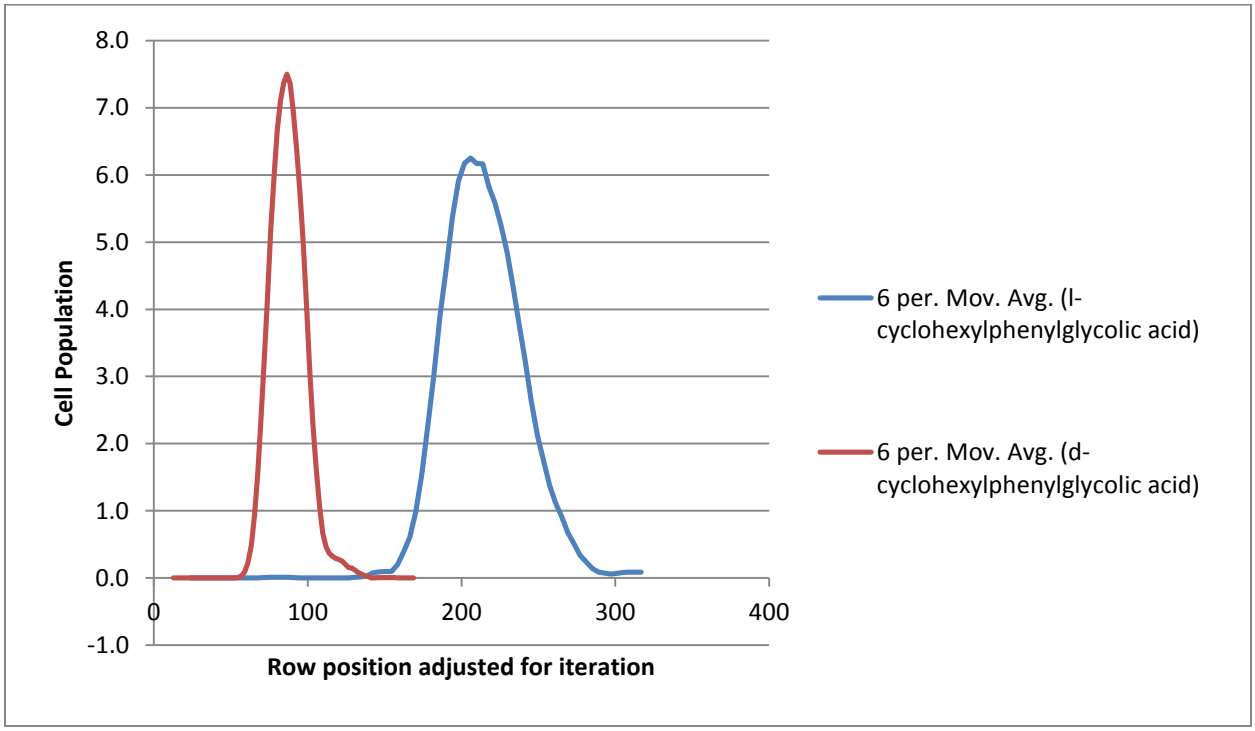

Figure 27: Excel chromatogram of cyclohexylphenylglycolic acid enantiomers at 57°C.

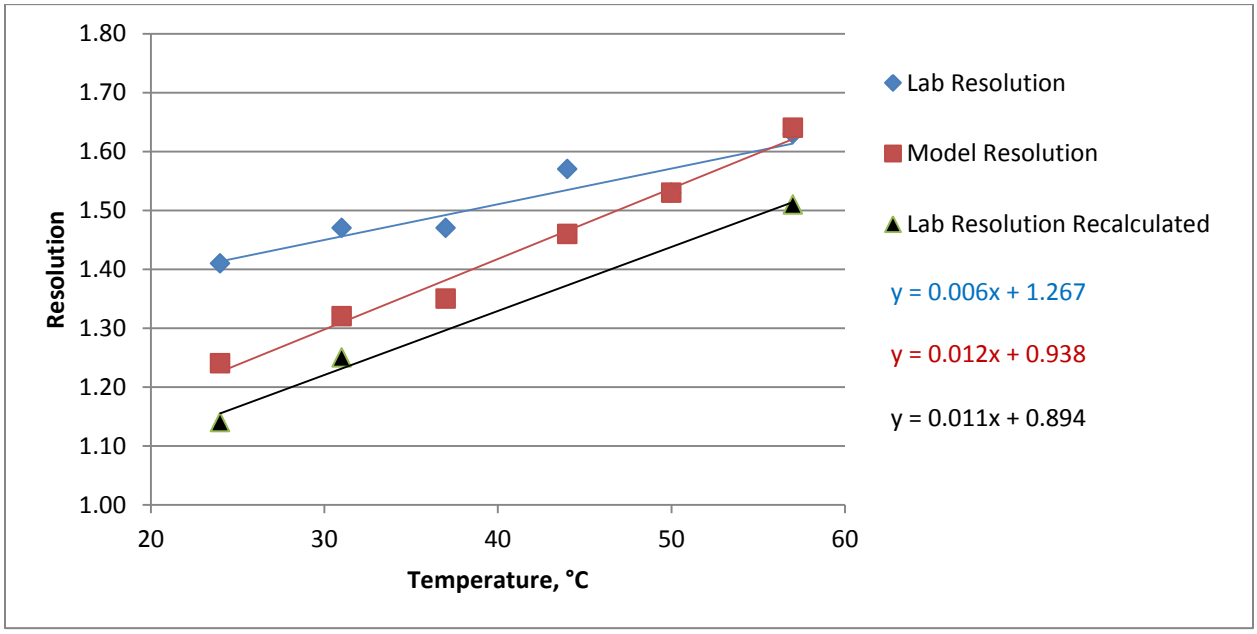

Figure 28: Chromatographic resolution of cyclohexylphenylglycolic acid enantiomers vs. temperature.

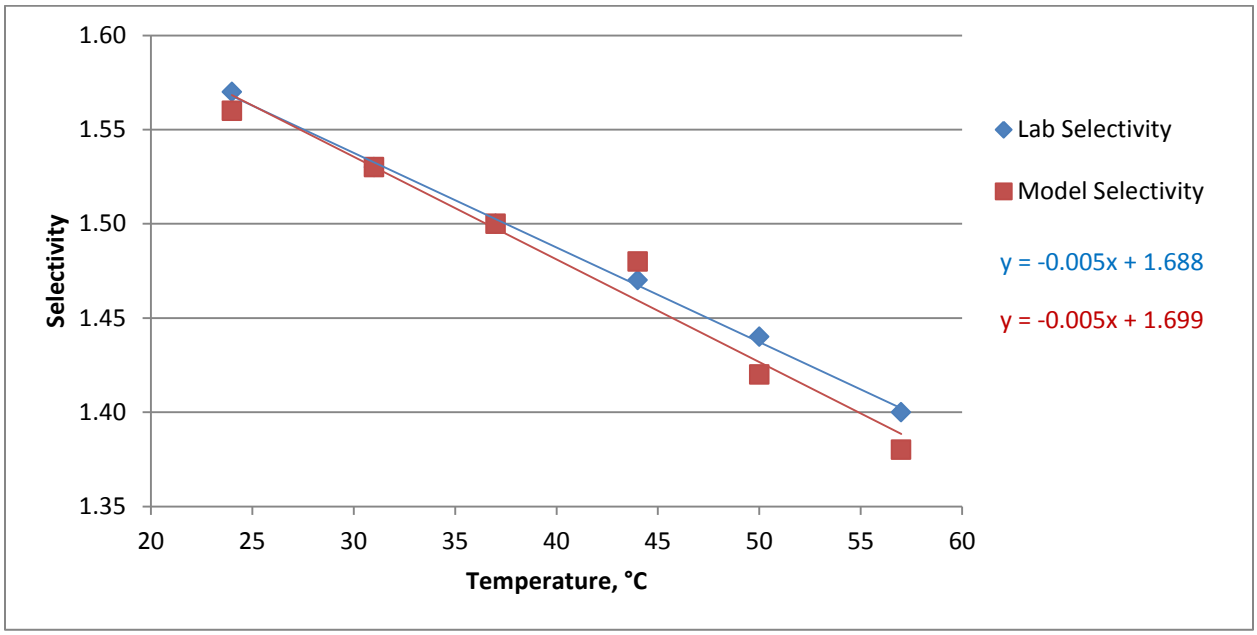

Figure 29: Chromatographic selectivity of cyclohexylphenylglycolic acid enantiomers vs. temperature.

4.4.2.3 Mobile phase flow variation

Although not evaluated in the laboratory separation of cyclohexylphenylglycolic acid enantiomers (Feitsma, Zeeuw et al. 1985), mobile phase flow impacts peak retention. How the model responds to an increase and decrease in mobile phase flow would be valuable to evaluate verses conventional chromatography behavior. The model has been run with a gravity factor of 2.0 (see section 2.4.1) representing the laboratory conditions of 1.0 mL/min. Flow will be modeled at ± 25% 1.0 mL/min, or a gravity factor of 1.5 and 2.5 for all mobile phase cells and analyte cells. In theory, selectivity, resolution, and tailing factors should not significantly change in a patterned manner. Although random fluctuation in these should be expected. Capacity factors of the peaks should increase with flow rate since the void volume is solely dependent on flow rate and analytes are dependent on flow rate and stationary phase retention that does not change proportionally with flow rate. The mobile phase flow was altered and runs were performed under conditions of from section 3.3.3.3-4 at 24°C. Results are summarized in Table 21.

Table 21: Modeled peak separation properties of cyclohexylphenylglycolic acid enantiomers at varying mobile phase flow rates

	d-cyclohexylphenylglycolic acid			l-cyclohexylphenylglycolic acid		
	75%	100%	125%	75%	100%	125%
Selectivity	1.44	1.56	1.51			
Resolution	1.11	1.24	1.40			
Tailing factor	1.12	1.13	1.10	1.15	1.15	1.15
Capacity factor	2.97	2.98	3.54	4.39	4.76	5.60

Selectivity between the cyclohexylphenylglycolic acid enantiomers should not decrease or increase in a particular direction with changes in flow rate, since flow rate should affect enantiomer retention nearly equally. At 75% of normal flow rate the selectivity decreased from 1.56 at 100% flow rate to 1.44; however, at a flow rate of 125% selectivity decreased to 1.51. Therefore, no pattern of change was observed and is consistent normal chromatographic behavior.

Resolution between the enantiomers increased steadily from 1.11 to 1.40 as mobile phase increased from 75% to 125%. At first this seams inconsistent with what would be expected. Examining factors that contribute to peak resolution, it's seen that selectivity was greater for 100% and 125% flow rates, which will increase peak resolution. Additionally, with a 125% flow rate, the tailing factor for d-cyclohexylphenylglycolic acid decreased to 1.10 versus the other flow rates of 75% and 100%, 1.12 and 1.13 respectively. This will further increase the resolution between the peaks. It appears that increases in peak resolution as flow rate increases is not a result of the mobile phase flow rate, but the result of random fluctuations in the selectivity and tailing factors.

Tailing factors for l-cyclohexylphenylglycolic acid remained constant at 1.15 throughout the mobile phase flow changes. While d-cyclohexylphenylglycolic acid had tailing factors that fluctuated slightly with no pattern.

Capacity factors were determined by:

$$k' = \frac{V_R - V_0}{V_0} \qquad \text{Eq. 18}$$

k', Capacity factor

V_R, Retention volume = retention iteration x flow rate (rows/iteration)

V_0, Void volume = void retention x flow rate (rows/iteration)

Capacity factors should increase with flow rate. Additionally, analytes that are retained longer should have capacity factors that increase more than peaks with less retention since their retention volume is less impacted by flow rate due to slower mass transfer with the stationary phase. d-cyclohexylphenylglycolic acid elutes first and had a capacity factor increase from 2.97 to 3.54, or a 119% overall increase from a flow rate of 75% to 125%. l-cyclohexylphenylglycolic acid elutes last and had a capacity factor increase from 4.39 to 5.60, or a 128% increase. Capacity factor changes were constant with what would be anticipated in a high performance liquid chromatography system.

4.4.2.4 Mobile phase pH variation

Changes in pH have been shown to have an effect on the chromatographic separation of cyclohexylphenylglycolic acid (Feitsma, Zeeuw et al. 1985). Mandelic acid, which is structurally similar, was previously modeled in section 4.4.1.2, where selectivity was shown to be mainly dependent on the interactions of the alpha hydroxyl acid with the secondary hydroxyl groups of the β-cyclodextrin. It is not unexpected then that the chromatographic separation of mandelic acid, with a pka of 3.85 (Weast 1988), is influenced by pH. Using the same buffered mobile phase (pH of 4.2) from the separation of cyclohexylphenylglycolic acid enantiomers, mandelic acid enantiomers

separated very slightly. When the pH was increased to 6.5, the mandelic acid enantiomers were no longer separated (Feitsma, Zeeuw et al. 1985).

Cyclohexylphenylglycolic acid only differs from mandelic acid by the substitution of the hydrogen on the chiral carbon of mandelic acid with cyclohexane. At a pH of 4.2 the enantiomers of cyclohexylphenylglycolic acid separate under laboratory conditions (Feitsma, Zeeuw et al. 1985) with a resolution of 1.14 (see Table 22). When the pH of the phosphate buffer in the mobile phase is raised to 6.5, the resolution of the peaks decreases to 0.67 under laboratory conditions. Although not fully understood, it was hypothesized by the authors that this is the result from differences in dissociations of the alpha hydroxy acids. This results in a change of hydrogen bonding with the secondary hydroxyl groups of the β-cyclodextrin, stronger for mandelic acid and cyclohexylphenylglycolic acid at a pH of 4.2 and weaker at 6.5. This hypothesis will be investigated by modeling changes in the breaking probability from section 3.3.3.3 of A0 and D0 (alpha hydroxy acid portion of cyclohexylphenylglycolic acid) with cell B0 (secondary hydroxyl groups of the β-cyclodextrin) from 0.05 for strong interaction to 0.50, a neutral interaction. Results of this model can be found in Table 22 and Figure 30.

Table 22: The effect of pH on peak resolution and selectivity of cyclohexylphenylglycolic acid enantiomers.

pH	4.2	6.5
Lab Resolution	1.14	0.67
Model Resolution	1.24	0.57
Lab Selectivity	1.57	1.29
Model Selectivity	1.56	1.06

Both the laboratory and model's resolution decreased significantly from a mobile phase pH of 4.2 to 6.5. The resolution differences between the laboratory and model results are small (±0.1) at both pHs. As can be seen visually in the Excel chromatograms (Figure 26 for pH 4.2 and Figure 30 for pH 6.5), at a pH of 4.2 the cyclohexylphenylglycolic acid enantiomer peaks are clearly retained longer based on row position and peak overlap versus a pH 6.5. Peak retention change is also consistent with laboratory results (Feitsma, Zeeuw et al. 1985), retention times decreasing with a pH of 6.5.

Peak selectivity was likewise compared. At a pH of 4.2, both the laboratory model results had a selectivity of 1.6. When the pH of the mobile phase was changed to 6.5, laboratory selectivity decreased to 1.3, while the model selectivity decreased to 1.1. Although slightly different, the selectivity results both decreased significantly.

Based on the model's changes in peak resolution and selectivity at different pH, results agree with laboratory outcomes. The model's results support the hypothesis that a change in hydrogen bonding between the alpha hydroxy acid group of cyclohexylphenylglycolic acid with the secondary hydroxyl groups of the β-cyclodextrin

plays a role in the enantiomeric separation. To verify this experimentally, cyclohexylphenylglycolic acid could be structurally altered to replace the carboxylic acid and hydroxyl group with structures incapable of hydrogen binding while maintaining the chiral center and not causing steric interference that might change the interaction with β-cyclodextrin. Run under the same chromatographic system, the separation should be similar to that of cyclohexylphenylglycolic acid at a pH of 6.5.

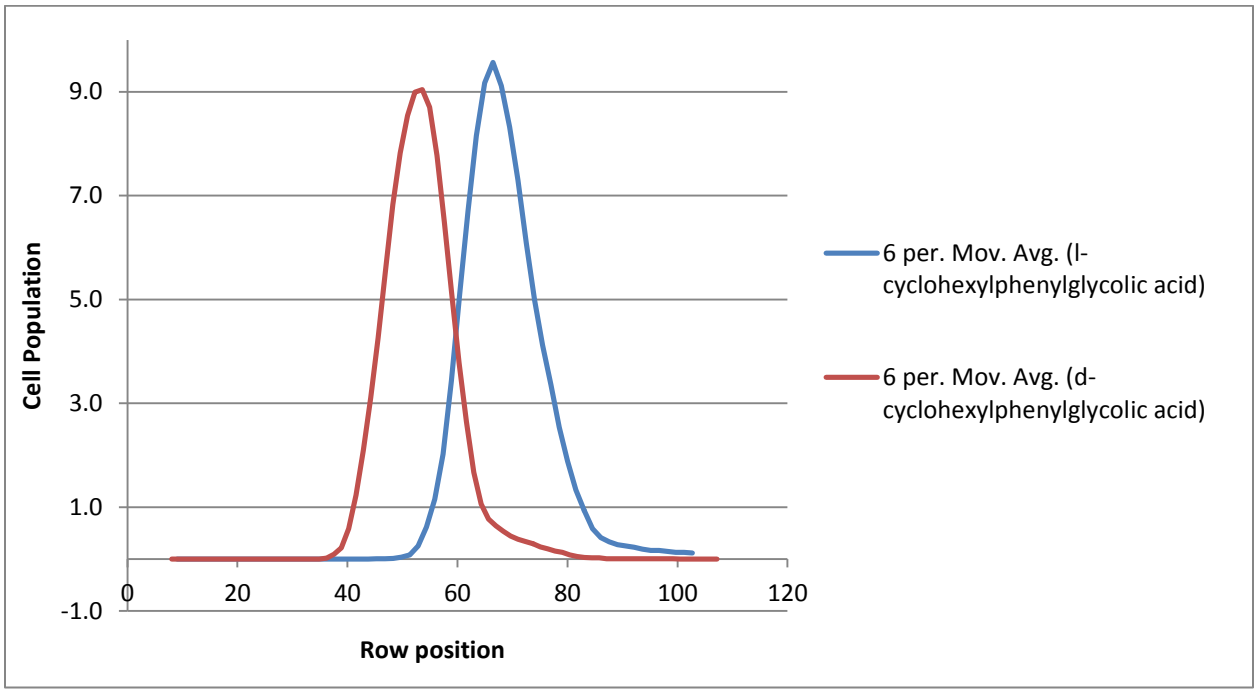

Figure 30: Excel chromatogram of cyclohexylphenylglycolic acid enantiomers at pH 6.5.

4.4.2.5 *Lowering sample injection vs. retention times*

In high performance liquid chromatography, retention of analytes on the stationary phase is affected by many factors. Selection of the proper stationary phase and mobile phase are critical; however, there are some factors that effect analyte retention that are not as easily to understand. In a linear chromatographic system, the distribution of analyte in the column is represented by (Jonsson 1996):

$$c_S = K_C \times c_M \qquad \text{Eq. 19}$$

c_s, Concentration of analyte in stationary phase

c_M, Concentration of analyte in mobile phase

K_C, Distribution constant

As can be seen from equation 19, analyte movement through the column should not be impacted by overall analyte concentration resulting in a linear isotherm. Under ideal conditions, changes in sample concentration should not change the analytes retention time.

In chromatographic systems where there is peak tailing, convex adsorption isotherms typically predominate resulting in increased retention time with decreased sample amounts (Heftmann 1983). However, when sample amounts are low, all distribution isotherms are likely to be linear (Jonsson 1996).

It has been observed with cyclohexylphenylglycolic acid enantiomers that as the amount of sample injected onto the column is reduced, the retention time of the analytes increases (Feitsma, Zeeuw et al. 1985). At the lowest concentrations the increase in retention time is greatest and still increasing in a non-linear manner. This phenomenon is not explained by traditional convex isotherms, since at lower concentrations the adsorption isotherm should become linear (Jonsson 1996).

Laboratory conditions involved injecting approximately 11μg of each cyclohexylphenylglycolic acid enantiomer onto the chromatographic system and sequentially reducing the amount in half, for concentration values of 100, 50, 25, 12.5, 6.3, 3.1, and 1.6 percent of the original concentration. To model this, enantiomer concentrations were changed similarly in concentration. The number of cells for each enantiomer has been 100 for each (see section 2.4.2). Enantiomer cell concentrations were reduced from 100 to 50, 25, 13, 6, 3, and 2 cells.

Determining retention time of enantiomers in the model could no longer be determined by 99% elution and peak shape as has been done to this point, since at lower cell concentration (i.e. 2 and 3 cells) there is no tradition peak shape. At these low levels of enantiomer cells, there is no cell population distribution to plot in Excel. Instead, retention time will be relatively compared by determining the iteration when the average cell concentration of one cell is past the stationary phase or beyond row 205. Using this approach, all cell concentrations can be compared in the same manner.`

Model results at the different concentrations were then compared to published laboratory results (see Table 23).

Table 23: Impact on enantiomer retention from amount injected into the stationary phase.

Relative Concentration	2	3	6	13	25	50	100
d-CHPGA lab retention	1.14	1.13	1.11	1.09	1.06	1.03	1.00
l-CHPGA lab retention	1.20	1.17	1.15	1.11	1.08	1.04	1.00
d-CHPGA model retention	1.35	1.24	1.19	1.11	1.06	1.05	1.00
l-CHPGA model retention	1.60	1.45	1.27	1.17	1.12	1.05	1.00

Sample amounts were relative to the 100% level (100 cells for each enantiomer) and rounded to eliminate decimals, since cell population must be modeled in integer values. For laboratory results, retention times were normalized against the retention at 100% sample concentration. Model retention iterations were normalized against the retention at 100 cell population. In both the laboratory and model results, the retention of the enantiomers increased as sample amount decreased. As can be seen in Figure 31, the model's retention was nearly identical to laboratory results until relative concentration levels reached 6% and below. Unlike laboratory conditions where dilution levels of 2% still result in many analyte molecules interacting, the model is limited to just 2 analyte cells. The model does predict the increase in retention with changes in analyte concentration; however, it's accuracy of the degree of change is limited when less than 13 cells were modeled.

There was peak tailing under all conditions (Feitsma, Zeeuw et al. 1985) in the chromatographic system studied, therefore, convex adsorption isotherms appear to drive the retention. Yet, even at the most diluted samples the isotherms do not become linear as would be expected (Jonsson 1996). This observation was not explainable by

the authors. With all other parameters being held constant, it was only the sample concentration that was changing and affecting retentions. The question is asked, since analytes have the ability to interact with each other, if the tendency towards analyte-to-analyte interaction changes, does this impact the retention of analytes and how would this affect a convex isotherm?

Previous model runs had a breaking probability between enantiomers of 0.5, meaning there is equal attraction and repulsion force between them. These breaking probabilities between enantiomer cells A0-3 and B0-3 will be changed to have less interaction between themselves with a value of 0.80. Analytes will be modeled for greater interaction between themselves with breaking probabilities of 0.20 and 0.35. Model runs and their interpretation will be the same as before. Run results are summarized in Table 24.

Table 24: Impact on enantiomer retention from amount injected into the stationary phase at varying analyte-to-analyte breaking probabilities.

Relative amount	2	3	6	13	25	50	100
d-CHPGA lab retention	1.14	1.13	1.11	1.09	1.06	1.03	1.00
d-CHPGA model retention, PB = 0.20	1.23	1.16	1.08	1.04	1.01	1.00	1.00
d-CHPGA model retention, PB = 0.35	1.31	1.23	1.10	1.07	1.03	1.01	1.00
d-CHPGA model retention, PB = 0.50	1.35	1.24	1.19	1.11	1.06	1.05	1.00
d-CHPGA model retention, PB = 0.80	1.38	1.30	1.21	1.11	1.08	1.04	1.00
l-CHPGA lab retention	1.20	1.17	1.15	1.11	1.08	1.04	1.00
l-CHPGA model retention, PB = 0.20	1.32	1.27	1.13	1.05	1.01	1.00	1.00
l-CHPGA model retention, PB = 0.35	1.50	1.33	1.23	1.13	1.05	1.03	1.00
l-CHPGA model retention, PB = 0.50	1.60	1.45	1.27	1.17	1.12	1.05	1.00
l-CHPGA model retention, PB = 0.80	1.64	1.50	1.34	1.18	1.10	1.06	1.00

Changing the strength of the interactions between enantiomers had an impact on the phenomenon of increasing retention time with decreased sample amounts. This can best be examined by looking at how the individual enantiomers changed versus laboratory results graphically (see Figures 32 and 33).

In Figure 32, the initial breaking probability conditions for d-cyclohexylphenylglycolic acid enantiomer-to-enantiomer interactions are displayed versus the laboratory results. As before, the model values for relative retention versus the 100% original amount of the enantiomer agrees with laboratory conditions at samples amounts greater 6%. When the breaking probability of enantiomer interactions is increased to 0.80, modeling less enantiomer interactions, the relative retention values do not change significantly from a breaking probability of 0.50. It may be that once repulsion between analytes reaches a certain strength and rapidly become dispersed in mobile phase, retention becomes solely driven by interactions with the stationary phase since analyte cells are no longer near each other. Therefore continuing to increase the analyte-to-analyte repulsion has minimal impact.

At sample amounts greater 6% the values remain similar to laboratory results, and at 6% and less retention increases significantly. When the analyte-to-analyte breaking probability is lowered to 0.20 and 0.35 the results change.

A breaking probability of 0.20 represents a stronger attraction between cyclohexylphenylglycolic acid cells. Model results show that this type of attraction shows no change in relative retention with dilution of the sample down to 25%. In this range there appears to be a linear isotherm. At dilution values of 13 and 6%, relative

retention begins to increase but is still below laboratory results. Not until dilution values of 3 and 2% do model values exceed experimental results and retain similarly as they did at higher breaking probabilities. A breaking probability of 0.35 was modeled for the enantiomer with relative retention results falling between the breaking probabilities of 0.20 and 0.50. Depicting a movement from a linear to a convex adsorption isotherm. Similar results were found for l-cyclohexylphenylglycolic acid in Figure 33.

This phenomenon is not explained by just a convex isotherm. Although a convex isotherm is present, it is proposed that analyte-to-analyte interaction is playing a role in retention in addition to a convex isotherm adsorption of analyte-to-stationary phase. As the attraction between analytes increases there is less of an increase in overall relative retention as sample amounts decreased. Additionally, as the sample concentration becomes so low that analyte-to-analyte interactions become less likely to occur, the less significant analyte attraction has on retention. Since changing the interactive forces between enantiomers would involve changing the mobile phase composition to make the environment more or less likely for solvation of the enantiomers, hence affecting analyte retention, this phenomenon would be difficult to analyze under laboratory conditions.

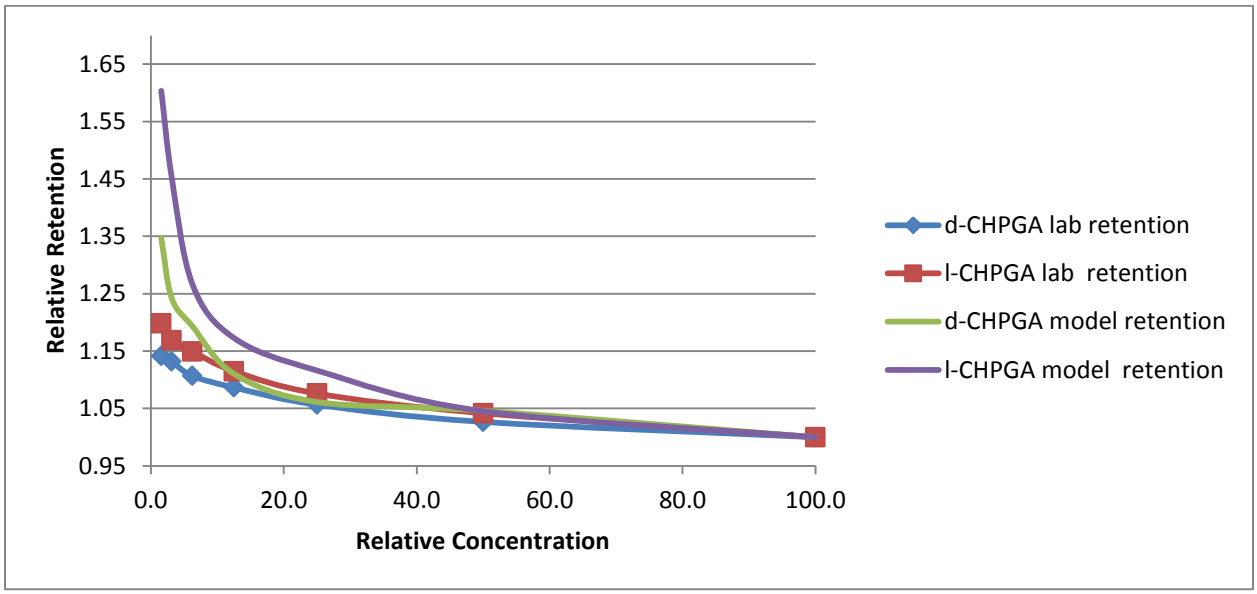

Figure 31: Relative concentration of enantiomers versus their relative retention under laboratory and model conditions.

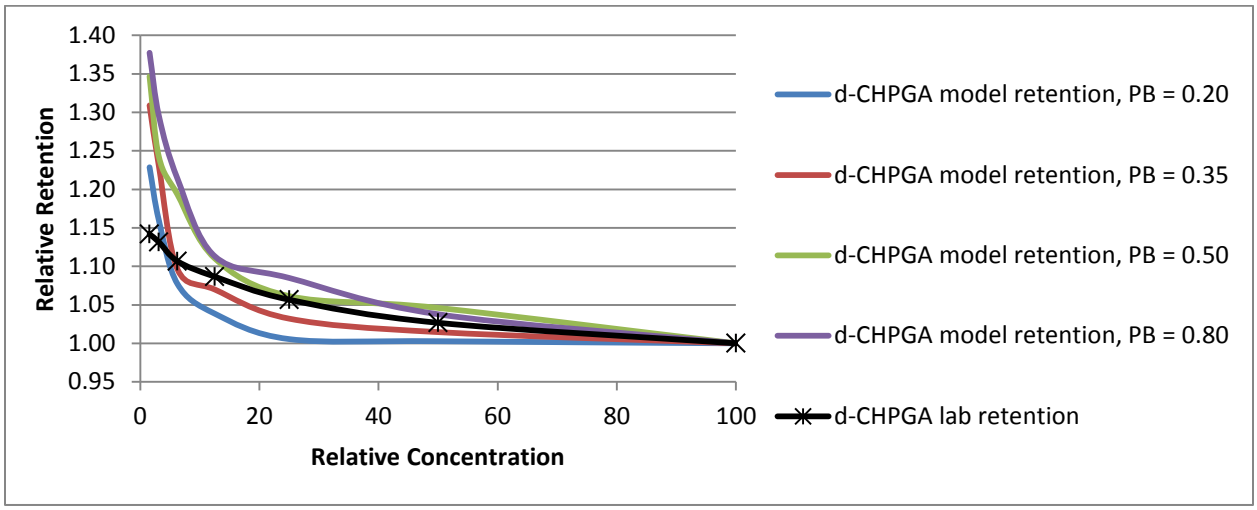

Figure 32: Relative concentration of d-cyclohexylphenylglycolic acid enantiomer at different breaking probability factors versus relative retention under laboratory and model conditions.

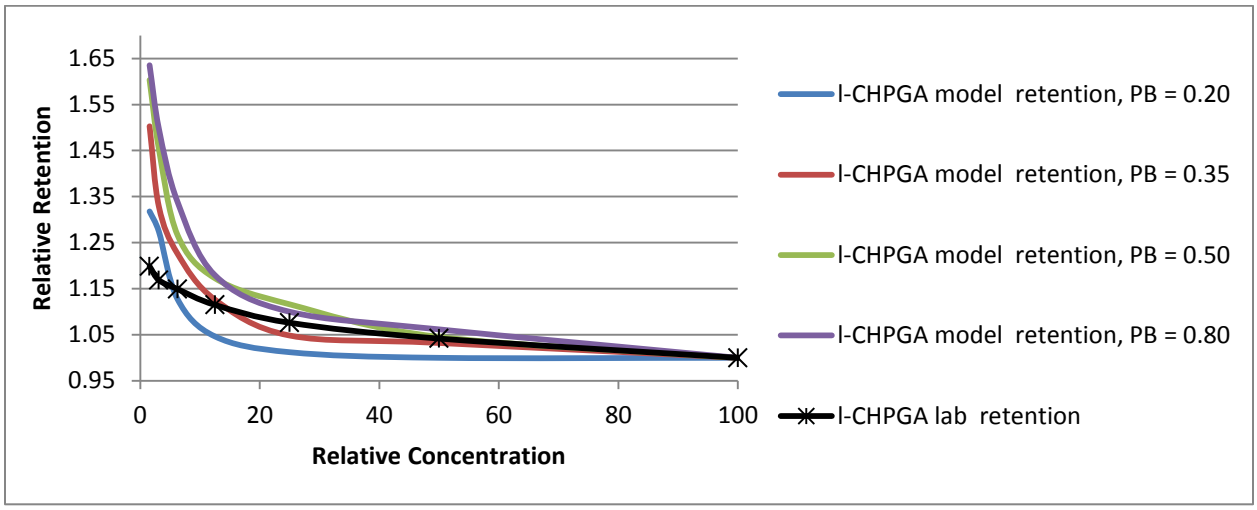

Figure 33: Relative concentration of l-cyclohexylphenylglycolic acid enantiomer at different breaking probability factors versus relative retention under laboratory and model conditions.

4.5 Conclusion

The proposed predictive model is based on correlation to experimentally determined complex stability constants and uses simple variable factors and probabilities to accurately determine the retention order of a wide variety of analytes and their complex strength to cyclodextrin stationary phases. By using such a diverse and large number (968) of analytes to develop the model's probability and factor equations, optimal modeling of one-to-one molecular binding strengths between analytes and cyclodextrins is achieved.

A cellular automata model using probability rules and factors that are based on generally accepted chromatographic bonding forces between enantiomers and β-cyclodextrin stationary phase gives a predictive tool for separation potential using chromatography. The cellular automata model agrees with published potential binding energies of six sets of enantiomer-(β-cyclodextrin) complexes and experimentally determined high performance liquid chromatography separation.

At chromatographic scale the model accurately predicted the lack of separation of mandelic enantiomers and the separation of brompheniramine enantiomers previously modeled in one-to-one interactions. By examining cyclohexylphenylglycolic acid enantiomers, the model accurately predicted both the selectivity and resolution of the enantiomer peaks at varying temperatures. Mobile phase flow rate changes in the model changed peak retention and shape in the same manner expected in traditional high performance liquid chromatography. Modeled changes in mobile phase pH agree with laboratory outcomes when examining peak resolution and selectivity. Changes in injection volume resulted in an increase in retention time of the modeled enantiomers as

was observed in the published laboratory results. However, the non-linearity of the change at low sample concentrations had not been explained. This phenomenon is not explained by just a convex isotherm. Although a convex isotherm is present, analyte-to-analyte interaction may be playing a role in retention in addition to a convex isotherm adsorption of analyte-to-stationary phase. Additionally, as the sample concentration becomes so low in the model that analyte-to-analyte interactions become less likely to occur, the less significance analyte attraction has on retention.

Chapter 5 Summary and Conclusions

A cellular automata model written as a Java™ application executed using Eclipse Classic as an integrated development environment was developed to analyze and predict the retention and chromatographic separation of enantiomers on β-cyclodextrin stationary phases. To date, the analytical process of high performance liquid chromatographic separation of enantiomers on cyclodextrins has not been modeled using cellular automata. Current published models of analyte to cyclodextrin stationary phase interaction focus on molecular binding thermodynamics, relying on physical concepts involving energies and forces to guide the actions of molecules expressed in terms of differential and non-linear equations. Results are wholly determined by the parameter sets used to describe the potential energy of the system on the initial conditions. This limits the scope of these models due to their complexity, making them difficult to study additional binding interactions. This first work in the area using cellular automata modeling, relies on mathematical systems of probability that are easily adaptable to different enantiomer analytical systems.

The model environment is designed in two main stages, one-to-one interactions and chromatographic scale. In one-to-one interactions between enantiomers and β-cyclodextrin, enantiomers are modeled and run individually to measure strength of the

interaction. Results were then compared between the enantiomers to predict whether or not chromatographic separation is likely.

In order for the model to be able to predict binding strengths of enantiomers to β-cyclodextrin, the relationship of the iterations of retention between an enantiomer and β-cyclodextrin versus complex stability constant (log K) is determined. Twenty eight value sets are used for breaking probabilities throughout the log K range of 0.25 – 5.5. A comparison of log (iterations to escape) vs. log K has a linear relationship (coefficient of determination, 0.9924) expressed as log(iterations to escape) = 0.5026 x log K +0.9394 (Figure 17). This demonstrates a linear relationship with no bias.

With enantiomer retention correlated to log K, the model was tested to see if it accurately predicts the retention order of different analytes when compared to experimental data. Using 65 analytes whose log Ks were experimentally determined (Blokzijl and Engberts 1993), one-to-one interactions were modeled with cyclodextrin stationary phase that spanned weak to strong retention with small to larger differences in log K. The model accurately predicted the relative retention strength of all 65 analytes (see Table 12).

Enantiomer retention was then modeled in on-to-one interactions to compare to published potential binding energies of the enantiomer-(β-cyclodextrin) complexes and high performance liquid chromatography selectivity data (see Table 13 (Durham, D. 1996; Han and Armstrong 1989) and Figure 19). Breaking probabilities between the enantiomers and β-cyclodextrin were determined for six sets of enantiomers.

The model predicted that brompheniramine would separate the most with a difference in iterations to escape (ΔITE) of 5.17. This agrees with the differences in

potential binding energy (ΔPBE) of brompheniramine-(β-cyclodextrin) complexes of 6.80 kcal/mole where a value greater than one predicts sufficient complexation for high performance liquid chromatography separation (Durham 1996). The model predicts that N-Methylphenobarbitone to have the next greatest separation with an ΔITE of 2.83. This agrees with a ΔPBE of 2.33 kcal/mole and a $\propto$ of 1.11. With model results of ΔITE of 1.17 pseudoephedrine has some separation potential. ΔPBE for pseudoephedrine is 0.57 kcal/mole indicating not much separation, however a chromatographic selectivity of 1.12 does. NMR analysis has demonstrated that pseudoephedrine separation occurs due to hydrogen bonding along the cyclodextrin outer edge (Mularz and Petersheim et al. 1988). Therefore, the separation occurring will be highly dependent on the surrounding mobile phase environment, which has not yet been accounted for in the model. Ibuprofen, mandelic acid, and ephedrine do not have significant chromatographic separation. This matches model predictions for ephedrine (ΔITE of 0.17) and mandelic acid (ΔITE of 0.67). Ibuprofen has an ΔITE of 1.33 predicting chromatographic separation. Other one-to-one modeling techniques have predicted separation of ibuprofen; however, chromatographic separation is less likely. It appears that one-to-one modeling is insufficient in predicting ibuprofen selectivity.

Model results are graphically displayed (see Figure 19) showing iterations to escape. It shows the separation of brompheniramine and N-Methylphenobarbitone enantiomers, with less separation for ibuprofen. It also demonstrates lack of separation of the other enantiomers. The model is able to predict enantiomer retention in β-cyclodextrins and the lack thereof, with the exception of ibuprofen.

One-to-one interactions do not take into account many factors that affect chromatographic separations. Therefore the model was expanded to represent a chromatographic scale. From the one-to-one modeled interactions, mandelic acid and brompheniramine were run under chromatographic model conditions to compare results. Mandelic acid had a laboratory selectivity 1.05 (Durham 1996), while model results by maximum row population gave a value of 1.01 and by iteration a value of 1.01. While these values are lower than laboratory results, the model accurately predicts the insufficient separation. Brompheniramine had a greater laboratory separation with a selectivity of 1.13, while the model predicted a row and iteration selectivity of 1.12 and 1.12, respectively. Consequently, the model accurately predicts the lack of chromatographic selectivity in mandelic acid while also predicting greater selectivity with brompheniramine enantiomers. Predicting selectivity is helpful, though it does not consider how well the peaks are separated. More information from the model was required to examine peak shape. Flow rate and void retention time were determined, and from this capacity factors. Tailing factors and resolution were determined manually from the Excel chromatograms so that enantiomer separation could be more closely examined.

Modeling the chromatographic system for cyclohexylphenylglycolic acid enantiomers, the model accurately predicted both the resolution and selectivity of the enantiomer peaks at varying temperatures (see Figures 28 and 29). Mobile phase changes in the model changed peak retention and shape in the same manner expected as in traditional chromatography. Modeled changes in mobile phase pH of 4.2 to 6.5 agree with laboratory outcomes when examining the loss of peak resolution and

selectivity at pH 6.5. Changes in sample amount on the column resulted in an increase in retention time of the modeled enantiomers as was observed in the published laboratory results (see Figure 31).

As a model for one-to-one enantiomer binding interactions with β-cyclodextrin, it has proven to be accurate in the prediction of binding strengths. In its expansion to the chromatographic scale, the model has been proven rugged under the varying chromatographic conditions studied that affect peak separation. Used as a tool for method development, the model has potential for reducing the time and cost in enantiomer separations using cyclodextrins.

References

Abate, T. “Need to preserve cash generates wave of layoffs in biotech industry.” San Francisco Chronicle, February 10, 2003:E1.

Allen, M. P. (1995). Observation, Prediction and Simulation of Phase Transitions in Complex Fluids, vol. 460 NATO ASI series C. Boston, MA, Kluwer Academic Publishers, M. Baus, L. F. Rull, and J. P. Ryckaert, Eds., pp. 339-356.

Aree, T., J. Jacob, W. Saenger, and H. Hoier (1998). “Crystal structure of α-cyclodextrin-acetonitrile-hexahydrate.” Carbohydr Res **307**: 191-197.

Blokzijl, W. and J. Engberts (1993). “Hydrophobic effects, opinions and facts.” Angew Chem Int Ed Engl **32**: 1545-1579.

Chaudhari, A., S. Lee (2004). “Density function study of hydrogen-bonded acetonitrile-water complex.” Int J Quantum Chem **102**: 106-111.

Chen, W., C. Chang, and M. Gilson (2004). “Calculation of cyclodextrin binding affinities: energy, entropy, and implications for drug design.” Biophysical Journal **87**: 3035-3049.

Choi, Y. J, S. K. Han, S. T. Chung and K. H. Row (2004). “Chromatographic separation of bupivacaine racemate by mathematical model with competitive Langmuir isotherm.” Korean J of Chem Eng **21**(4): 829-835.

Choi, Y. H., C. Yang, H. Kim, and S. Jung (2000). "Monte Carlo simulations of the chiral recognition of fenoprofen enantiomers by cyclomaltoheptaose (β-cyclodextrin)." Carbohydrate Res **328**(3): 393-397.

Conners, K. A. (1997). "The stability of cyclodextrin complexes in solution." Chem Rev **97**: 1325-1358.

Dimitrova, M., S. Ilieva, and B. Galabov (2004). "Reactivity descriptors for the hydrogen bonding ability of pyridine bases." SAR and QSAR in Environmental Res **15**: 311-319.

Durham, D. (1996). "Application of force field calculations to the prediction of chirally discriminating chromatographic behavior for cyclodextrins." Chirality **8**: 58-66.

Ege, S. (2003). Organic Chemistry: Structure and Reactivity. 5th ed. Boston, MA, Houghton Mifflin Company, pp. 30-33.

Feitsma, K. G., J. Bosman, B. F. H. Drenth, and R. A. De Zeeuw (1985). "A study of the separation of enantiomers of some aromatic carboxylic acids by high-performance liquid chromatography on a β-cyclodextrin-bonded stationary phase." J Chrom **333**: 59-68.

Geiger, A., F. H. Stillinger, and A. Rahman (1979). "Aspects of the percolation process for hydrogen bonded networks in water." J Phys Chem **70**: 4186.

Grimme, S. (2008). "Do special noncovalent π-π staking interactions really exist?" Angewandte Chemie International **47**: 3430-3434.

Han, S. M. and D. W. Armstrong (1989). Chiral separations by HPLC: Applications to pharmaceutical compounds. A.M. ed. United Kingdom, Taylor & Francis Ltd, Chap 10.

Heftmann, E. (1983). “Chromatography fundamentals and applications of chromatographic and electrophoretic methods, part A: fundamentals and techniques.” J Chrom Library **22A**: A32-33.

Hinze, W. L. (1981). “Applications of cyclodextrins in chromatographic separations and purification methods.” Sep Purif Methods **10**(2): 159-237.

Hummer, G., S. Garde, A. E. Garcia, A. Pohorille, and L. R. Pratt (1996). “An information theory model of hydrophobic interaction.” Proc Nat Acad Sci **93**: 8951-8955.

Jonsson, J. A. (1996). “Nomenclature for non-linear chromatography.” Pure & Appl Chem **68**(8): 1591-1595.

Jorgensen, W. L., J. Gao, and C. Ravimohan (1985). “Monte carlo simulations of alkanes in water: hydration numbers and hydro-phobic effect.” J Phys Chem **89**: 3470-3477.

Kakitani, T., H. Kakitani, and S. Yomosa (1980). “Hydrophobic bond energy of non-polar molecules: application to β-Ionone and 11-cis Retinal.” Biophys Struct Mech **7**: 101-106.

Kano, K., K. Mori, B. Uno, M. Goto and T. Kubota (1990). “Voltammetric and spectroscopic studies of pyrroloquinoline quinone coenzyme under neutral and basic conditions.” J Am Chem Soc **112**: 8645-8649.

Khimenko, M. T. and N. N. Gritsenko (1980) Zh.Fiz.Khim **54**: 198-199.

Kier, L. B. and C. K. Cheng (1994). “A cellular automata model of water.” J Chem Inf Comput Sci **34**: 647.

Kier, L. B., C. K. Cheng, and H. T. Karnes (2000). “A cellular automata model of chromatography.” Biomed Chrom **14**: 530-534.

Kier, L. B., C. K. Cheng, and P. Seybold (2000). **“**Cellular automata models of chemical systems.” SAR QSAR Environ Res **11**: 79-98.

Kier, L. B., P. G. Seybold, and C. Cheng. (2005). Modeling Chemical Systems using Cellular Automata, 1st ed. Netherlands, Springer.

Kim, H., K. Jeong, S. Lee, and S. Jung (2003) “Molecular modeling of the chiral recognition of propranolol enantiomers by a β-Cyclodextrin.” Bull Korean Chem Soc. **24**(1): 95-98.

Kitagawa, M., H. Hoshi, M. Sakurai, Y. Inoue, and R. Chujo (1988). “A molecular orbital study of cyclodextrin inclusion complexes: the calculation of the dipole moments of α-cyclodextrin aromatic guest complexes.” Bull Chem Soc Jpn **61**: 4225-4229.

Leach, A. R. (1996). Molecular Modeling: Principles and Applications, 1st ed. Harlow, England, Longman.

Linyong, M., H. Harold, and K. Stine (2002). “Simple lattice simulation of chiral discrimination in monolayers.” J Chem Inf Comput Sci **42**:1179-1184.

Liu, L. and Q. Guo (2002). “The driving forces in the inclusion complexation of cyclodextrins.” J of Inclusion Phenomena and Macrocyclic Chem **42**: 1-14.

Mao, L., H. H. Harris, and K. J. Stine (2002). “Simple lattice simulation of chiral discrimination in monolayers." J Chem Inf Comput Sci **42**: 1179-1184.

Matsui, Y. and K. Mochida (1979). “Binding forces contributing to the association of cyclodextrin with alcohol in an aqueous solution.” Bulletin of the Chem Soc of Japan **5**: 2808-2814.

Miertus, S., V. Frecer, E. Chiellini, F. Chiellini, R. Solaro and J. Tomasi (1998). "Molecular interactions and inclusion phenomena in substituted β-cyclodextrins. Simple inclusion probes: H2O, C, CH4, C6H6, NH4+, HCOO-." J of Inclusion Phenomena and Macrocyclic Chem **32**: 23-46.

Mularz, E. A., L. J. Cline-Love, and M. Petersheim (1988). "Structural basis for enantiomeric resolution of pseudoephedrine and the failure to resolve ephedrine by using β-cyclodextrin mobile phases." Anal. Chem **60**: 2751-2755.

Ohmine, L. and H. Tanaka (1993). "Fluctuation, relaxations and hydration in liquid water, hydrogen bond rearrangement dynamics." Chem Rev **93**: 2545.

Regiert, M. (accessed Nov. 20, 2007) "The structure of cyclodextrins." www.cyclodextrin.org/pc/seminarFolieDateien/fullscreen.htm.

Rekharsky, M. V. and Y. Inoue (1998). "Complexation. Thermodynamics of cyclodextrins." Chem Rev **98**: 1875-1917.

Saenger, W., J. Jacob, K. Gessler, T. Steiner, D. Hoffmann, H. Sanbe, K. Koizumi, S. M. Smith, and T. Takaha (1998). "Structures of the common cyclodextrins and their larger analogues beyond the doughnut." Chem Rev **98**: 1787-1802.

Sakurai, M., M. Kitagawa, H. Hoshi, Y. Inoue (1988). "CNDO-electrostatic potential maps for α-cyclodextrin." Chem Letters **17**: 895-898.

Sanemasa, I., Y. Wu, Y. Koide, T. Fujii, H. Takahashi, and T. Deguchi (1994). "Stability on drying of cyclodextrin precipitates of volatile nonelectrolytes." Bulletin of the Chem Soc of Japan **67**: 2744-2750.

Schwartz, A. T. (1997). Chemistry in Context: Applying Chemistry to Society, 2nd ed. Dubuque, IA, Wm. C. Brown Publishers, A. T. Schwartz, Ed.

Skoog, D. A. (1985). Principles of Instrumental Analysis, 3rd ed. New York, NY, Saunders College Pub. pp. 735-739.

Tildesley, D. J. (1998). The Molecular Dynamics Method, 1st ed. Boston, MA, Kluwer Academic Publishers, pp. 23-47.

Tropsha, A., P. Gramatica, and V. Gombar (2003). "The importance of being earnest: validation is the absolute essential for successful application and interpretation of QSPR models." QSAR Comb Sci **22**: 69-77.

Weast, R. C. (1988). CRC Handbook of Chemistry and Physics, 69th ed. 1988-1989 Boca Raton, FL, CRC Press Inc., pp. D-162, F-10.

Wolfram, S. (1983). "Cellular automata." Los Alamos Science **9**: 1-21.

Wolfram, S. (2002). A New Kind of Science, 1st ed. Champaign, IL, Wolfram Media, J. Progen and C. Small, Eds., pp. 49-50.

Zhoa, Y., M. Abraham and A. Zissimos (2003). "Fast calculation of van der Waals volume as a sum of atomic and bond contributions and its application to drug compounds." J Org Chem **68**: 7368-7373.

APPENDIX A

Model program and manual

1. On the disk included, copy the folder “desoi” onto any location on computer
2. Install the 32 or 64 bit version of Eclipse SDK on the computer
3. Open Eclipse and Import the existing project “desoi”
4. Key files to modify
    a. “b.txt”
        i. Under the main project open b.txt to change the following parameters (example): desoi2 desoi2 7000 1000 50 10 0
            1. Name of file simulation
            2. Name of variation, should be same name as simulation file
            3. Number of iterations to run, 7000
            4. Start recording at iteration 1000
            5. Number of runs to average, 50
            6. Record data every 10 iterations
            7. Graphics turned off, 1 for on
    b. “desoi2.inf”, to modify grid layout and cell population
    c. “desoi2.prb”, to change to probabilities and absolute gravity (mobile phase flow) of cells

d. “desoi2.inf”, to change cell design

5. Once parameters are set run simulation
6. Model run result file is found in the main project folder in a folder name “CAOutput”

APPENDIX B

Java cell layout file for chromatographic scale, “desoi2.inf”

The file name is:desoi2.inf
desoi2.str is the Str file on which the prb file is based
40 Num of Columns
800 Num of Rows

The number of cells per cell types are below:

cell type	number of cells
A	100
D	100
B0	200
B1	200
B2	300
W1	13376
W2	6271

First row of β–cyclodextrin cells (B0, 1, and 2)

LUX	LUY	RBX	RBY	CellType	CellNum	Orient
5	10	5	10	2	1	2
5	14	5	14	2	1	0
6	10	6	10	3	1	2
6	14	6	14	3	1	0
7	11	7	13	4	3	0
13	10	13	10	2	1	2
13	14	13	14	2	1	0
14	10	14	10	3	1	2
14	14	14	14	3	1	0
15	11	15	13	4	3	0
21	10	21	10	2	1	2
21	14	21	14	2	1	0
22	10	22	10	3	1	2
22	14	22	14	3	1	0
23	11	23	13	4	3	0
29	10	29	10	2	1	2
29	14	29	14	2	1	0
30	10	30	10	3	1	2
30	14	30	14	3	1	0
31	11	31	13	4	3	0
37	10	37	10	2	1	2
37	14	37	14	2	1	0
38	10	38	10	3	1	2
38	14	38	14	3	1	0
39	11	39	13	4	3	0

Second row of β–cyclodextrin cells (B0, 1, and 2)

LUX	LUY	RBX	RBY	CellType	CellNum	Orient
1	20	1	20	2	1	2
1	24	1	24	2	1	0
2	20	2	20	3	1	2
2	24	2	24	3	1	0
3	21	3	23	4	3	0
9	20	9	20	2	1	2
9	24	9	24	2	1	0
10	20	10	20	3	1	2
10	24	10	24	3	1	0
11	21	11	23	4	3	0
17	20	17	20	2	1	2
17	24	17	24	2	1	0
18	20	18	20	3	1	2
18	24	18	24	3	1	0
19	21	19	23	4	3	0
25	20	25	20	2	1	2
25	24	25	24	2	1	0
26	20	26	20	3	1	2
26	24	26	24	3	1	0
27	21	27	23	4	3	0
33	20	33	20	2	1	2
33	24	33	24	2	1	0
34	20	34	20	3	1	2
34	24	34	24	3	1	0
35	21	35	23	4	3	0

Placement of enantiomers (A & D) and mobile phase

LUX	LUY	RBX	RBY	CellType	CellNum	Orient
0	0	39	9	0	100	0
0	0	39	9	1	100	0
0	0	39	799	5	13376	0
0	0	39	799	6	6271	0

APPENDIX C

Java cell types for chromatographic scale, “desoi2.inf”

The file name is:desoi2.str
14 number of side types
Their names are:
a0
a1
a2
a3
d0
d1
d2
d3
b0
b1
b2
c0
w1
w2

Their colors are:
0 Black
1 Blue
2 Green
3 Red
4 Brown
5 Yellow
6 Orange
0 black
8 Burgundy
9 White
0 black
11 Violet
1 Blue
2 Green

7 number of cell types
Their names are:
A
D
B0
B1
B2
W1
W2

Their side types are			
(4 for 4slice, and 1 for solid):			
a0	a1	a2	a3
d0	d1	d2	d3
b0	c0	c0	c0
b1	c0	c0	c0
c0	c0	c0	b2
w1			
w2			